SITE - SPECIFIC CHARACTERIZATION, MODELING AND SPATIAL ANALYSIS OF SUB-SOIL COMPACTION (HARDPAN) FOR PRECISION AGRICULTURE ON SOUTHEASTERN US SOILS

by

MEHARI ZEWDE TEKESTE

(Under the Direction of Randy L. Raper and Ernest W. Tollner)

ABSTRACT

Natural and machinery traffic-induced subsoil compacted layers (soil hardpans) that are found in many southeastern US soils limit root growth with detrimental effects on crop productivity and the environment. Due to the spatial variability of hardpans, tillage management systems that use site-specific depth tillage applications may reduce fuel consumption compared to the conventional uniform depth tillage. The success of site-specific tillage or variable depth tillage depends on an accurate sensing of the hardpan layers, field positioning, and controlling the application of real-time or prescribed tillage. The over arching objective of the work was to understand and advance the art and science of soil compaction analysis and prediction with an eye towards compaction management in precision farming. The specific objectives were (1) To investigate the influences of soil parameters (soil moisture and bulk density), and the soil-cone frictional property on the interpretations of cone penetrometer data in predicting the magnitude and depth of hardpans, (2) To determine spatial variability for creating hardpan maps and (3) To investigate a passive acoustic based real-time soil compaction sensing method. The soil cone

penetration problems were also modeled using finite element modeling to investigate the soil deformation patterns and evaluate the capability of the finite element method to predict the magnitude and depth of the hardpan. Laboratory experiments in a soil column study indicated that the soil cone penetration resistances were affected by soil moisture, bulk density and cone material type. Soil drying increased the magnitude of soil cone penetration resistance and slightly decreased the predicted depth of the hardpan. The small difference (approximately 2 cm) of the predicted depth of the hardpan due to soil drying may imply that cone index measurements for prediction of the depth to the hardpans are less sensitive to soil moisture variations. Cone index readings varied due to the type of cone material. The cone index obtained with Teflon cone material was less as compared to using a stainless steel (ASAE 1999a). By coating dry powder Teflon on the stainless steel cone, the cone index values were between the stainless steel and Teflon.

The spatial variability and the theoretical semivariogram model parameters for Kriging prediction were significantly affected by soil drying in determining the magnitude of soil strength contained in the soil hardpan. The spatial variability of the predicted depth of soil hardpans, however, showed less spatial correlations at dry soil moisture conditions. The magnitude of the soil hardpan was more strongly affected by soil drying than the predicted depth of the hardpan. Precision tillage that varies across the field according to the spatial structure of soil hardpan attributes can be prescribed on soils of the southeastern US to improve the sustainability of crop production.

Besides soil cone penetrometer based hardpan characterization, real-time acoustic compaction layer detection system was developed using a microphone-fitted cone mounted on a tine. The detection of the location of hardpans was carried out on the highest frequency range of

the acoustic signals (termed "detection edge"), which was band filtered on the fast Fourier transformed acoustic signal. High levels of agreement were found between cone index measurements and associated sound levels, which clearly demonstrated the methods' potential to detect hardpans.

INDEX WORDS: Soil compaction, Soil Hardpan, Soil Cone Penetrometer, Finite Element Method, Acoustics-soil compaction, Precision Tillage.

SITE - SPECIFIC CHARACTERIZATION, MODELING AND SPATIAL ANALYSIS OF SUB-SOIL COMPACTION (HARDPAN) FOR PRECISION AGRICULTURE ON SOUTHEASTERN US SOILS

by

MEHARI ZEWDE TEKESTE

B.S. The University of Asmara, Eritrea 1996

M.S. The University of Wageningen, the Netherlands 2000

M.S. The University of Wisconsin, Madison, USA 2001

A Dissertation Submitted to the Graduate Faculty of The University of Georgia in Partial Fulfillment of the Requirements for the Degree

DOCTOR OF PHILOSOPHY

ATHENS, GEORGIA

May 2006

SITE - SPECIFIC CHARACTERIZATION, MODELING AND SPATIAL ANALYSIS OF SUB-SOIL COMPACTION (HARDPAN) FOR PRECISION AGRICULTURE ON SOUTHEASTERN US SOILS

by

MEHARI ZEWDE TEKESTE

Co-Major Professor:	Randy L. Raper
	Ernest W. Tollner
Committee:	Glen C. Rains
	David R. Radcliffe
	Lynne Seymour

Electronic Version Approved:

Maureen Grasso
Dean of the Graduate School
The University of Georgia
May 2006

DEDICATION

This dissertation is dedicated to honor and glorify my God in heaven and my Lord Christ Jesus for the infinite mercy, grace and the power through the Holly Spirit who has established the work of my hands.

ACKNOWLEDGEMENTS

I sincerely thank and acknowledge my advisors Dr. Randy L. Raper from USDA-ARS-National Soil Dynamics Laboratory (NSDL) in Auburn, AL and Dr. Ernest W. Tollner from the Department of Biological and Agricultural Engineering at UGA for their guidance and mentorship during my PhD work. I also would like to express my gratitude to the members of the graduate committee; Dr. David Radcliffe from the Department of Crop and Soil Sciences, Dr. Lynne Seymour from the Department of Statistics and Dr. Glenn Rains from the Department of Biological and Agricultural Engineering. I would also like to extend my gratitude to the employees of USDA-ARS-NSDL in Auburn, AL and Auburn University; Dr. Thomas R. Way and Dr. Tony R. Grift for their invaluable suggestions and comments; Eric Schwab, Morris Welch, Dexter LaGrange, John Walden and others employee of the NSDL for their help in data collection and preparation of the soil bin. I would also like to acknowledge Dr. Clarence Johnson from Auburn University and Dr. Bailey from the NSDL for allowing me to use their tri-axial test data and invaluable contributions in using the NSDL-AU soil compaction model for the finite element modeling work.

Last but not least, my special gratitude goes to my beloved wife and sister in Christ Jesus, Tirhas Ghebrehiwet Kelati for her encouragement, steady fast prayers and patience; my beloved family in Eritrea for their encouragement and prayers; and friends and family in Victory Life Church in Athens, GA for their persistent help and prayers.

TABLE OF CONTENTS

CHAPTER 1

INTRODUCTION

In the southeastern US, soil compaction is a severe soil physical problem that negatively affects crop productivity, and may accelerate erosion and runoff. Crop revenues are reduced substantially due to soil compaction. Highly compacted subsoil layers (hardpans) found in many southeastern US soils restrict root growth and decrease soil moisture availability that results in a decline in crop productivity, particularly during drought periods. Farmers apply uniform subsoiling either on an annual or a biannual basis to mechanically disrupt the hardpan layers such that roots can easily access the soil moisture and nutrient reserves for optimal crop growth. With the current subsoiling practice, the tillage implements are set at uniform depth for the entire field. Such tillage practices may incur unnecessary fuel consumption as the hardpans exhibit substantial field variability. Application of tillage practices that address the field variability of soil compaction may reduce tillage energy and fuel costs and also create the desired soil conditions for crop growth.

Precision (site-specific) tillage is a management strategy whereby deep tillage could be applied at variable depths according to the soil compaction needs. The success of precision tillage depends on the availability of accurate methods and standardized procedures to determine the hardpan layers, quantifying the field variability, field positioning, and controlling the application of real-time or prescribed tillage. Spatial variability analysis of soil compaction and

application of precision tillage management have not progressed as much as precision agricultural applications of fertilizers and chemicals. Research is needed to develop methods to precisely characterize the relative strength and depth of hardpans and determine their spatial pattern for precision (site-specific) tillage management to improve sustainability of crop production in the southeastern US.

A soil cone penetrometer is a device widely used to assess soil compaction. The device measures the penetration force required to vertically insert a cylindrical rode with a steel cone down through the soil. The data are reported as soil cone index (penetration force / cone base area) as a function of depth. The tool's design specifications and measurement procedures have been standardized (ASAE 1999a, b). Standardization of the cone penetrometer data interpretation has not developed to characterize compacted layers or hardpans for heterogeneous soil conditions and layering. In the past, the use of soil cone penetrometers for soil compaction management depended mainly on users' experiences with the data and field conditions. Limited research has been conducted that study the influence of soil parameters and layering on the cone penetrometer readings in characterizing soil hardpan layers. The mechanical reactions of layered soils to cone penetration are also less investigated. In precision tillage, a precise detection of the relative strength and depth of hardpans is important because errors of a few centimeters could cause variations in accurately locating the hardpan layers and site-specific tillage depth recommendations.

Studies on cause and effect relationships between cone index and soil properties in layered soils, modeling of soil deformation during cone penetration and determining the field variability of soil hardpans were needed to evaluate the existing knowledge and develop procedures in using soil cone index measurements for precision tillage management.

A Global Positioning System (GPS) assisted Multiple-Probe-Soil-Cone-Penetrometer (MPSCP) that has the capability to acquire large amounts of cone index profile data in a relatively short period, was used in the soil bin and field experiments. Algorithms for cone index analysis were developed to predict the relative strength and depth of hardpans. With the help of GPS field positioning, accurate characterization, and within-field management of soil hardpans, precision tillage management may improve the sustainability of crop and animal production systems by reducing tillage energy consumption often associated with the conventional uniform tillage practices in the southeastern US. The application of precision tillage management can potentially be applied for both conventional and conservation cropping systems.

In the future, with the advancement of micro-controller and control engineering in agriculture, the actuation of real-time soil compaction measurement and application of tillage may be a reality in the management of agricultural systems. Besides to the soil cone penetrometer based soil hardpan characterization, investigation was made in soil bin study to develop and evaluate on-the-go/ real-time sensors based on passive acoustic method in predicting location and strength of hardpan.

The over arching objective of the work was to understand and advance the art and science of soil compaction analysis and prediction by evaluating the “stop and go” cone index measurement in characterizing soil hardpan and the potential of “on-the-go” acoustic based soil hardpan sensing with the intent of soil compaction management in precision farming on southeastern US soils. The specific objectives were (1) To investigate the influences of soil parameters (soil moisture and bulk density), and the soil-cone frictional property on the interpretations of cone penetrometer data in predicting the magnitude and depth of hardpans, (2)

To determine spatial variability for creating hardpan maps and (3) To investigate a passive acoustic based real-time soil compaction sensing method.

CHAPTER 2

LITERATURE REVIEW

Soil compaction has been recognized as one of the major problems in crop production (Voorhees, 1991; Soane and Van Ouwerkerk, 1994 and Hamza and Anderson, 2005). Soil compaction is a process of soil particle rearrangement that reduces the soil porosity, in particular the air-filled fraction. The reduction in soil porosity causes a decrease in soil aeration and hydraulic conductivity, and an increase in soil bulk density and soil strength (Al-Adawi and Reeder, 1996 and Hillel, 1998). Soil compaction can occur naturally due to soil particle size variability, soil moisture variation and soil formation processes (Hillel, 1998) and can be created by forces exerted from machinery traffic, tillage, and animal trampling (Radcliffe et al., 1989; Da silva et al., 2003; Raper and Reeves, 2004a and Raper, 2005).

There are two types of soil compaction, namely surface and subsurface (subsoil) compaction that occurs within normal tillage depth and below the normal tillage depth, respectively. Some magnitude of surface soil compaction may be necessary to obtain firm contact between seed and soil aggregates for uptake of nutrients and soil moisture during germination. Surface soil compaction problems can be removed by cultivation tillage. Subsurface compaction is of greater concern than surface compaction because once it occurs; its removal requires energy intensive tillage practices and often the benefits may not last long (Jones et al., 2003; Hamza and Anderson, 2005 and Raper, 2005).

Many soils in the southeastern US have compacted subsoil layers, commonly called hardpan, that occur at an approximate depth range of 15 to 35 cm (Campbell et al., 1974;

Radcliffe et al., 1989; Raper et al., 2000; Khalilian et al., 2002 and Busscher et al., 2005). Depending on the mode of formation, soil pans can be classified as: 1) genetic pans which are formed naturally and have low hydraulic conductivity and different soil physical and chemical properties from the soil layers above or below the pan; or, 2) pressure (tillage) pans that are formed by external forces such as machinery traffic and tillage and are characterized by a higher bulk density and a lower total porosity than the soil layers directly above or below the pans (Internet Glossary of Soil Science Terms, http://www.soils.org/sssagloss). In the southeastern Coastal Plains region, hardpans occur in the E horizon (Campbell et al., 1974 and Khalilian et al., 2002). Radcliffe et al. (1989) identified soil hardpans near the top of the Bt horizon in soils of the southern Piedmont region. The formation of the hardpans in the southeastern US could be associated to the low organic matter, weak soil structure and soil particle size variability (Spivey et al., 1986 and Radcliffe et al., 1988). Vehicle traffic and tillage increase the magnitude of soil compaction and natural reconsolidation could occur quickly after deep tillage (Busscher et al., 2002 and Raper et al., 2004a).

The excessively compacted hardpans impede root growth below the plow depth thereby resulting in crop yield reduction especially during drought periods when soil moisture and nutrients reserves in the lower soil strata are critical for crop growth (Taylor and Gardner, 1963; Camp and Lund, 1968, Busscher and Bauer, 2003 and Raper et al., 2004a). The presence of soil hardpan layers also reduces soil water infiltration, which can accelerate erosion and runoff of nutrients.

Farmers in the region apply uniform depth subsoiling annually to mechanically disrupt the hardpan layers and improve the root environment for optimal crop growth (Busscher and Bauer, 2003 and Raper et al., 2004a). The application of this energy intensive uniform subsoiling

is based on the assumption that the compacted layers are located at a constant depth. The relative strength and depth of the hardpans, however, vary from field to field and within fields (Fulton et al., 1996; Clark, 1999; Goodson et al., 2000; Raper et al., 2000 and Kenan et al., 2003). With uniform depth subsoiling, tillage may be applied in areas of the field where there is no soil compaction problem or at depths that do not necessarily correspond to the hardpan depth. This may incur unnecessary fuel consumption or the desired soil conditions may not be attained.

Precision or site-specific tillage where tillage is adjusted to the actual field location and depth of hardpans may be a sustainable alternative tillage management system. The introduction and development of precision agriculture management strategies owes to the advancement of precise information, sensing technologies and GPS (Hermann, 2001 and Rains et al., 2001). The precision agriculture management strategies that have shown promising successes in describing within field variability and variable rate applications of fertilizers, lime and chemicals could potentially be applied to precision tillage management. Naiqian et al. (2000) explained the benefits of precision agriculture on crop profitability, ecology and the environment. Precision tillage in particular is geared towards achieving the goals of sustainable agriculture by determining within-field variability and providing more accurate records of soil compaction; and eventually reducing tillage energy and fuel consumption. Many studies (Fulton et al., 1996; Khalilian and Hallman, 1996; Raper et al., 2000 and Khalilian et al., 2002) have reported the potential of precision tillage as compared to the conventional uniform depth tillage. Raper et al. (2000) estimated about 50% reduction in energy requirements for shallow tillage (approximately 18cm) versus deep tillage (approximately 33cm). Fulton et al. (1996) reported a fuel consumption reduction of 50% by precision tillage compared to subsoiling the entire field. Khalilian et al. (2002) found that approximately 75 % of the test area required tillage operations

shallower than the commonly used tillage depth for Coastal Plain soils. They reported energy and fuel savings of 42.8% and 28.4% respectively by adopting variable depth tillage as compared to uniform depth tillage.

The success of precision tillage depends on the availability of economical, rapid, easy and precise soil strength sensing methods, management of within field variability, accuracy of field positioning and controlling the application of real-time or prescribed precision tillage. The most important and basic requirement is the development of a soil strength sensing method followed by the management of within – field variability and controlling the application of tillage depths.

MEASUREMENT AND PREDICTION OF SOIL COMPACTION

Measurement and predictions of soil compaction behaviors are important for sustainable soil management, trafficability, simulation of root penetration, and design of soil engaging tools. Reviews on soil compaction measurement methods; the history and development of the cone penetrometer; fundaments of stress and strain relationships in soils and constitutive relationships; soil failure models during cone penetration and spatial variability studies were made in this section of the dissertation.

A soil body is comprised of solid materials (mineral and organic matter) and voids that contain air, water or both. When soil experiences compressive force; its volume may decrease; that results in turn a decrease in porosity or an increase in bulk density (mass of dry soil per unit soil volume). Soil compaction can be quantified by direct measurement of bulk density or porosity; or indirect measurement of soil behavioral changes to cone penetrometer insertion, air permeability or hydraulic conductivity (Gill and VandenBerg, 1968; Stafford and Hendrick, 1988 and Hillel, 1998). Bulk density and soil strength are the two widely measured parameters to

determine the state of soil compaction. Measurement of soil bulk density for large fields is tedious and time consuming. Soil cone penetrometer, a device that measures force required to insert a cone into the soil, is an easy and quick tool to measure relative soil strength in layered soils (ASAE 1999a, b). Soil strength as measured by a soil cone penetrometer was a critical impedance factor for root penetration on sandy soils (Taylor and Gardner, 1963). In addition to the magnitude of soil strength, the depth of the compacted layer is also a very important quantity for precision tillage that can be predicted from cone penetrometer data.

Recently the labor shortage, environmental constraints and spatial variability (Tollner et al., 2002), which drive precision agriculture and future robotic farming, enhanced research and development of real-time (on-the-go) and non-destructive soil compaction measurement technologies (Raper et al., 1990; Lui et al., 1993; Sudduth et al., 1998; Hall et al., 2000 and Andrade et al., 2004). Raper et al. (1990) was able to detect a soil hardpan with ground penetrating radar (GPR) that showed good agreement with cone penetrometer prediction of the hardpan for Norfolk sandy loam and Decatur clay loam soil bins at the USDA-ARS National Soil Dynamics laboratory. According to Raper et al. (1990) the amount and distribution of soil moisture along the profile ought to be uniform for accurate GPR detection of a soil hardpan. Under field conditions it is often unlikely to obtain uniform soil moisture profiles. Sudduth et al. (1998) successfully sensed the topsoil depth on claypan soils of central Missouri from soil electrical conductivity measurement by a non-contact, electromagnetic induction-based sensor (EM38) and a coulter-based sensor (Veris 3100). Hall et al. (2000) developed an on-the-fly mechanical impedance sensor to measure horizontal soil wedge penetration resistance. They reported similar results between the “wedge index” and cone index with the “wedge index” being less sensitive to soil moisture. In real-time sensing of soil compaction, the main problem is

identifying a dynamic soil quantity (e.g. air permeability, mechanical impedance, or electromagnetic properties of soils) that uniquely responds to soil compaction or soil strength with less sensitivity to the variations of other soil properties. As an alternative to the above mentioned real-time measurement technologies, sensing acoustic properties of soils can potential be used to develop on-the-go hardpan characterization method. Studies have shown some applications of acoustics in soils to measure soil texture (Liu et al., 1993) and soil surface roughness using acoustic backscatter (Oelze et al., 2003). Oelze et al. (2002) also studied the sound propagation velocity in soils. The acoustic sensors (microphone), which are availability in small size and inexpensive, can be easily embedded into production tillage sub-soiler shanks. DeRoock and Cooper (1967) conducted active compression wave propagation velocities measurement in soil using two accelerometers, which were separated by a measured distance. The differences in time of arrival of the sound signal pulses at the two accelerometers as it passes through the soil were related to propagation velocity. They found a linear relationship between wave propagation velocity and penetrometer resistance. Passive measurement of acoustics created as tillage tool passed through a layered soil that varied in soil strength could be potential developed for real-time measurement of soil compaction.

History of Cone Penetrometer

The history of the penetrometer dates back to 1846 when a French engineer, Collin, developed a 1mm diameter needle shaped penetrometer to estimate the cohesion of different clay types (Sanglerat, 1972). The Waterways Experiment Station (WES, 1948) later developed a circular cone penetrometer with an apex angle of 30-deg and base area of 1.61 cm^2 that was mounted on a graduated shaft of 0.95 cm diameter and 91.4 cm long. Historical perspectives on the cone penetrometer design (sizes and shape) and operation procedures are described in the

literature (Sanglerat, 1972 and Perumpral, 1987). Soil cone penetrometers have numerous applications in agriculture and off-road traffic studies that include in-situ soil compaction assessment, predicting trafficability, and bearing capacity for foundations (Perumpral, 1987) and simulation of root growth (Tollner and Verma, 1984). In developing their modified soil cone penetrometer, which was called soil impedometer, Tollner and Verma (1984) used polymer and water as cone lubricating agents. The American Society of Agricultural and Biological Engineering (ASABE) has established standards for a 30-deg circular stainless steel cone penetrometer and procedures for using and reporting data obtained with the soil cone penetrometer (ASAE 1999a, b). The standard (ASAE 1999a) recommended two cone base types: 20.27 mm diameter cone base with 15.88 mm diameter shaft for soft soils; and 12.83 mm diameter cone base with 9.53 mm diameter shaft for hard soils (Fig. 2.1). The penetrometer should be inserted at a uniform rate of 30 mm/s either manually or mechanically with the unit mounted on a tractor, truck, or a trailer. The data are reported as cone index defined as force of insertion per unit cone base area. Recent advances in the equipment design have been reported for multiple- probe cone penetration resistance reading and real-time cone penetration measurement (Raper et al., 1999 and Price, 2002). The interpretation of cone penetrometer data, however, has not progressed well mainly due to the influences of soil factors and soil material heterogeneity in space and time.

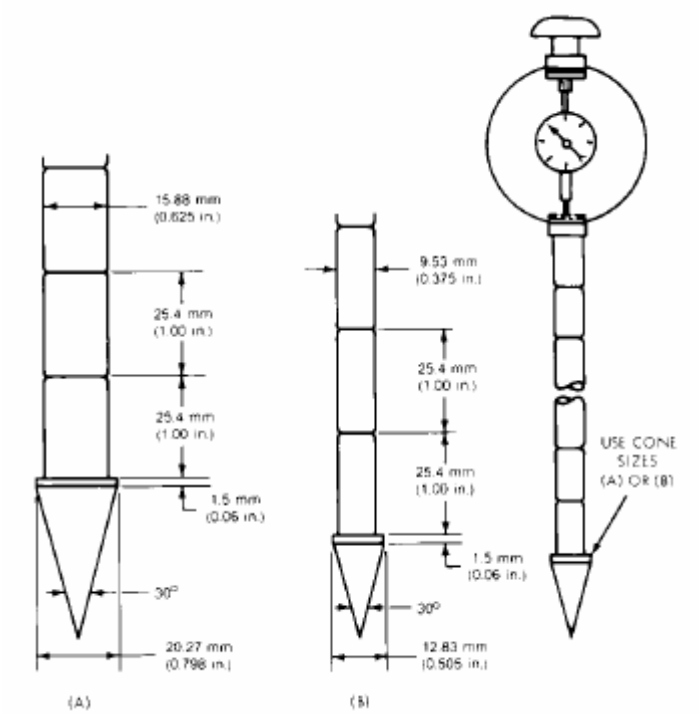

Figure 2.1. ASAE standard cone penetrometer (Used with permission from the ASABE).

Prediction and Modeling of Soil Compaction

Understanding the concepts of stress and strain in soils is essential for modeling soil reactions under loading from wheel traffic, tillage operation and plant roots. The fundamental engineering concepts on stresses and strains are available in books on mechanics of materials (Beer et al., 2005 and Coduto, 1999). When an infinitely small cubic soil element (Fig. 2.1a) with an area (δA) is subjected to force systems (δF_i), the stress (P_i), a quantity that expresses the intensity of force, can be obtained by solving the limit in equation 2.1 as the area (δA) approaches zero.

$$P_{ij} = \lim_{\delta A \to 0} \frac{\delta F_{ij}}{\delta A} \qquad 2.1$$

The force systems (F_{ij}) acting on the soil body could be normal to the plane resulting in normal stresses denoted by σ_{ij} and/or tangential to the plane resulting shear stresses (τ_{ij}). The

notation in the subscript for the normal stress indicates a plane perpendicular to the direction of force and for shear stress the first and second subscripts denote the planes normal and parallel to the direction of the tangential force, respectively. In response to the applied force, the soil element produces deformation. Strain expresses the deformation of the soil element in terms of its original dimension. Similar to the stress components, the state of strain can also be described as the normal strain (ε) and shear strain (γ) (Eq. 2.2). Shear strain (γ) is the angular deformation that measures the shape changes of the soil element.

$$\varepsilon = \frac{l - l_o}{l_0} \qquad 2.2$$

Where ε=engineering strain, l_0= original length of the element and l= length of the element after load is applied. In large strains, which are typical soil characteristics under loading from agricultural practices, natural strains instead of engineering strains are often used (Bailey and Johnson, 1989). Natural strains are determined by dividing the change in dimension (deformation) by the current dimension (instantaneous dimension). Natural strain ($\bar{\varepsilon}$) and engineering strain (ε) are related by:

$$\bar{\varepsilon} = \int_{l_o}^{l} \frac{dl}{l} = \ln\left(\frac{l}{l_0}\right) = \ln(1+\varepsilon) \qquad 2.3$$

The state of stress and strain at a point in a soil body can be described mathematically using stress and strain tensors (Table 2.1). Both for the stress and strain tensors, the diagonal variables are normal components and the off diagonal variables are the shear components. Solving the force equilibrium, the stress tensor has a symmetric property ($\tau_{xy}=\tau_{yx}$; $\tau_{xz}=\tau_{zx}$; and

$\tau_{yz}=\tau_{zy}$) and, hence, six independent variables as shown in Table 2.1 can fully describe the complete stress and strain tensors.

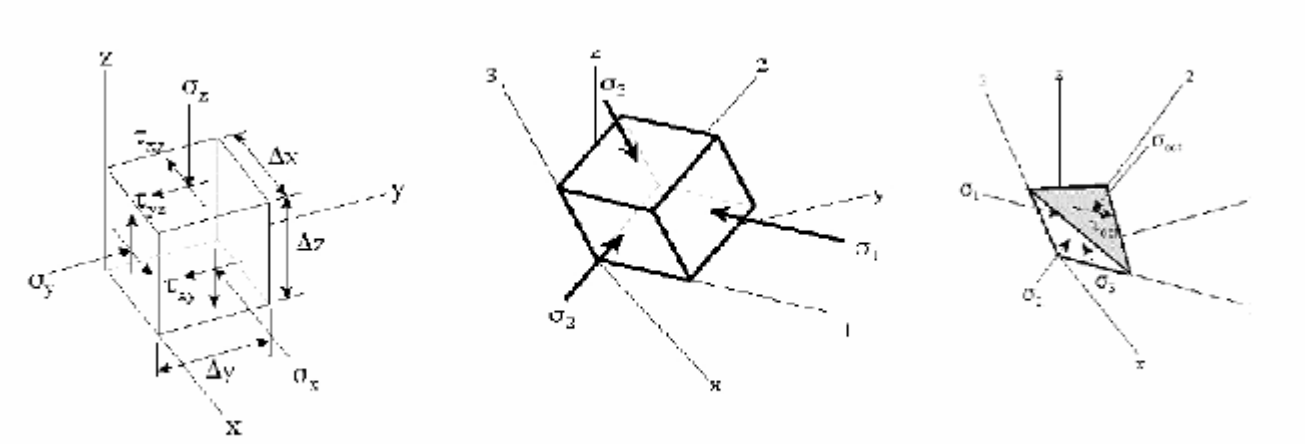

Figure 2.2 Stress state at a point in a continuum in (a) x, y and z coordinate system; (b) Principal stress system ; and (c). Octahedral plane. (After Johnson and Bailey, 2002).

The stress components at a point can vary depending on the orientation of the coordinate system chosen. The cartesian coordinate system in x, y, and z axes (Fig. 2.2a) can be reoriented into a new orthogonal plane called the principal stress plane on which there are no shear stresses (Fig. 2.2b). The stresses in the principal stress plane are called the major principal stress (σ_1), intermediate principal stress (σ_2) and minor principal stress (σ_3). In a cylindrical stress state, $\sigma_2 = \sigma_3$ and are both minor principal stresses. The coordinate system reorientation and symmetric properties of stress variables also apply to the strain variables (Table 2.1). Another important property of tensors is the existence of invariants, which are functions of the stress and strain components. Invariants are independent of the coordinate systems. Table 2.2 shows stress and strain invariants and their relationships.

Table 2.1 Stress and strain tensors for the different coordinate systems.

Systems	Stress tensor	Strain tensor
General coordinates	$[\sigma]=\begin{pmatrix}\sigma_{xx} & \tau_{xy} & \tau_{xz}\\ \tau_{yx} & \sigma_{yy} & \tau_{yz}\\ \tau_{zx} & \tau_{zy} & \sigma_{zz}\end{pmatrix}$	$[\varepsilon]=\begin{pmatrix}\varepsilon_{xx} & \varepsilon_{xy} & \varepsilon_{xz}\\ \varepsilon_{yx} & \varepsilon_{yy} & \varepsilon_{yz}\\ \varepsilon_{zx} & \varepsilon_{zy} & \varepsilon_{zz}\end{pmatrix}$
Symmetric property	$[\sigma]=\begin{pmatrix}\sigma_{xx} & \tau_{xy} & \tau_{xz}\\ & \sigma_{yy} & \tau_{yz}\\ & & \sigma_{zz}\end{pmatrix}$	$[\varepsilon]=\begin{pmatrix}\varepsilon_{xx} & \varepsilon_{xy} & \varepsilon_{xz}\\ & \varepsilon_{yy} & \varepsilon_{yz}\\ & & \varepsilon_{zz}\end{pmatrix}$
Principal state plane	$[\sigma]=\begin{pmatrix}\sigma_1 & 0 & 0\\ 0 & \sigma_2 & 0\\ 0 & 0 & \sigma_3\end{pmatrix}$	$[\varepsilon]=\begin{pmatrix}\varepsilon_1 & 0 & 0\\ 0 & \varepsilon_2 & 0\\ 0 & 0 & \varepsilon_3\end{pmatrix}$

Constitutive Relationship in Soil Modeling

The stress and strain relationships for a material under loading can be established using constitutive equations. Engineering standard tests such as triaxial testing can be used to uniquely define the stress and strain relationships in the constitutive equation. The constitutive relationships depend on many factors including homogeneity, isotropy, material continuity and reaction to various loading conditions (Chen and Mizuno, 1990). Loading in agricultural practices can vary depending on duration, rate and magnitude of loading, and loading paths (Koolen and Kuiper, 1983 and Wulfsohn and Adams, 2002). In production agriculture and forestry, the main force systems can be categorized into load bearing and soil loosening (Gill and Vanden Berg, 1968 and Koolen and Kuiper, 1983). Gill and Vanden Berg (1968) prepared a handbook on soil dynamics in tillage and traction that explained the engineering mechanics of soil-tillage tools and soil-traction systems. Agricultural soils are heterogeneous, as they vary in soil moisture content, bulk density, soil structure, mineral compositions and layering. Gill (1968) and Koolen and Kuiper (1983) described soil deformation modes that could occur in soil-tool-

machinery interactions as: soil compaction (change in volume); soil distortion at constant volume (plastic flow); distortion combined with compaction; expansion (dilation) that could occur with shear failure and tensile failure; and cutting. The soil deformation types vary depending on the soil moisture contents, bulk density and loading. Wet and deformable soils (e.g. high clay content soils) may exhibit deformation at constant volume. Relatively dry soils under high lateral to axial stress ratio, distortion combined with compaction predominates the soil deformation. In dense soils (e.g. high sand content soils) and soils with relatively low lateral to axial stress ratios, failure planes with dilation could occur.

Table 2.2. The stress and strain invariants for general coordinate and octahedral systems.

System	Stress invariants	Strain invariants
Invariants of normal stresses	$I_{1\sigma} = \sigma_1 + \sigma_2 + \sigma_3$ $I_{2\sigma} = \sigma_x\sigma_y + \sigma_x\sigma_z + \sigma_y\sigma_z - \tau^2_{xy} - \tau^2_{xz} - \tau^2_{yz}$ $= \sigma_1\sigma_2 + \sigma_1\sigma_3 + \sigma_2\sigma_3$ $I_{3\sigma} = \sigma_x\sigma_y\sigma_z + 2\tau_{xy}\tau_{xz}\tau_{yz} - \sigma_x\tau^2_{yz} - \sigma_y\tau^2_{xz} - \sigma_z\tau^2_{xy}$ $= \sigma_1\sigma_2\sigma_3$	$I_{1\varepsilon} = \varepsilon_1 + \varepsilon_2 + \varepsilon_3 = \varepsilon_v$ $I_{2\varepsilon} = -(\varepsilon_x\varepsilon_y + \varepsilon_x\varepsilon_z + \varepsilon_y\varepsilon_z)$ $I_{3\varepsilon} = \varepsilon_x\varepsilon_y\varepsilon_z$
Invariants of deviatoric or shear stress	$J_1 = \sigma_1 + \sigma_2 + \sigma_3 = I_{1\sigma}$ $J_2 = \frac{1}{6}\sqrt{(\sigma_x - \sigma_y)^2 + (\sigma_y - \sigma_z)^2 + (\sigma_x - \sigma_z)^2} + \tau^2_{xy} + \tau^2_{yz} + \tau^2_{xz}$ $= \frac{1}{6}\sqrt{(\sigma_1 - \sigma_2)^2 + (\sigma_2 - \sigma_3)^2 + (\sigma_3 - \sigma_1)^2}$ $= \sqrt{\frac{2}{9}(I^2_{1\sigma} - 3I_{2\sigma})}$	$I_1 = I_{1\varepsilon}$
Octahedral plane	$\sigma_{oct} = \frac{1}{3}(\sigma_1 + \sigma_2 + \sigma_3) = \frac{1}{3}I_{1\sigma}$ $\tau_{oct} = \frac{1}{3}\sqrt{(\sigma_1 - \sigma_2)^2 + (\sigma_2 - \sigma_3)^2 + (\sigma_3 - \sigma_1)^2}$ $= \sqrt{\frac{2}{9}(I^2_{1\sigma} - 3I_{2\sigma})}$	$\varepsilon_{oct} = \frac{1}{3}(\varepsilon_1 + \varepsilon_2 + \varepsilon_3) = \frac{1}{3}I_{1\varepsilon}$ $\gamma_{oct} = \frac{2}{3}\sqrt{(\varepsilon_1 - \varepsilon_2)^2 + (\varepsilon_2 - \varepsilon_3)^2 + (\varepsilon_3 - \varepsilon_1)^2}$

(After Koolen and Kuiper, 1983 and Wulfsohn and Adams, 2002).

Constitutive modeling of soil behavior under general loading and field soil conditions could be complicated. In modeling soil constitutive relationships, idealization of the soil material

behavior and assumptions of continuum mechanics are essential. For stress and strain analysis, soil is assumed to be a continuum material even though it is a multiphase material with inter-and intra-soil pores. Continuum mechanics based stress and strain analysis has solved numerous engineering problems using the finite element method (Upadhyaya, 2002). Idealization of soil material for the development of a constitutive relationship should reflect the important characteristics of the experimental data or soil failures related to the simulated engineering problem.

Soil deformation contains elastic (recoverable) and plastic (irrecoverable) strains upon loading and unloading paths. Elastic strains account for small fractions of the total soil deformation (Koolen and Kuiper, 1983 and Shen and Kushwaha, 1998). The reversible behavior of elastic strains upon removal of loading could be of linear or non-linear forms (Chen and Mizuno, 1990). The simplest form of linear-elastic constitutive relationship for an isotropic soil material that incorporates the volumetric and distortional (shape change) effects is shown in equation 2.4 (Wulfsohn, 2002).

$$\begin{Bmatrix} \varepsilon_v^e \\ \varepsilon_s^e \end{Bmatrix} = \begin{bmatrix} 1/K & 0 \\ 0 & 1/G \end{bmatrix} \begin{Bmatrix} p \\ q \end{Bmatrix} \qquad 2.4$$

Where: $K = \frac{E}{3(1-2\nu)}$ is bulk modulus; $G = \frac{E}{2(1+\nu)}$ is shear modulus; P = $\sigma_{oct} = \frac{1}{3}(\sigma_1 + \sigma_2 + \sigma_3)$ is octahedral normal stress and q = $(\sigma_1 - \sigma_3)$ is deviatoric stress.

Non-linear elastic models could be of bi-linear, multi-linear and hyperbolic forms and the material parameters (bulk modulus (K) and shear modulus (G)) are not constant but depend on stress and/or strain invariants (Chen and Mizuno, 1990 and Shen and Kushwaha, 1998). Soil behaviors under loading are generally considered having non-linear elastic-plastic properties

with geometric non-linearity (large strain deformation) (Upadhyaya, 2002). A review on deformation or flow theory of plasticity that can be used to model the plastic behaviors of the stress and strain relationships is given in Chen and Mizuno (1990). Formulation of plastic theories requires the definition of yield criteria that mathematically defines the stress conditions under which plastic deformation occurs. Yielding in soils define the onset of plasticity or the point at which elastic behavior ceases. Gill and VandenBerg (1968) and Koolen (1994) noted yielding in soil could be of compression; shear failure (change in shape and volume); or plastic flow (shearing with out change in volume). A yield criterion, *f*, is a function of stress and could be defined as:

$$f\left(\sigma_{ij},k\right)=0 \qquad 2.5$$

The yield criterion assumes that the plastic strain occurs when the stress states (σ_{ij}) reach a critical value, *k,* which could be a constant value for a perfectly plastic material or a variable for work hardening or softening materials (Chen and Mizuno,1990 and Wulfsohn, 2002). Soil behavior under wheels often exhibits work hardening as the soil becomes stronger by compaction (Koolen, 1994). The yield surface may change in size and shape as soil behavior attains work hardening (Koolen and Kuiper, 1983 and Wulfsohn, 2002).

Numerous yield criteria have been proposed for constitutive soil models that are generally defined when a maximum stress state (e.g. shear stress) or maximum strain energy reaches a critical value (Chen and Mizuno, 1990 and Shen and Kushwaha, 1998). The Mohr-Coulomb failure criterion, Drucker-Prager's yield criterion, and Cam-Clay yield criteria (Table 2.3) have important applications in soil mechanics (Atkinso and Bransby, 1978; Chen and Mizuno, 1990 and Wood, 1990). Chen and Mizuno (1990) provided the developments of each

criterion, advantages and disadvantages of them. The bases for yield criteria definitions for soils were the Tresca's and von Misses yield criteria, which were originally developed for metals.

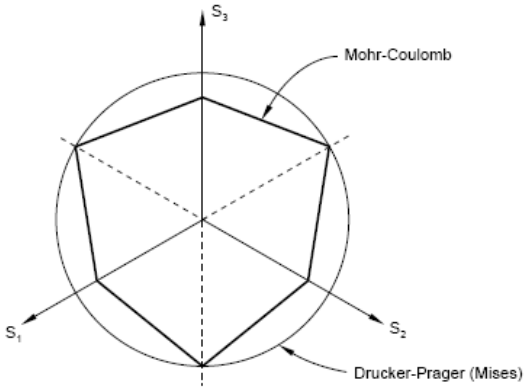

Figure 2.3. Yield surfaces in deviatoric plane; (After Shoop, 2001 and ABAQUS, 2004).

The model parameters of the constitutive models are defined in the pressure-deviatoric plane (p-q plane) and/or the pressure-volume plane (v-p or v-ln p plane). The Drucker-Prager, and Mohr-Coulomb yield surfaces in deviator plane as shown in figure 2.3 (Shoop, 2001 and ABAQUS, 2004). The volume parameter could be defined using bulk density, void ratios, bulk weight volume (1/bulk density) or natural volumetric strain (Koolen and Kuiper, 1983; Bailey and Johnson, 1989 and Wood, 1990).

Table 2.3. Yield criteria soil constitutive models.

Yield criterion	Yield equation	Description
Mohr-Coulomb	$f(\sigma_{ij}) = \sigma_1 - \sigma_3 - [\sin\phi(\sigma_1 - \sigma_3) + 2c\cos\phi]; k_o = 0$	Simple frictional model; based on Mohr-Coulomb law ($\tau = c + \sigma\tan\phi$); hexagonal pyramid surface on hydrostatic axis; and corner of the surface complicates in finite element analysis
Drucker-Prager	$f(\sigma_{ij}) = \alpha I_1 + \sqrt{J_2} = k$	Constants α and k may be related to Coulomb's material constants c and phi; this is *extended von Mises criterion*
Cam-Clay	$f(\sigma_{ij}) = \frac{q}{p\ln(p_c / p)}; k = M$	Based on critical state soil and can be separated into three components: critical state line (CSL) q=Mp; normal consolidation line (NCL) q=0, $V = N - \lambda \ln p$ and unloading-reloading line (URL) $V = V_k - \kappa \ln p$

Several soil behavioral models have been developed to predict the effects of force systems from surface loads, tires and soil engaging tools on the bases of yield criteria in Table 2.3 and pseudo-analytic theories such as Bousinnesq and Froehlich (Söhne, 1958; Raper and Erbach, 1990; Gupta and Raper, 1994; Markauskas et al., 2002; Chrioux et al., 2005 and Foster et al., 2005). The Drucker-Prager criterion based constitutive modeling was used in finite element analysis for solving various soil-tool interaction problems (Fielke, 1999; Mouazen and Ramon, 2002 and Upadhyaya et al., 2002). Drucker-Prager yield criterion is a modified form of the well-known Mohr Coulomb criterion that simplifies the mathematical formulation of the yield function (Chen and Mizuno, 1990). In the meridional plane (p vs q), the shape of the yield surface of Drucker-Prager can have a linear form, hyperbolic form, and a general exponent form (ABAQUS, 2004). The linear Drucker-Prager form (Fig. 1), which is the only available one in ABAQUS/Explicit (ABAQUS, 2004) is intended for applications where compressive stresses are

dominant. The linear yield criterion (*F*) (Chen and Mizuno, 1990 and ABAQUS, 2004) is written as;

$$F = t - p\tan(\beta) - d = 0 \qquad 2.6$$

Where $t = \frac{1}{2}q\left[1 + \frac{1}{k} - \left(1 - \frac{1}{k}\right)\left(\frac{r}{q}\right)^3\right]$; β = slope of the linear yield surface in p-t stress plane which is also referred as angle of friction of the material; *d* = cohesion of the material; and *k* = ratio of the yield surface in triaxial tension to the yield stress in triaxial compression. *p* and *q* are the normal and deviator stresses, respectively. For *k* =1, *t*=*q*;

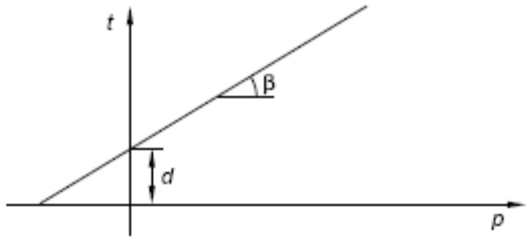

Figure 1. Linear Drucker Prager Yield Criterion: F= t-p tan β - d=0 in the p-t plane.

Bailey et al. (1986) developed a non-linear elastic model to predict natural volumetric strains of unsaturated agricultural soils under hydrostatic stress. Bailey and Johnson (1989) modified the hydrostatic stress compaction model by Bailey et al. (1986) to include soil behaviors under compressive normal and shearing stresses. The model which is also called National Soil Dynamics Laboratory-Auburn University (NSDL-AU) soil compaction model was developed from triaxial tests on four different soil types, each at a specific soil moisture contents. The details on the NSDL-AU model parameters and their descriptions are available in the later chapter on finite element modeling. The three dimensional yield diagrams of NSDL-AU are related to the Critical State Soil Mechanics theory and its parameters are compared with the

modified Cam-clay model (Bailey and Johnson, 1996). Raper and Erbach (1990) developed a finite element program that used the hydrostatic stress and natural volumetric strain NSDL-AU model to predict soil stresses under flat plate and spherical disc loads. Their finite element predicted soil stresses were fairly similar to the stresses measured by soil Stress State Transducers (SST) that were placed within the soil profile. Raper et al. (1994) reported improvements in the finite element predictions of soil stresses when they used the modified NSDL-AU soil constitutive model which accounted both the normal and shearing stresses. Numerous models of soil compaction due to traffic have been evaluated by Defossez and Richard (2002).

Further details on soil deformation-load related soil physical properties, measurement methods and soil-plant dynamics are available in ASAE monographs "Compaction of Agricultural Soils" (Barnes et al., 1971) and "Advances in Soil Dynamics-volume 1" (Upadhyaya et al., 1994).

SOIL BEHAVIOR MODELING DUE TO CONE PENETRATION

Soil behavior under cone penetration involves a combination of cutting, compression, shear or plastic failures, or any combination of these (Gill, 1968). Various approaches (Farrell and Greacen, 1965; Rohani and Baladi, 1981; Tollner and Verma, 1984; Tollner et al., 1987; Yu and Mitchel, 1998) have been considered to study the soil responses in cone penetration including (1) bearing capacity theory; (2) cavity expansion theory; (3) steady state deformation; (4) finite element (FE) analysis; and (5) laboratory experimental methods. Most of these approaches used analytical methods whereby a shape of soil failure surface was assumed and then limit equilibrium of forces over the soil-tool system was solved. Analytical approaches have limitations to explain soil dynamic responses in cone penetration, in particular in layered and

heterogeneous soil conditions because of the difficulty in pre-defining the soil failure shape and complexity of force equilibrium analysis (Shen and Kushwaha, 1998). Tollner et al. (1987) have conducted experiments in plastic chambers to study soil responses to cone penetration from lubricated and non-lubricated cone penetrometers using X-ray computer tomography (CT). With the availability of powerful machines with high computational speeds and FE codes that contain advanced material models, the FE method can be implemented in solving the soil cone penetration problem (Markauskas et al., 2002; Huang, 2004; Foster et al., 2005; Chrioux et al., 2005). In modeling cone penetration using the finite element method, availability of soil constitutive models that account for soil behaviors that occur in cone penetration and meshing techniques for the soil and cone contact problems have to be selected and developed for the simulation to be successful. These important properties of modeling cone penetration in heterogeneous soil conditions and layering have been investigated in this work.

SOIL STRENGTH SPATIAL VARIABILITY

Cone penetrometers have been used in numerous applications in crop production systems, including comparing tillage implements, comparing conservation and conventional cropping systems effect on soil compaction, simulation of root penetration and prediction of the root restriction layers for subsoiling operations. Being a point measurement, the sampling designs and interpolations of point cone penetrometer measurements for field or landscape level requires an understanding of the spatial continuity of soil strength (cone penetration resistance). As a result of the influences of soil forming factors (climate, vegetation, geologic parent materials, topography and time) and management practices, soil properties exhibit inherent spatial variability within fields, across landscapes and on a regional scale (Mulla and McBratney, 1999). Many soil properties exhibit spatial dependence that spatially less separated variables are more

similar than the far apart pairs. Geostatistical technique appropriately describes spatial variability analysis better than classical statistical methods, which assume random distribution of residuals and spatial independence of variables. Analysis and modeling of spatial variability involves estimation of semivariances, fitting theoretical variogram models and kriging for spatial interpolations (Isaaks and Srivastava, 1989; Mulla and McBratney, 1999 and Donald and Ole, 2003).

Spatial variances are quantified by estimating the semivariances according to equation 2.6 (Isaaks and Srivastava, 1989).

$$\gamma(h) = \frac{1}{2N(h)} \left\{ \sum_{i=1}^{N(h)} [Z(x_i + h) - Z(x_i)]^2 \right\} \qquad 2.6$$

Where $\gamma(h)$ is the semivariance for interval class h, N(h) is the number of pairs separated by lag distance, $Z(x_i)$ is a measured variable at spatial location x_i, $Z(x_i + h)$ is a measured variable at spatial location $x_i + h$. The semivariogram models are used to define the distribution of semivariances. The spatial structure ($\gamma(h) = C_o + C$) of a semivariogram can be described by three basic parameters: *nugget effect* (C_o), *sill* ($C_o + C$), and *range*. The *nugget effect* is the variation due to sampling errors, micro-scale variability, and/or measurement errors and occurs at a scale finer than the sampling interval. The *sill* is the asymptote of the semivariogram model. The *range* is a separation distance at which the semivariogram levels off at the sill and it indicates the distance over which the pairs of values of the variable are spatially dependent. The best theoretical semivariogram models are fitted to the estimated semivariances distribution using non-linear fitting techniques. Theoretical models such as spherical, exponential, Gaussian, linear, or power

could be considered in model fitting. The best-fitted semivariogram model is then used in creating a weighting matrix of the kriging procedure for interpolations.

Precise topographic mapping of the soil hardpan attributes is important for the success of variable depth tillage. Field positioning of the sampling points could be acquired using Global Positioning System (GPS). GPS is a worldwide radio-navigation system capable of determining positions (latitude and longitude) on the earth's surface. The system consists of 24 GPS satellites and multiple ground stations for microwave electromagnetic signal receiving and error corrections (Jan van Sickle, 2001). The positional accuracies of GPS can be improved by selecting the appropriate GPS ground receivers. Differential GPS (DGPS) and Real-Time Kinematic (RTK) systems that have single and double frequency receivers, respectively, have good accuracy. The RTK Trimble AgGPS® 214 receiver gives accuracy to a centimeter level and is widely used in precision agriculture applications.

CURRENT APPLICATIONS OF CONE INDEX MEASUREMENTS

The cone penetrometer has been modified for precision tillage by incorporating GPS and improving data acquisition (Clark, 1999 and Raper et al., 1999). Raper et al. (1999) developed a tractor mounted multiple–probe–soil-cone-penetrometer (MPSCP) that has five probes and the capability of rapidly obtaining high-density cone index readings. The device still offers an easy and economical method of soil compaction evaluation. Cone index has also a good relationship with the fundamental soil strength properties (cohesion and angle of friction) (Rohani and Baladi, 1981). Research also showed that soil penetration resistance is a good indicator of root impedance (Taylor and Gardner, 1963). Precision farming has further promoted the use of the cone penetrometer in evaluating the potential of real-time soil compaction measurement systems.

The main constraints of the cone penetrometer as a tool in precision tillage could be the influence of its readings by soil factors, mainly soil moisture and bulk density, and the difficulty in data interpretation especially in layered soils characterized by varying soil moisture contents and soil strength profiles. Researchers (ASAE 1999b, Schuler et al., 2000 and Soil quality – Agronomic Technical Note No. 17, 2003) have recommended that (1) Measurement of soil cone penetration should be taken under wet soil conditions; (2) Depth to peak (maximum) cone index or critical cone index value (2 MPa) characterizes the hardpan layers; (3) Compacted layers or hardpan location as predicted from cone index-depth data is generally not affected by soil moisture content variations and (4) Tillage depth should be set 3 cm below the predicted depth of the layer. Detection of the hardpan is done by evaluating the cone index vs. depth profile. Interpretation of soil cone index-depth data is difficult due to layering, compactibility of soils, soil conditions and soil-tool interactions (Farell and Greacen, 1966; Gill, 1968; Gill and VandenBerg, 1968; Sanglerat, 1972; Mulqueen et al., 1977 and Lunne at al., 1997). Gill (1968) and Mulqueen et al. (1977) showed that formation of a soil wedge in front of the cone could erroneously increase the soil penetration resistance. ASAE (1999b) recommends soil cone penetrometer measurements be taken at soil moisture content near field capacity to minimize the effect of varying soil moisture on the cone index data. The difficulty to discern single soil moisture content in layered soils, spatio-temporal soil moisture variability and appropriate sampling time could make cone index sampling at soil moisture near field capacity very difficult. In precision tillage, accurate soil hardpan detection is important because errors of a few centimeters could cause variations in precision tillage depth recommendations. Real-time soil strength sensing methods are intended to detect hardpan at soil moisture conditions similar to the tillage operation, which often is expected under dry soil moisture conditions for maximum

performance (Al-Adawi and Reeder, 1996 and Raper and Sharma, 2004). Appropriate evaluation of real-time (on-the-go) soil strength sensing methods with the cone index measurement in predicting soil hardpan would require study of the influences of soil moisture and layering on soil cone penetration resistance.

REFERENCES

Al-Adawi and Reeder, 1996. Al- Adawi, S. S. and R. C. Reeder. 1996. Compaction and sub-soiling effects on corn and soybean yields and soil physical properties. *Trans. ASAE* 39 (5): 1641-1649.

Andrade, P., U. A. Rosa, S. K. Upadhyaya, B. M. Jenkins, J. Aguera, and M.Josiah. 2004. Field evaluation of the improved version of the UC Davis compaction profile sensor. ASAE Paper No. 01-1037. St. Joseph, Mich.: ASAE.

ASAE Standards, 46 Ed. 1999a. S313.3. Soil cone penetrometer. St. Joseph, Mich.: ASAE.

ASAE Standards, 46 Ed. 1999b. EP542. Procedures for using and reporting data obtained with the soil cone penetrometer. St. Joseph, Mich.: ASAE.

Atkinson, J.H. and Bransby, P.L. 1978. The mechanics of soils: An introduction to critical soil mechanics. McGraw Hill, London.

Barnes, K.K., W.M. Carleton, H.M. Taylor, R.I., Throchmorton and G.E. Vanden Berg. 1971. Compaction of Agricultural Soils. ASAE monograph no. 1, St. Joseph, MI. 126-153.

Bailey, A.C., C.E. Johnson, and R.L. Schafer. 1986. A model for agricultural soil compaction. *J. Agric. Eng. Res.* 33:257-262.

Bailey, A.C. and C.E. Johnson. 1996. Soil critical state behavior in the NSDL-AU model. ASAE Paper 96-1064. St. Joseph, Mich.: ASAE.

Bailey, A.C. and C.E. Johnson. 1996. A soil compaction model for cylindrical stress states. *Trans. ASAE* 32(3): 822-825.

Beer F.P., E.R. Johnson and J.T. DeWolf. 2005. Mechanics of materials. 3rd ed. McGraw Hill, London.

Busscher, W.J., P.J. Bauer and J.R. Frederick. 2006. Deep tillage management for high strength southeastern USA Coastal Plain Soils. *Soil Till. Res.* 85:178-185.

Busscher, W.J. and P.J. Bauer. 2003. Soil strength, cotton root growth and lint yield in a southeastern USA coastal loamy sand. *Soil Till. Res.* 74:151-159.

Busscher, W.J., P. J. Bauer, and J.R. Fredercik. 2002. Recompaction of a coastal loamy sand after deep tillage as a function of subsequent cumulative rainfall. *Soil Till. Res.* 68: 49-57.

Camp, Jr. C. R. and Z. F. Lund. 1968. Effect of mechanical impendence on cotton root growth. *Trans. ASAE*: 189-190.

Campbell, R.B., D.C. Reicosky and C.W. Doty. Physical properties and tillage of Paleudults in the southeastern Coastal Plains. *J. Soil and Water Conservation.* 29(4):220-224.

Chen, W.F. and E. Mizuno. 1990. Non-linear Analysis in soil mechanics: Theory and Implementation. Developments in geotechnical engineering vol. 53. Elsevier Science Publishing Company Inc. 655 Avenu of the Americas, New York, NY 10010, U.S.A.

Chiroux, R.C., W.A. Foster Jr., C.E. Johnson, S.A. Shoop and R.L. Raper. 2005. Three-dimensional finite element analysis of soil interaction with rigid wheel. *Applied Mathematics and Computation*. 162:707-722.

Clark, R. L. 1999. Evaluation of the potential to develop soil strength maps using a cone penetrometer. ASAE Paper No. 993109. St. Joseph, Mich.: ASAE.

Coduto, D.P. 1999. Geotechnical engineering principles and practices. Prentice-Hall, Inc. Upper Saddle River, New Jersey.

Da silva, A. P., S. Imhoff and M. Corsi. 2003. Evaluation of soil compaction in an irrigated short-duration grazing system. *Soil Till. Res.* 70:83-90.

Defossez, P. and G. Richard. 2002. Models of soil compaction due to traffic and their evaluation. *Soil Till. Res.* 67: 41-64.

DeRoockm B, and A.W. Cooper. 1967. Relation between propagation velocity of mechanics waves through soil and soil strength. *Trans. ASAE* 10 (4): 471-474.

Donald R.N. and Ole, W. 2003. Spatial and temporal statistics. Sampling field soils and their vegetation. Catena Verlag GMBH, 35447 Reiskirchen, Germany.

Farell, D.A. and E.L. Greacen. 1966. Resistance to penetration on fine probes in compressible soil. *Australian Journal of Soil Res.* 4:1-17.

Fielke, J.M. 1999. Finite element modeling of the interactions of cutting edge of tillage implements with soil. *J. Agric. Engg. Res.* 74: 91-101.

Foster,Jr. W.A., C.E. Johnson, R.C. Chiroux and T.R. Way. 2005. Finite Element Simulation of Cone Penetration. *Applied Mathematics and Computation.* 162: 735-749.

Fulton, J. P., L. G. Wells, S. A. Shearer, and R. I. Barnhisel. 1996. Spatial variation of soil physical properties: a precursor to precision tillage. ASAE Paper No. 96-1002. St. Joseph, Mich.: ASAE.

Gill, W.R. 1968. Influence of compaction hardening of soil on penetration resistance. *Trans. ASAE* 11(6): 741-745.

Gill, W.R. and G.E. VandenBerg. 1968. Soil dynamics in tillage and traction. Agriculture Handbook No. 316. USDA-Agricultural Research Service, Washington. D.C.

Goodson, R., R. Letlow, D.Rester, and J. Stevens. Use of precision agriculture technology to evaluate soil compaction. 23 rd Annual Southern Conservation Tillage Conference for Sustainable Agriculture, Monroe, Louisiana, June 19-21, 2000.

Gorucu, S., A. Khalilian, Y.J. Han, R.B. Dodd, F.J. Wolak, and M. Keskin. 2001. Variable depth tillage based on geo-referenced soil compaction data in Coastal Plain region of South Carolina. ASAE Paper No. 011016. St. Joseph, Mich.: ASAE.

Gupta, S.C., R.L. Raper. 1994. Prediction of soil compaction under vehicle. In: Soane, B.D., van Ouwerkerk, C. (Eds.), Soil Compaction in Crop Production, Development in Agricultural Engineering, Vol. 11. Elsevier, Amesterdam, pp. 53-71.

Hall, H.E., R.L. Raper, T.E. Grift, and D.W. Reeves. 2000. Development of an on-the-fly mechanical impedance sensor and evaluation in a coastal plains soil. Proceedings of the 15th ISTRO Conference, Ft. Worth, TX.

Hamza, M.A. and W.K. Anderson. 2005. Soil compaction in cropping systems a review of the nature, causes and possible solutions. *Soil Till. Res.* 82:121-145.

Hermann Auernhammer. 2001. Precision farming-the environmental challenge. *Computers and electronics in agriculture.* 30: 31-43.

Hillel, D. 1998. Environmental soil physics. Academic Press, a division of Harcourt Brace and Company, San Diego, CA, USA.

Huang, W., D. Sheng, S.W. Sloan and H.S. Yu. 2004. Finite element analysis of cone penetration in cohesionless soil. *Computers and Geotechnics.* 31(7):517-528.

Isaaks, E.H. and R.M. Srivastava. 1989. An introduction to applied geostatistics. Oxford University Press, Inc. New York, New York.

Jones, R.J.A., G. Spoor and A.J. Thomasson. 2003. Vulnerability of subsoils in Europe to compaction: a preliminary analysis. *Soil Till. Res.* 73:131-143.

Kenan, K., E. Ozgoz, and F. Akbas. 2003. Assessment of spatial variability in penetration resistance as related to some soil physical properties of two fluvents in Turkey. *Soil Till. Res.* 76:1-11.

Khalilian, A. and R. R. Hallman. 1996. Energy requirements of conservation tillage tools in Coastal Plain soils. 1996 Proceedings, 19th Annual Southern Conservation Tillage Conference for Sustainable Agriculture, Jackson, TN, July 23-25, 1996.

Khalilian,A., Y.J. Han, R.B. Dodd, M.J. Sullivan, S. Gorucu, and M. Keskin.2002. A control system for variable depth tillage. ASAE Paper No. 02-1209. St. Joseph, Mich.: ASAE.

Kitchen, N.R., K.A. Sudduth, D.B. Myers, S.T. Drummond, and S.Y. Hong. Delineating productivity zones on claypan soil fields using apparent soil electrical conductivity. *Computers and Electronics in Agriculture* 46: 285–308.

Koolen, A.J. and H. Kuipers. 1983. Agricultural soil mechanics. Advanced series in agricultural sciences 13. Springer-Verlan Berlin Heidelberg, Germany.

Lui, W., L. D. Gaultney, and M. T. Morgan. 1993. Soil texture detection using acoustic methods. ASAE Paper No. 931015. St. Joseph, Mich.: ASAE.

Lunne, T., P.K. Robertson, and J.J.M. Powell. 1997. Cone penetration testing in geotechnical practices. Blackie academic and professional, London, UK.

Markauskas, D. , R. Kacianauskas, M. Suksta. 2002. Modeling the cone penetration test by the finite element method. *Foundation of Civil and Environmental Engineering*. No. 2. Poznan University of Technology,Poznan, Poland.

Mouazen, A. M. and M. Neményi. 1999. Finite element analysis of subsoiler cutting in non-homogeneous sandy loam soil. *Soil Till. Res.* 51(1-2): 1-15.

Mulla, D.J. and A.B. McBratney. 1999. Soil spatial variability. In: Hand book of soil science. M.E. Summer. Editor-in Chief. CRC Press LLC, 2000 N.W. Corporate Blvd., Boca Raton, Florida. U.S.A.

Mulqueen, J., J.KV. Stafford and D.W. Tanner. 1977. Evaluation of penetrometers for measuring soil strength. *Journal of Terramechanics* 14(3):137-151.

Naiqian, Z.,W. Maohua, and W. Ning.2000. Precision agriculture- a worldwide review. ICETS Session 6: *Technology Innovation and Sustainable Agriculture*: 112-122.

Oelze, M. L., W. D. O'Brien, and R. J. Darmody. 2002. Measurement of attenuation and speed of sound in soils. *SSSA J.* 66(3): 788-796.

Oelze, M. L., J. M. Sabatier, and R. Raspet. 2003. Roughness measurements of soil surfaces by acoustic backscatter. *SSSA. J.* 67(1): 241-250.

Perumpral, J.V. 1987. Cone penetrometer applications-A review. *Trans. ASAE* 30(4):939-944.

Radcliffe, D.E., G. Manor, R.L. Clark, L.T. Langdale, and R.R. Bruce. 1989. Effect of traffic and in-row chiseling on mechanical impedance. *Soil Sci. Soc. Am. J.* 53:1197-1201.

Radcliffe, D. E., E. W. Tollner, W. L. Hargrove, R. L. Clark, and M. H. Golabi. 1988. Effect of tillage practices on soil strength and infiltration of a Southern Piedmont soil after ten years. *Soil Sci. Soc.Am J.* 52:789-804.

Rains, G.C., D.L. Thomas, and G. Vellidis. Soil sampling issues for precision management of crop production. *App. Eng. Agr.* 17(6): 769-775.

Raper, R.L. 2005. Vehicle traffic impacts on soil. *Terramechanics Journal*. 42(3-4):259-280

Raper, R. L., B. H. Washington, J.D. Jarrell. 1999. A Tractor - Mounted – Multiple Probe - Soil Cone - Penetrometer. *App. Eng. Agr.* 15(4): 287-290.

Raper, R.L., C.E. Johnson and A.C. Bailey. 1994. Coupling normal and shearing stresses to use in finite-element analysis of soil compaction. *Trans. ASAE* 37(5):1417-1422.

Raper, R.L., D.W. Reeves, and C.H. Burmester. 1998. Cotton yield response and energy requirements of matching tillage depths to root-impeding layers. ASAE Paper No. 981112. St. Joseph, MI.: ASAE.

Raper, R.L., D.W. Reeves, and C.H. Burmeste and E.B. Schwab. 2000. Tillage depth, tillage timing and cover crop effects on Cotton yield, soil strength and tillage energy requirements. *App. Eng. Agr.* 16(4): 379-385.

Raper, R.L., and D.W. Reeves. 2004a. Reducing soil compaction with in-row subsoiling and controlled traffic. In: Proceedings of Session IV of the 2004 CIGR International Conference, October 11-14, 2004, Beijing, China.

Raper, R. L., D.W. Reeves, J.N. Shaw, E. van Santen, and P.L. Mask. 2004b. Site-specific subsoiling benefits for coastal plain soils. 26 th Southern Conservation Tillage Conference, Raleigh, NC, June 8-9, 2004.

Raper, R.L. and D.C. Erbach, 1990b. Prediction of soil stresses using the finite element method. *Trans. ASAE,* 33: 725–30.

Raper, R.L., E. B. Schwab, and S.M. Dabney. 2005. Measurement and variation of site-specific hardpans for silty upland soils in the Southeastern United States. *Soil Till. Res.*84:7-17.

Raper, R.L., E. B. Schwab, and S.M. Dabney. 2000. Spatial Variation of the depth of the root-restricting layer in an upland soils of Northern Mississippi. Second International Conference of Geospatial Information in Agriculture and Forestry, Lake Buena Vista, Florida, January 10-12, 2000.

Raper, R.L., L.E. Asmussen, and J.B. Powell. 1990. Sensing hardpan depth with ground penetrating radar. *Trans. ASAE,* 31(1): 41-46.

Raper R. L. and A.K. Sharma. 2004. Soil moisture effects on energy requirements and soil disruption on subsoiling a Coastal Plain soils. *Trans. ASAE,* 47(6): 1899-1905.

Rohani, B. and G. Y. Baladi. 1981. Correlation of mobility cone index with fundamental engineering properties of soil. International Society for Terrain-Vehicle Systems. Vol 3:959-990. Alberta, Canada.

Sanglerat, G. 1972. Interpretation of penetration diagrams- theory and practice. Developments in geotechnical engineering. Elsevier publishing company. Amsterdam, The Netherlands.

Schomberg, H.H., G.H. Langdale, A.J. Franzluebbers, and M.C. Lamb. Comparison of tillage types and frequencies for cotton on Southern Piedmont soil. *Agron. J.* 95:1281-1287.

Schuler, R.T., W.W. Casady, R.L. Raper. 2000. Soil Compaction. In *Conservation Tillage Systems and Management.* MWPS-45 p 70-76.

Shen, J. and R.L. Kushwaha, 1998. Soil–Machine Interaction, A Finite Element Perspective. New York: Marcel Dekker, Inc.

Spivey, L.D., W.L.Busscher, R.B. Campbell. 1986. The effect of texture on strength of southeastern Coastal Plains soils. *Soil Till. Res.* 6:351-363.

Soane, B. D., and C. Van Ouwerkerk. 1994. Soil compaction problems in world agriculture. In *Soil Compaction in Crop Production*, p 1-22. B.D. Soane, and C. Van Ouwerkerk. (Eds.). Amsterdam, The Netherlands, Elsevier.

Soil quality –Agronomic Technical Note No 17. Soil compaction: Detection, prevention and alleviation. 2003. USDA-NRCS Soil Quality Institute. Auburn, AL.

Söhne, W. 1958. Fundamentals of pressure distribution and soil compaction under tractor tyres. Agric. Eng. 39,276-281.

Shoop, S.A. 2001. Finite element modeling of tire-terrain interaction. Technical report ERDC/CRREL TR-01-16.

SSSA. 2001. Internet Glossary of Soil Science Terms: 29 September 2005. Available at: www.soils.org/sssagloss.

Stafford, J.V. and J.G. Hendrick. 1988. Dynamic sensing of soil pans. *Trans. ASAE* 31(1):9-13.

Sudduth, K.A., N.R. Kitchen, and S.T. Drummond. 1998. Soil conductivity sensing on claypan soils: comparison of electromagnetic induction and direct methods. Proceedings of the 4th International Conference on Precision Agriculture. St. Paul. MN.

Taylor, H. M. and Gardner, H. R. 1963. Penetration of cotton seedling taproots as influenced by bulk density, moisture content and strength of soil. *Soil Sci.* 96:153-545.

Tekeste, M. Z., T.E. Grift, and R.L. Raper. 2002. Acoustic compaction layer detection. ASAE Paper No. 021089.St. Joseph, Mich.: ASAE.

Tollner, E. W., R.L. Schafe, and T.K. Hamrita. 2002. Sensors and controllers for primary drivers and soil engaging implements. In *Advances in Soil Dynamics Volume 2*, 179- 224. St. Joseph, Mich.: ASAE.

Tollner, E. W. and B.P. Verma. 1984. Modified cone penetrometer for measuring soil mechanical impedance. *Trans. ASAE*: 331-336.

Tollner E. W., B.P. Verma, and J.M. Cheshire. 1987. Observing soil-tool interactions and soil organics using X-ray computer tomography. *Trans. ASAE* 30 (6): 1605-1610.

Upadhyaya, S.K., U.A. Roasa, and D.Wulfsohn. 2002. Application of the finite element method in agricultural soil mechanics. In *Advances in Soil Dynamics Volume 2*, 117- 147. St. Joseph, Mich.: ASAE.

Upadhyaya, S. K., W. J. Chancellor, J. V. Perumpral, R. L. Schafer, W. R. Gill, and Glen E. VandenBerg (editors). 1994. Advances in Soil Dynamics. Vol. 1. American Society of Agricultural Engineers. 313p.

U.S. Army Corps of Engineers. 1948. Trafficability of soils—Development of testing instruments. Technical memo 3-240, 3d suppl. Vicksburg, MS:U.S. Army Corps of Engineers Waterways Experiment Station.

Voorhees W.B. 1991. Compaction effects on yield-are they significant? *Trans. ASAE* 34(4): 1667-1672.

Wood, M.D. 1990. Soil behavior and critical state soil mechanics. Cambridge University Press: Cambridge.

Wulfsohn, D., and B. A. Adams. 2002. Elastoplastic soil mechanics. In *Advances in Soil Dynamics Volume 2*, 1- 116. St. Joseph, Mich.: ASAE.

Yu, H.S., and J.K. Mitchell, 1998. Analysis of cone resistance: review of methods. *J Geotechnical and Geoenvironmental Engg.* 141 (2): 140-149.

CHAPTER 3

Soil Drying Effects on Soil Cone Penetration Resistance for Norfolk Sandy Loam Soil[1]

[1] Mehari Z. Tekeste, R.L. Raper and E.B. Schwab. To be submitted to the *Transactions of the ASABE*

ABSTRACT: Site-specific detection of a soil hardpan is an important step in precision farming. Different methods have been developed including the ASAE standard soil cone penetrometer to detect the hardpan layer. Most of the newly developed methods use results obtained by a soil cone penetrometer as a reference to validate their potential. Soil factors, mainly soil moisture and bulk density, may influence the cone index measurement and the determination of the relative strength and depth of the hardpan layer. In this study, magnitude and location of soil hardpan were characterized by peak cone index, depth to the peak cone index and depth to the top of the hardpan layer. The effects of soil drying on peak cone index, depth to the peak cone index and depth to the top of the hardpan layer were studied for three compaction levels on a Norfolk Sandy Loam soil in a soil bin. The soil bin was wetted to near saturation and then subjected to four levels of soil drying. A Multiple-Probe-Soil-Cone-Penetrometer (MPSCP) was used to measure soil cone index. The results showed that soil drying had a significant effect on peak cone index for the single pass compaction (1.66 Mg m^{-3}) but not for the double pass compaction (1.76 Mg m^{-3}). A trend existed that showed that the predicted depth to the peak cone index and the top of the hardpan layer decreased with soil drying.

Keywords: Precision tillage, Soil hardpan, Soil drying, Cone index.

INTRODUCTION

In the southeastern USA, Coastal Plains soils typically have a highly compacted subsoil layer commonly called a hardpan that restricts root growth and reduces soil water infiltration (Taylor and Gardner, 1963; Camp and Lund, 1968; and Raper et al, 2000).

Both natural and human induced forces mainly from wheel traffic and tillage cause the hardpan formation. The excessive soil compaction created within the subsoil layer decreases available water to crops, reduces aeration and restricts root growth, and consequently reduces crop yield. The effect is highly pronounced during drought periods when soil moisture reserves in the subsoil layer are inaccessible to roots. Natural processes have limited capability to loosen this root-restricting layer (Bernier et al., 1989). Thus, mechanical subsoiling has been used as an effective practice to disrupt this hardpan layer.

Many farmers apply energy-intensive uniform subsoiling that assumes a uniform depth to soil hardpan. However, the depth to the hardpan layer and its relative strength vary across the field (Clark, 1999; Raper et al., 2000; and Utset and Greco 2001). Site-specific tillage that takes into account the depth variability of the soil hardpan could be the best alternative subsoiling practice. It has also the potential to reduce tillage energy and fuel consumption as compared to uniform depth tillage (Fulton et al., 1996; Raper et al., 1998; and Raper et al., 2004).

Technologies using either stop-and-go or on-the-go soil strength measurement methods have been developed to precisely identify the hardpan layer to assist with the objective of site-specific tillage. A soil cone penetrometer apparatus (ASAE, 1999a) has been used traditionally to assess soil compaction. The results are reported as cone index (penetration force / cone base area) as a function of depth (ASAE, 1999b). The system has been automated and modified to improve the data acquisition rate and evaluated to produce soil strength maps (Clark, 1999;

Raper et al., 1999). Raper et al. (1999) developed a tractor mounted multiple–probe–soil-cone-penetrometer (MPSCP) that is capable of rapidly taking high-density cone index readings with five probes.

Many studies also have reported the potential of on-the-go soil hardpan or soil compaction detection methods (Raper et al., 1990; Lui et al., 1993; Hall et al., 2000; Andrade et al., 2001; and Tekeste et al., 2002). Raper et al. (1990) was able to detect a soil hardpan with ground penetrating radar (GPR) that showed good agreement with cone penetrometer prediction of the hardpan for Norfolk sandy loam and Decatur clay loam soils. The amount and distribution of soil moisture along the profile affected the GPR results. Better results would require uniform soil moisture distribution throughout the soil profile that may not necessarily be obtained under field conditions. Hall et al. (2000) developed an on-the-fly mechanical impedance sensor that measures horizontal soil wedge penetration resistance. They reported similar results between the "wedge index" and cone index with the "wedge index" being less sensitive to soil moisture. Tekeste et al. (2002) studied the potential of an acoustic method to detect the depth of a soil hardpan. Their results showed good agreement with cone penetrometer detection of the soil hardpan layer.

One can observe that the use of a standardized cone penetrometer apparatus and procedures (ASAE, 1999a and ASAE, 1999b) is and will remain to be an important tool in precision tillage technology. The measurement system has been continuously modified for site-specific tillage and offers an easy and economical method of soil compaction evaluation. Besides, most of the on–the-go soil compaction detection methods use measurements obtained by soil cone penetrometer as a reference to validate their potential.

The influences of soil parameters, mainly soil moisture and bulk density, on cone index may affect the use of cone penetrometer in hardpan detection. Many studies have addressed the effect of soil moisture and bulk density on cone index in laboratory and field scale studies (Ayers and Perumpral, 1982; Rajaram and Erbach, 1998; Raper et al., 2000; and Utset and Cid, 2001).

Ayers and Perumpral (1982) studied soil moisture-bulk density-cone index relationships on artificial soils obtained by mixing different quantities of zircon, sand and clay. According to their report, the cone index decreased with increased soil moisture. The effect of bulk density varied with soil moisture such that at low soil moisture, the influence of soil bulk density on cone index was high and at high soil moisture, cone index was less dependent on bulk density.

Clark (1999) investigated the use of a cone penetrometer to map soil strength. The author reported that producing an accurate field soil strength map required large amount of cone index data. He also observed that the relationship between the maximum cone index and soil moisture (0 -15 cm) was contrary to what was normally expected with high cone index values being associated with low soil moisture. It was reported that plots with high maximum cone index had high soil moisture. The author recommended the need for depth-specific soil moisture measurement in determining the relationship between maximum cone index and soil moisture.

Raper et al. (2000) determined the depth of the hardpan and its spatial variability in upland soils of Northern Mississippi, USA. The authors found a good correlation between the depth of hardpan and soil moisture in the depth ranges of 0-15 cm and 0-30 cm for trafficked and non-trafficked soils, respectively. However, the average depth to trafficked hardpan (21 cm) was not within the soil moisture sampling depth range (0-15 cm).

Rajaram and Erbach (1998) studied the effect of drying stress induced by a wetting and drying cycle on soil physical properties of a clay loam soil. It was observed that cone penetration

resistance measured at 50, 100 and 150 mm depths increased with increased drying stress. The study was conducted in a uniform soil density profile.

Further studies on soil moisture-bulk density-cone index related to a stratified soil strength profile would still be needed to enhance the understanding of using cone index measurement as a tool to determine the depth of site-specific hardpan. One major area that needs further studies could be the site-specific soil moisture variations and its effect on the magnitude and relative position of soil hardpan. Measuring soil moisture over short depth increments may provide better understanding on the soil moisture-cone index relationship.

Limited information is available to ascertain whether the predicted depth of the hardpan remained the same or shifted upward or downward due to soil moisture variations. Most of the previous studies emphasized on the relationship between soil moisture and the magnitude of soil hardpan. Different procedures have been developed to predict the magnitude and relative position of the hardpan layer from a cone index profile observed as the cone penetrometer approaches and passes through the hardpan layer. Clark (1999) and Raper et al. (2000) determined the depth to peak cone index as a value for the depth to the hardpan layer. Fulton et al. (1996) used the depth to a critical cone index value (2 MPa) as the site-specific tillage depth. At this critical value plant root growth is severely impeded (Taylor and Gardner, 1963). In this study, it was hypothesized that peak cone index value and its depth, and the depth to the top of the hardpan could fully characterize the hardpan layer.

Thus, the objectives of this study were:

- To investigate the effect of soil drying on peak cone index,
- To investigate the effect of soil drying on the depth to the peak cone index, and
- To investigate the effect of soil drying on the depth to the top of the hardpan.

MATERIALS AND METHODS

SOIL PREPARATION AND EXPERIMENTAL DESIGN

The experiment was conducted in summer 2002 in a Norfolk sandy loam (*Typic Paleudults*) soil bin located at the USDA-ARS National Soil Dynamics Laboratory in Auburn, AL. The soil bin is 7-m wide, 58-m long and 1.5-m deep. The soil consisted of 72 % sand, 17 % silt and 11 % clay (Batchelor, 1984). For the soil hardpan creation, the soil was first wetted to workable soil moisture and then mixed with a rotary tiller so that the soil bin attained uniform soil moisture. By varying the number of passes of a rigid compression wheel, soil hardpan layers with three different soil strength levels were created. Forward and backward movements of the rigid wheel created a single pass compaction level. The single pass procedure was repeated to create the double pass compaction level. No hardpan was installed for the no pass compaction level. The soil surface was leveled using a blade. The entire soil bin was then wetted using a mobile sprinkler vehicle. Wetting was repeated one day later to ensure the soil bin was saturated.

A split plot experimental design with a randomized complete block design (RCBD) at the whole plot level was used to conduct the experiment. The soil bin was divided into four blocks (replicates). Each block consisted of three whole plot experimental units where the three-compaction treatments (No, Single and Double passes) were randomly applied. Each whole plot experimental unit was further divided into four sub-plot experimental units. Within each sub-plot, cone index data were collected at 25Hz sampling rate using a soil bin vehicle mounted multiple-probe-soil-cone-penetrometer (MPSCP) (Raper et al., 1999) at four positions (20 cm apart) to a depth of about 40cm for each of four consecutive days (days 1, 2,

3 and 4). The four measurement days were considered as four levels of the subplot treatment factor (soil moisture). The soil bin was open to the atmosphere for drying. A total of 320 (1 compaction x 4 positions x 5 probes per position x 4 days x 4 replicates) data points were obtained for each compaction treatment.

Core samples for soil moisture determination on a gravimetric basis were taken immediately after cone index measurement at depth ranges of 0-2.5, 2.5-5, 5-7.5, 7.5-10, 10-12.5, and 12.5-15 cm. Soil moisture on a dry basis was determined after oven drying the samples at 105 ^{o}C for 72 hrs. Soil cores using a cylinder of 5 cm inner diameter were collected above and with the hardpan for dry soil bulk density determination.

CONE INDEX DATA ANALYSIS

The digitally obtained cone penetrometer data averaged for each position was analyzed to extract the hardpan parameters, namely peak cone index, the depth to the peak cone index, and the depth to the top of the hardpan layer. The peak cone index value was assumed as the numerically greatest value of cone index in the soil profile. Cone index values at depths deeper than the hardpan were not considered in the analysis as they may have been created by the previous history of the soil in the bin. To determine the depth to the peak cone index and the depth to the top of the hardpan layer, the location of the soil surface was determined by observing the change in cone index as the probes of the penetrometer were moved from air to the soil. A cone index value, the mean cone index for the open-air run plus 5 kPa, was first calculated. The location of the soil surface was assumed as the depth that has this calculated cone index (maximum tolerance of 2 kPa).

The first rapid abrupt changes in cone index data occurred at the interface between loose soil above the hardpan and the hardpan. Thus, the hardpan was assumed to start where

cone index increased rapidly with a minimum change in depth. The depth to the top of the hardpan layer was estimated as the depth where at least three consecutive slope (Δ Depth /Δ Cone Index) values were between 0.0 and 0.01 cm/kPa.

Fig. 1 shows the graphical representation of how the depth to the peak cone index (D_{Peak}) and the depth to the top of the hardpan ($D_{Hardpan}$) were determined.

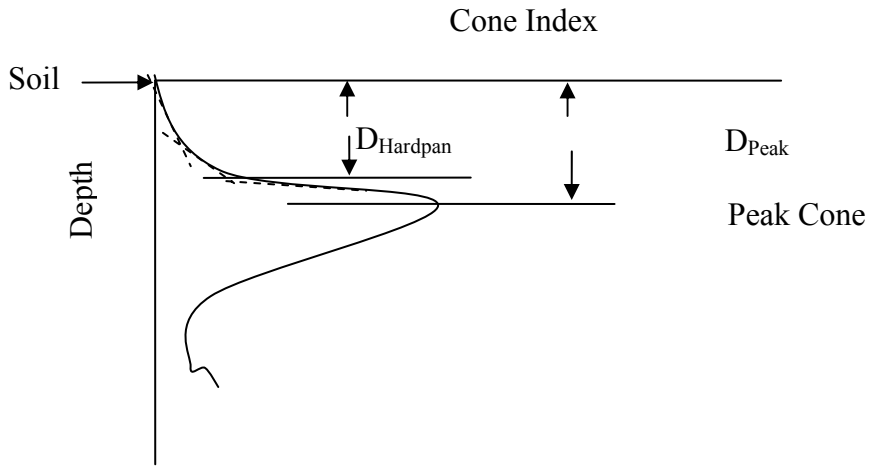

Figure 1. Cone index vs. depth to determine the depth to the peak cone index (D_{Peak}) and the depth to the top of the hardpan layer ($D_{Hardpan}$). The instantaneous slope values are shown as dashed lines.

The effects of the four levels of soil drying and three compaction levels on peak cone index, the depth to the peak cone index and the depth to the top of the hardpan were analyzed using PROCGLM procedure in SAS (SAS. Release 8.02 SAS Institute Inc., Cary, NC, 2001). An F-statistic with an alpha (α) level of 0.05 was used for all statistical comparisons.

Table 1. Soil bulk density (g/cm^3) above and within hardpan for no pass, single pass and double pass compaction for Norfolk sandy loam soil.

Compaction Level	Above Hardpan		Within Hardpan	
	mean -Mg m^{-3}-	S.D. -Mg m^{-3}-	mean -Mg m^{-3}-	S.D. -Mg m^{-3}-
No pass compaction	1.27 (a)	0.03	1.22(c)	0.04
Single pass compaction	1.42 (a)	0.16	1.66(b)	0.02
Double pass compaction	1.42(a)	0.10	1.76(a)	0.03

For above and within hardpan layers, means with the same letter are not significantly different ($LSD_{\alpha=0.05}$).

RESULTS AND DISCUSSION

Within the hardpan, soil bulk density values of the three-compaction treatments were significantly different (Table 1, $P \leq 0.0001$). The single pass and double pass compaction resulted in a 36 % and 44 % increase in soil bulk density as compared to the no pass compaction, respectively. Above the hardpan layer, all compaction levels were not statistically different in soil bulk density.

Soil compaction and depth affected the soil moisture profile distribution which decreased as the sampling days passed for the no pass and single pass compaction treatments (Fig. 2). For the double pass compaction treatment, the average soil moisture throughout the soil profile remained nearly the same after the second sampling day and the variation in depth was insignificant below 5.5 cm. This indicates the highly compacted hardpan layer (1.76 Mg m^{-3}) reduced soil moisture drying.

The magnitude of soil dryness was quantified using soil drying index (Eq. 1) computed by comparing the average soil moisture in each sampling day with the soil moisture of day-1 (wet soil moisture). The soil drying index values were affected both by the number of days passed and the amount of soil compaction. As more days passed, the drying index values increased, except

for the double pass compaction in which the values appeared to vary insignificantly after the second day (Fig. 3).

$$Soil\ Drying\ Index\,(\%) = \left| \frac{Soil\ moisture_{\ day-i} - Soil\ moisture_{\ day-1}}{Soil\ moisture_{\ day-1}} \right| * 100 \qquad (1)$$

Where:

i = day index 1, 2, 3 and 4 that shows the four sampling days.

The effects of soil drying on cone index profile for the three compaction levels are indicated in Fig. 4. Results and discussion would mainly be focused on the hardpan parameters: peak cone index, the depth to the peak cone index, and the depth to the top of the hardpan layers. The effect of soil drying on these parameters were not analyzed for the no pass compaction, as there was no hardpan installed in the no pass experimental units.

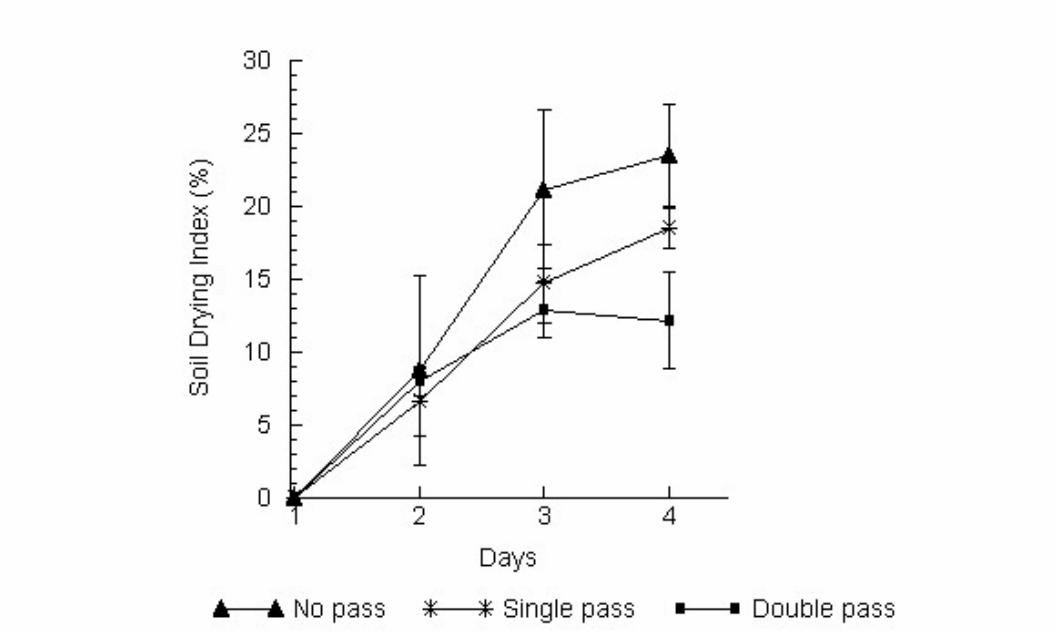

Figure 2. Soil drying index vs. measurement days for No pass, Single pass and Double pass compaction. Vertical bars indicate standard deviations.

Soil compaction, soil moisture and their interactions affected the peak cone index significantly ($P \leq 0.0001$). The peak cone index values increased for the single and double pass compaction treatments as the soil dried. The differences in the average peak cone index for the four measurement days were statistically significant for the single pass compaction (Fig. 5 (A), $P \leq 0.0001$). However, for the double pass compaction level, the average peak cone index values did not vary significantly (Fig.5 (B), $P \leq 0.265$). For the single pass compaction, as the measurement days passed from day - 1 to day - 4 (18 % soil drying index), the average peak cone index value increased by 68 %. For the double pass compaction, the average peak cone index increased only 6 % as measurement days passed from day - 1 to day - 4 (12 % soil drying index). The small differences in the peak cone index values in the double pass treatment could be due to the reduced variation in soil moisture.

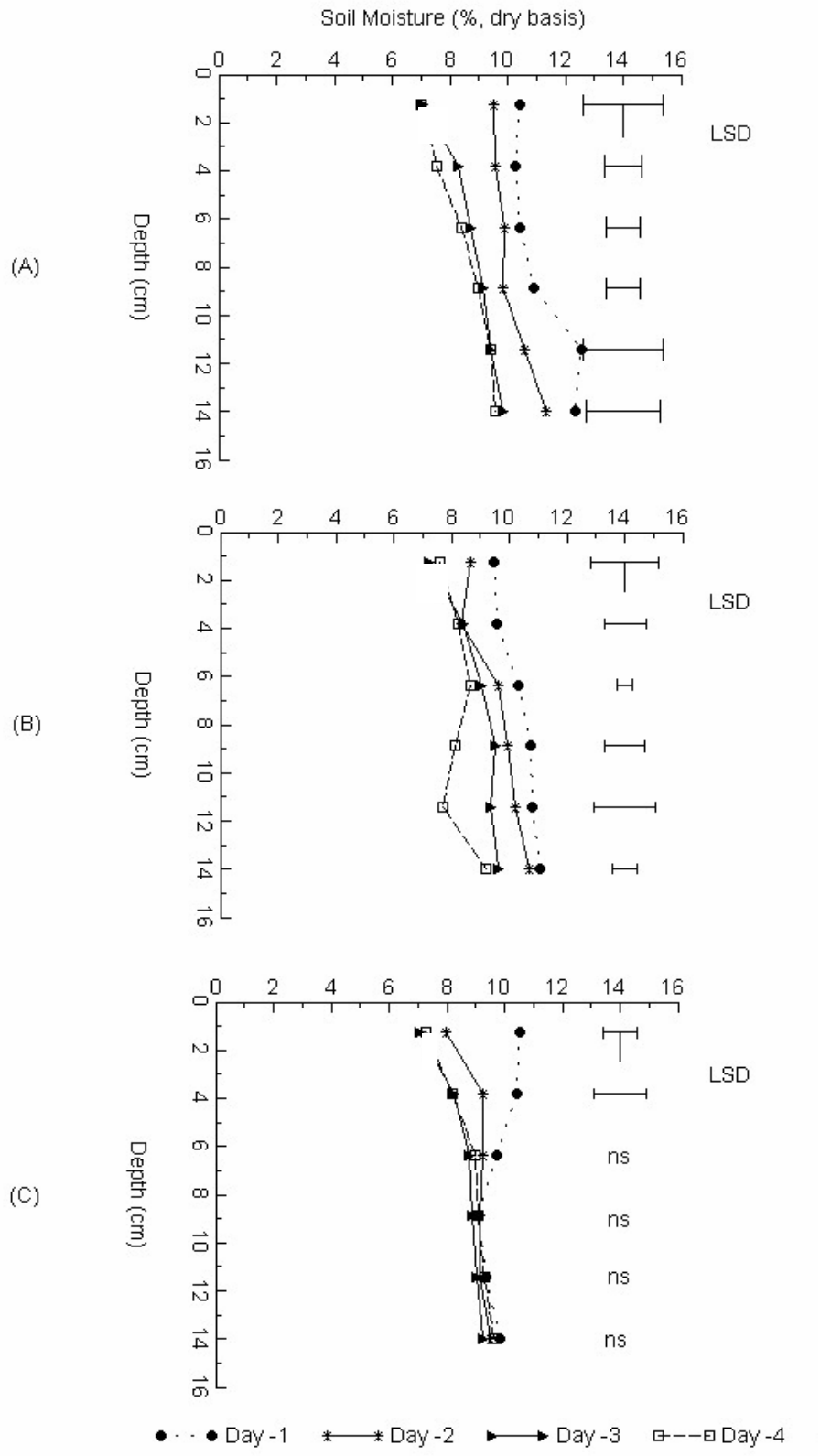

Figure 3. Soil moisture distribution throughout soil profile of the four measurement days for (A) No pass compaction, (B) Single pass compaction and (C) Double pass compaction (C). Horizontal bars indicate LSD $_{\alpha=0.05}$.

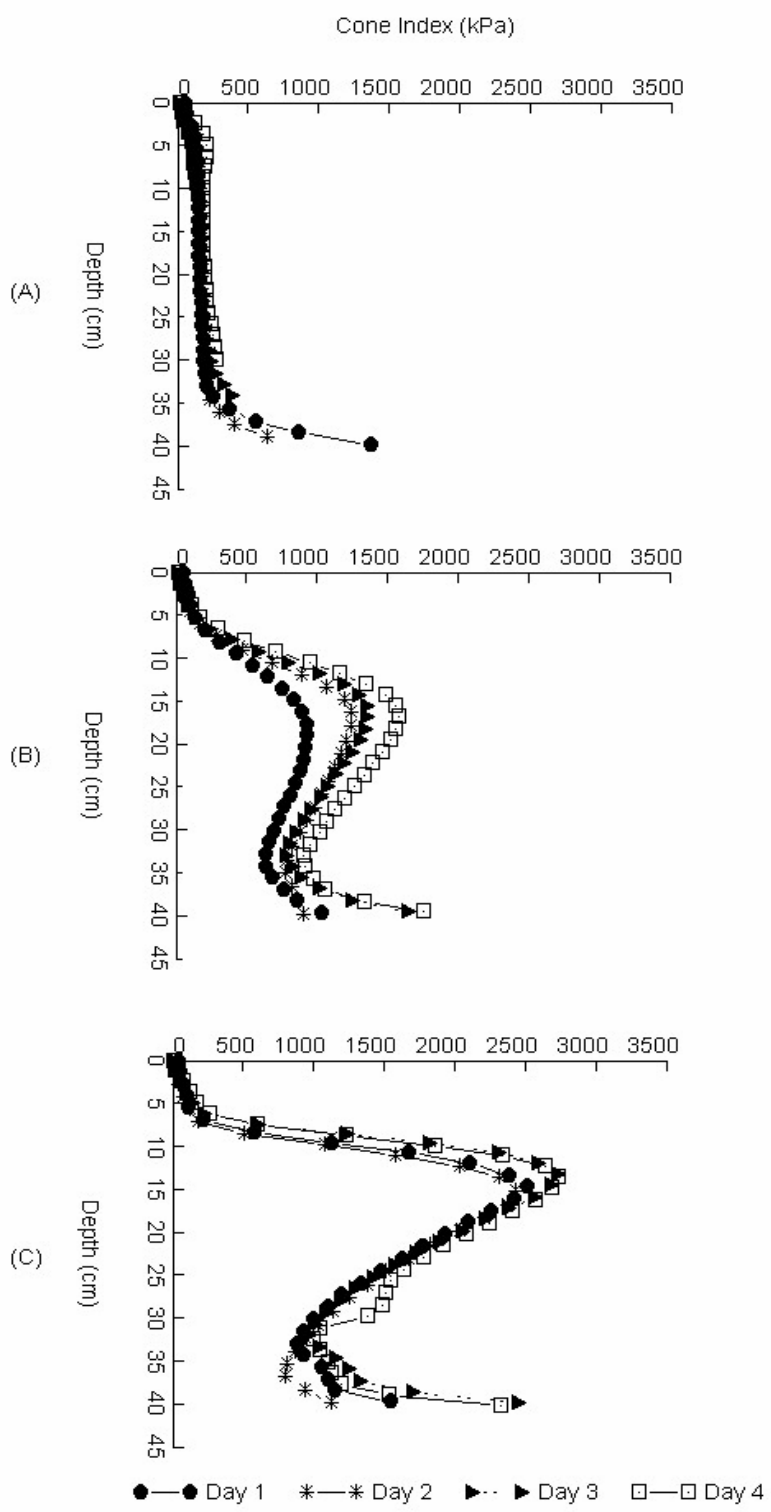

Figure 4. Cone index profile as a function of depth of the four measurement days for (A) No pass compaction, (B) Single pass compaction and (C) Double pass compaction.

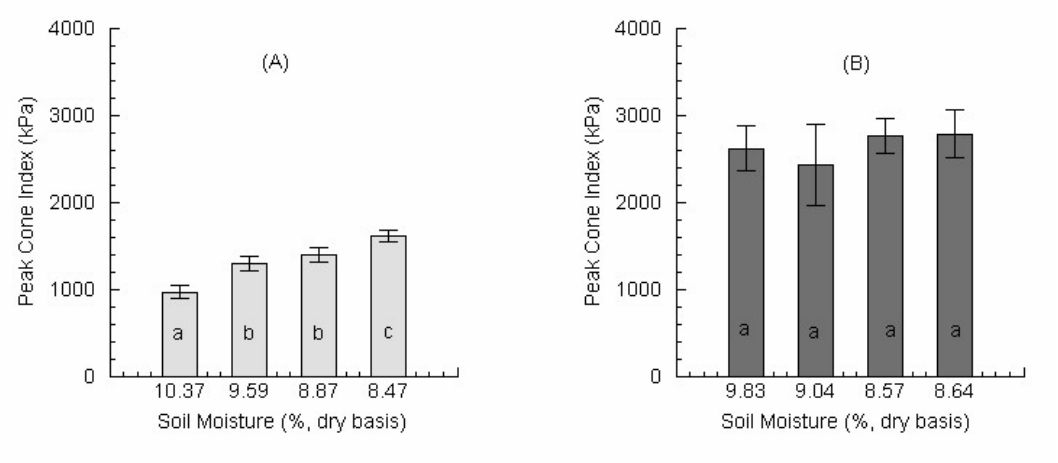

Figure 5. Peak cone index vs. soil moisture of the four measurement days (A) Single pass compaction and (B) Double pass compaction. For each compaction level, means with the same letter are not significantly different, LSD $_{\alpha=0.05}$. Vertical bars indicate standard deviations.

The strength of relationship between peak cone index and average soil moisture for the single pass and double pass compaction treatments was determined by the coefficient of determination (r^2). Soil moisture variation was highly correlated to the peak cone index for the single pass ($r^2 = 0.96$, $P \leq 0.02$) but was not for the double pass ($r^2 = 0.20$, $P \leq 0.55$).

Both soil compaction ($P \leq 0.0002$) and soil moisture ($P \leq 0.0216$) significantly affected the depth to the peak cone index. No soil compaction and soil moisture interaction existed on the depth to the peak cone index ($P \leq 0.367$). The values of this depth ranged from 14.9 to 18.2 cm for the single pass compaction and 12.3 to 14.1 cm for the double pass compaction with the highest and the lowest values occurring at the wet and dry soil conditions. It appeared that the predicted depth to the peak cone index decreased with soil drying.

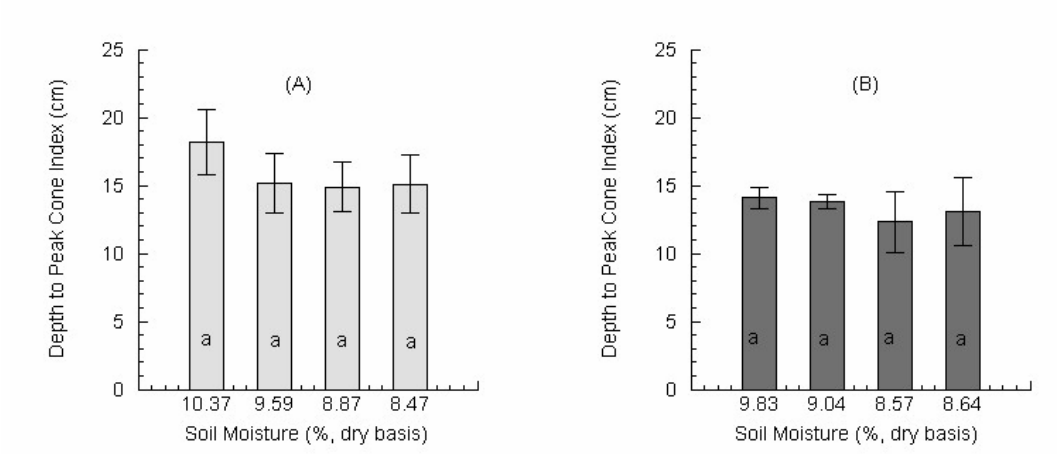

Figure 6. Depth to the peak cone index (cm) vs. soil moisture of the four measurement days (A) Single pass compaction and (B) Double pass compaction. For each compaction level, means with the same letter are not significantly different, LSD $_{\alpha=0.05}$. Vertical bars indicate standard deviations.

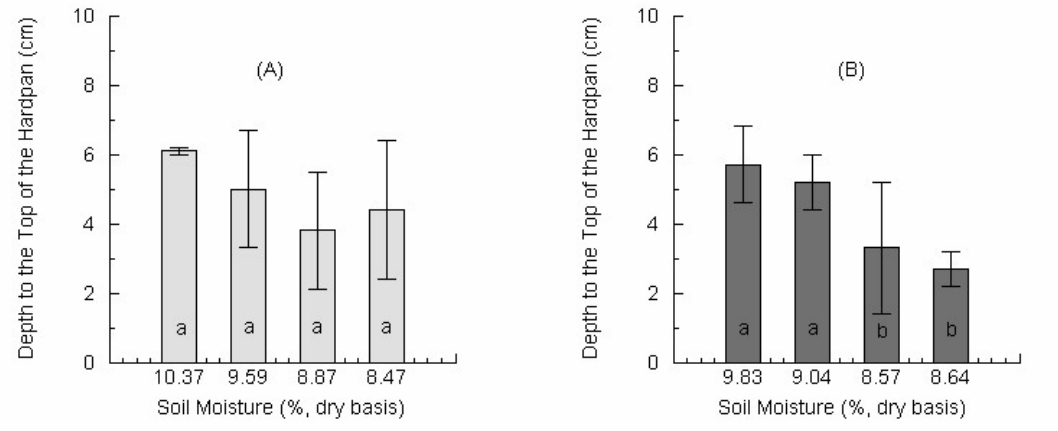

Figure 7. Depth to the top of the hardpan (cm) vs. soil moisture of the four measurement days for (A) Single pass compaction and (B) Double pass compaction. For each compaction level, means with the same letter are not significantly different, LSD $_{\alpha=0.05}$. Vertical bars indicate standard deviations.

The depths to the top of the hardpan ranged from 3.8 to 6.1 cm and 2.7 to 5.7 cm for the single pass and double pass compactions, respectively. The largest and the smallest values were observed under wet and dry soil conditions, respectively. The differences in the predicted depths to the top of the hardpan were significant for the double pass compaction (Fig. 7 (B), $P \leq 0.0086$) but not for the single pass compaction (Fig.7 (A), $P \leq 0.2487$).

At dry soil conditions the decrease in predicted depth implies that the hardpan was sensed before the cone actually reached the layer. This effect could be due to the influence of soil layering and soil compressibility at the tip of the cone as explained by Sanglerat (1972); and Koolen and Kuipers (1983). As a cone passes from soft to hard layer, it can start to sense the hard layer before the tip of the cone reaches it (Lunne et. al., 1997). According to Lunne et. al. (1997), the distance over which the cone starts to sense depends on material stiffness and thickness of the stiff layer; in soft materials the diameter of zone of soil influenced could be two to three times of the cone diameter, where as in stiff materials it can reach up to 10 to 20 cone diameters. Soil drying appeared to magnify this effect.

CONCLUSIONS

Based on the discussions mentioned above, the following conclusions can be drawn;

a). Depth-specific soil moisture variations were observed at short soil depth increments when a Norfolk sandy loam soil bin was subjected to drying. The soil moisture distributions were affected by the degree of compaction and amount of drying. In the double pass compaction (1.76 Mg m^{-3}), the changes in soil moisture were very small in the deeper soil profile (below 5.5 cm).

b). The effects of soil drying on predicted hardpan parameters in the Norfolk sandy loam soil bin were dependent not only on the magnitude of soil drying index (intensity of soil dryness) but also on the bulk density of the hardpan. The higher the antecedent bulk density (1.76 Mg m^{-3}) of the hardpan in the double pass compaction treatment, the lesser was the soil moisture variation and its effect on the peak cone index and the depth to the peak cone index. For the single pass compaction (1.66 Mg m^{-3}), peak cone index increased and its depth appeared to decrease with

soil drying. The effect of soil drying on the predicted depth to the top of the hardpan layer was significant only for the double pass compaction treatment.

c). Further research is needed to observe the soil moisture effects at higher degrees of soil drying, particularly under natural field conditions when there is crop growth.

REFERENCES

Andrade, P., U. A. Rosa, S. K. Upadhyaya, B. M. Jenkins, J. Aguera, and M. Josiah. 2001. Soil profile force measurements using an instrumented tine. ASAE Paper No. 01-1060. Sacramento, CA.: ASAE.

ASAE Standards, 46 Ed. 1999a. S313.3. Soil cone penetrometer. St. Joseph, Mich.: ASAE.

ASAE Standards, 46 Ed. 1999b. EP542. Procedures for using and reporting data obtained with the soil cone penetrometer. St. Joseph, Mich.: ASAE.

Ayers, P. D. and J. V. Perumpral. 1982. Moisture and density effect on cone index. Trans. ASAE.: 1169-1172.

Batchelor, J. A. 1984. Properties of bin soils. National Tillage Machinery Laboratory, USDA-ARS, Auburn, AL.

Bernier, H., G. Bostock , G. S. V. Raghavan, and R. S. Broughton. 1989. Sub-soiling effects of moisture content and bulk density in the soil profile. App. Eng. Agr. 5 (1): 24-28.

Camp, Jr. C. R. and Z. F. Lund. 1968. Effect of mechanical impendence on cotton root growth. Trans. ASAE: 189-190.

Clark, R. L. 1999. Evaluation of the potential to develop soil strength maps using a cone penetrometer. ASAE Paper No. 993109. Toronto, Ontario, Canada:ASAE.

Fulton, J. P., L. G. Wells, S. A. Shearer, and R. I. Barnhisel. 1996. Spatial variation of soil physical properties: a precursor to precision tillage. ASAE Paper No. 96-1002. St. Joseph, Mich.: ASAE.

Hall, H.E., R.L. Raper, T.E. Grift, and D.W. Reeves. 2000. Development of an on-the-fly mechanical impedance sensor and evaluation in a coastal plains soil. Proceedings of the 15th ISTRO Conference, Ft. Worth, TX.

Koolen, A.J. and H. Kuipers. 1983. Agricultural soil mechanics. Advanced series in agricultural sciences 13. Springer-Verlag Berlin, Germany.

Liu, W., L. D. Gaultney, and M. T. Morgan. 1993. Soil texture detection using acoustic methods. ASAE Paper No. 931015. St. Joseph, Mich.: ASAE.

Lunne, T., P.K. Robertson, and J.J.M. Powell. 1997. Cone penetration testing in geotechnical practices. Blackie academic and professional, London, UK.

Rajaram, G. and D.C. Erbach. 1999. Effect of wetting and drying on soil physical properties. Journal of Terramechanics 36: 39 –49.

Raper, R.L., L.E. Asmussen, and J.B. Powell. 1990. Sensing hardpan depth with ground penetrating radar. Trans. ASAE 31(1): 41-46.

Raper, R.L., D.W. Reeves, and C.H. Burmester. 1998. Cotton yield response and energy requirements of matching tillage depths to root-impeding layers. ASAE Paper No. 981112. St. Joseph, MI.: ASAE.

Raper, R. L., B. H. Washington, J.D. Jarrell. 1999. A Tractor - Mounted - Multiple – Probe Soil Cone Penetrometer. App. Eng. Agr. 15(4): 287-290.

Raper, R.L., E. B. Schwab, and S.M. Dabney. 2000. Spatial variation of the depth of the root-restricting layer in an upland soil of Northern Mississippi. Second International Conference of Geospatial Information in Agriculture and Forestry, Lake Buena Vista, Florida, January 10-12, 2000.

Raper, R. L., D.W. Reaves, J.N. Shaw, E. van Santen, and P.L. Mask. 2004. Site-specific subsoiling benefits for coastal plain soils. 26 th Southern Conservation Tillage Conference, Raleigh, NC, June 8-9, 2004.

Sanglerat, G. 1972. Interpretation of penetration diagrams- theory and practice. Developments in geotechnical engineering. Elsevier publishing company. Amsterdam, The Netherlands.

SAS/STAT 1999-2001 by SAS Institute Inc., Cary, NC, USA.

Taylor, H. M. and Gardner, H. R. 1963. Penetration of cotton seedling taproots as influenced by bulk density, moisture content and strength of soil. Soil Sci. 96:153-545.

Tekeste, M. Z., T.E. Grift, R.L. Raper. 2002. Acoustic compaction layer detection. ASAE Paper No. 021089. Chicago, IL.: ASAE.

Utset, A. and C. Greco. 2001. Soil penetrometer resistance spatial variability in a Ferrasol at several soil Moisture conditions. Soil Till. Res. 61:193-202.

CHAPTER 4

Spatial Variability of Soil Cone Penetration Resistance as influenced by Soil Moisture on Pacolet sandy loam soil in the Southeastern United States [2]

[2] Mehari Z. Tekeste, Randy L. Raper, Eric B. Schwab and Lynne Seymour to be submitted to soil and tillage research journal

Abstract: Soil hardpans found in many of the Southeastern USA soils reduce crop yields by restricting the root growth. Site-specific soil compaction management to alleviate this problem requires determination of the spatial variability and mapping of soil hardpans. The objective of this study was to determine the spatial variability of soil hardpan as influenced by soil moisture. Geo-referenced soil cone index measurements were taken in 200 grid cells (10 X 10 m^2 grid cell size) on Pacolet sandy loam soil (*Fine, kaolinitic, thermic Typic Kanhapludults*) in Auburn, AL (USA) on June 29, 2004 and August 25, 2004 representing wet and dry soil measurement dates. Core samples were also taken in 5 cm depth increments up to a depth of 65 cm for soil moisture and bulk density determinations. Statistical and geostatistical methods were used for the data analysis. In the 0-35 cm depth, the soil moisture had dried significantly by August 25, 2004 (Dry) as compared to the soil moisture on June 29, 2004 (Wet; $P < 0.0001$). An isotropic spherical semivariogram model best fit the semivariances of the peak cone index for wet ($R^2 = 0.98$) and dry ($R^2 = 0.97$) soil conditions. Soil drying increased the peak cone index and the maximum semivariance value (sill). Small but statistically significant differences ($P < 0.0001$) were also observed on the predicted depth to the peak cone index as the soil dried in the 0-35 cm depth. In the dry soil condition, the semivariances of the predicted depth to the peak cone index were nearly constant over the separation distances suggesting that the depth to the hardpan did not exhibit spatial dependence.

Keywords: Soil hardpan, cone index, semivariogram, soil moisture and bulk density

1. Introduction

Soil compaction has been recognized as one of the major problems in crop production (Soane and Van Ouwerkerk, 1994). Soil hardpan layers found in many Southeastern US soils restrict root growth that in turn limits crop yield, especially during drought (Taylor and Gardner, 1963;

and Camp and Lund, 1968). These excessively compacted layers may also reduce soil aeration and soil water infiltration that could accelerate erosion and runoff. Farmers annually apply uniform depth tillage to disrupt this root-restricting layer for optimum root growth environment (Raper et al., 2004b and Busscher et al., 2005). Many researchers have found that the soil hardpan layers exhibit spatial variability within a field (Fulton et al., 1996; Kenan et al., 2003 and Raper et al., 2004b). Studies have also suggested that site-specific tillage has potential in reducing tillage energy and fuel consumptions as compared to the conventional uniform depth tillage (Fulton et al., 1996; Raper et al., 2000; Gorucu et al., 2002 and Raper et al. 2004b). Raper et al. (2000) estimated about 50% reduction in energy requirements for shallow tillage (approximately 18cm) as compared to deep tillage (approximately 33cm). Gorucu et al. (2002) found that approximately 75 % of the test area required tillage operations shallower than the commonly used tillage depth for Coastal plain soils. Site-specific tillage is a component of precision agriculture management strategy that employs detailed site-specific soil and crop information to precisely manage the production inputs (Naiqian et al., 2002). Site-specific tillage in particular is geared towards achieving the goals of sustainable agriculture by determining within field variability and providing more accurate soil compaction records, and optimizing the tillage input within the field where root limiting soil compaction exists. The success of site-specific tillage depends on the availability of economical, rapid, easy and precise soil strength sensing technology, management of within field variability, accuracy of field positioning and controlling the application of real-time or prescribed site-specific tillage.

A soil cone penetrometer has been used widely to assess soil compaction, root penetration resistance; and to predict trafficability and bearing capacity for foundations (Perumpral, 1987 and Raper et al., 2004b). The soil cone penetrometer measures the soil penetration resistance,

reported as cone index, as a function of depth (ASAE 1999a, b). The influence of soil factors, mainly soil moisture, on the cone index reading and the difficulty in data interpretation in layered soils varying by soil moisture and soil strength, are the main challenges in using the soil cone penetrometer for site-specific tillage (Gill, 1968; Sanglerat, 1972 and Mulqueen et al., 1977). Gill (1968) and Mulqueen et al. (1977) showed that a soil wedge formed in front of the cone could erroneously increase the soil penetration resistance. In precision tillage, an accurate prediction of soil hardpan is important because errors of a few centimeters variations in site-specific tillage depth recommendations.

Spatial variability analysis of soil compaction and application of site-specific tillage management has not progressed as the precision/site-specific application of fertilizers and chemicals due to lack of appropriate technology or procedures to characterize soil physical properties. Hence, research was needed to accurately characterize the soil hardpan and define its spatial pattern as influenced by soil moisture on landscape level for site-specific tillage applications. Analysis of spatial variability and mapping of soil hardpans may further improve our understanding of soil compaction variability and the precision tillage decision making process for Southeastern US soils.

Therefore, our objectives were to:

- determine the effect of soil moisture on the peak cone index and its depth, and to
- determine the field spatial variability and spatial structure of the peak cone index and the depth to the peak cone index as influenced by soil moisture.

2. Materials and methods

2.1. Site description

The experiment was conducted during summer 2004 at the Auburn University experimental field plot in Auburn, AL and is located at a latitude 32^0 21′ 15″N and a longitude 85^0 17′ 30″ W. Pacolet sandy loam (*Fine, kaolinitic, thermic Typic Kanhapludults*) is the dominant soil series in the site. The area receives an average annual precipitation of 1440 mm and the mean annual temperature is 18 ^{o}C (Siri et al., 2002). The soil physical and chemical properties of the site are shown in Table 1.

Table 1

Descriptive statistics for the soil physical and chemical properties of a Pacolet sandy loam soil

Soil parameters	Depth -cm-	Mean	Median	Standard deviation	Coefficient of variation	Minimum	Maximum	95 % Confidence interval	Kurtosis	Skewness
Soil moisture (%)										
June 29,2004	0-35	11.25	11.01	2.30	20.40	8.54	17.52	10.42-12.08	2.57	1.59
	35-65	15.80	15.51	3.39	21.46	14.58	17.03	10.71-22.02	0.36	-0.72
August 25,2004	0-35	9.83	9.11	2.17	22.08	7.36	14.84	9.05-10.61	0.40	1.02
	35-65	17.82	17.09	4.43	24.88	16.22	19.42	11.13-23.23	-0.08	-1.58
Cone Index (Mpa)										
June 29,2004	0-35	2.61	2.63	0.54	20.56	1.75	4.00	2.42-2.81	0.74	1.11
	35-65	3.93	3.86	0.76	19.25	2.86	5.78	3.65-4.20	0.91	0.65
August 25,2004	0-35	2.87	2.83	0.72	25.15	1.62	4.56	2.61-3.13	0.50	0.38
	35-65	2.97	2.91	0.90	30.23	1.48	4.72	2.64-3.29	0.20	-0.40
Bulk density (Mg m^{-3})	0-35	1.39	1.41	0.04	3.11	1.29	1.48	1.38-1.41	-0.67	-0.03
	35-65	1.36	1.37	0.08	6.01	1.22	1.50	1.33-1.39	0.06	-1.07
Soil Organic Carbon (%)	0-35	0.70	0.72	0.13	19.01	0.42	0.90	0.65-0.75	-0.24	-1.21
	35-65	0.37	0.31	0.14	36.89	0.23	0.71	0.32-0.42	0.94	0.06
Clay (%)	0-35	8.63	6.79	5.36	62.11	2.14	26.07	6.70-10.56	1.20	1.90
	35-65	25.74	27.29	12.80	49.74	3.33	45.83	21.12-30.36	-0.30	-0.87
Silt (%)	0-35	14.76	14.73	2.01	13.62	10.18	18.21	14.03-15.48	-0.40	0.17
	35-65	13.08	12.92	3.86	29.49	5.00	18.96	11.67-14.47	-0.33	0.03
Sand (%)	0-35	76.61	77.86	5.92	7.73	59.11	84.11	74.48-78.75	-0.80	0.71
	35-65	61.18	59.27	12.96	21.19	42.71	91.67	56.51-65.85	1.00	0.97

2.2. Experiment design

The field was divided into 200 grid cells each with a 10 X 10 m^2 covering an area of 2 ha. Because the objective of the experiment was to determine the spatial variability of soil hardpan, sampling patterns associated with crop management and trafficking were not considered. In the north and east directions of the field, a 10 meter transect distance was used for cone index

sampling. A tractor mounted Multiple Probe Soil Cone Penetrometer (MPSCP) that has five probes was used to acquire cone index data at 25 Hz sampling rate (ASAE, 1999 a, b and Raper et al., 1999).

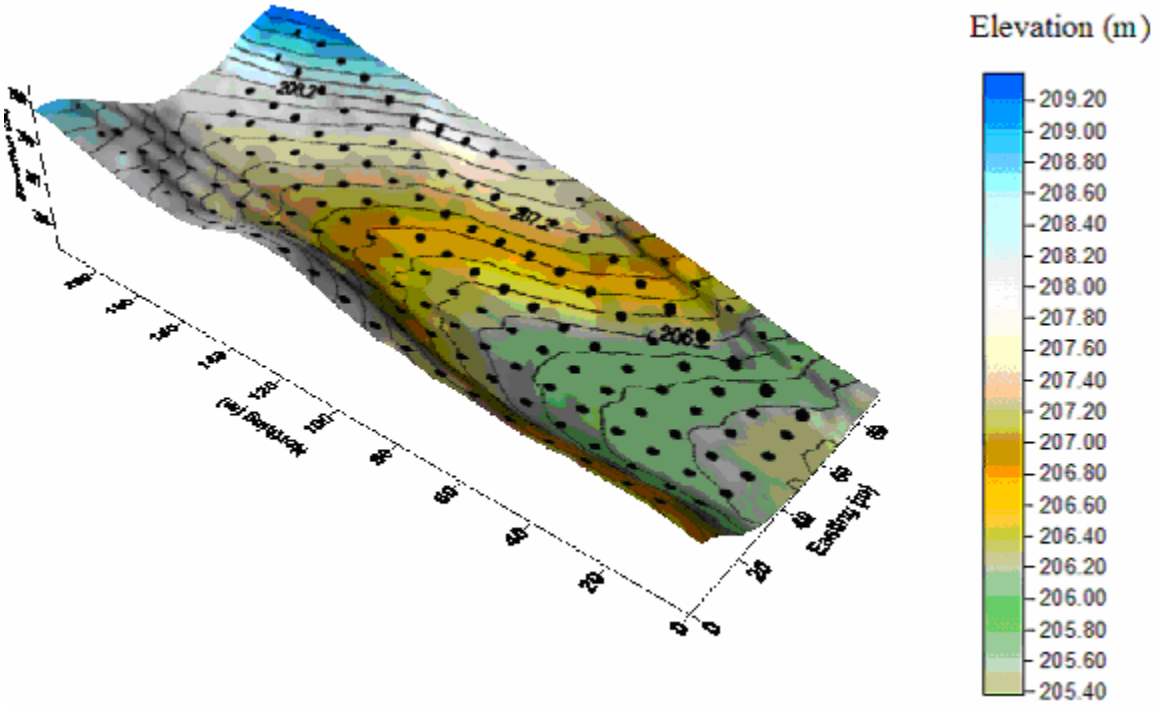

Fig. 1. Elevation of the sampling field of Pacolet sandy loam soil. The marks indicate the sampling points for cone index measurement.

Two sets of cone index measurements were obtained in each of the grid cells using the tractor mounted MPSCP equipped with GPS for field positioning. A dual-frequency RTK, *Ag*GPS® 214, GPS receiver was also used to obtain elevation data across the field. Soil core that has an inner diameter of 5 cm were collected for soil moisture and bulk density determinations. The soil core samples were collected at every 5-cm depth increments to a depth of 65 cm in two replicates at 54 randomly selected grid cells near where the cone indices were sampled. The soil core samples were oven dried at 105 ^{0} C for 72 hrs to determine gravimetric soil moisture and bulk density. Soil particle size distributions and soil organic matter were also analyzed on the soil core samples from the 32 grid cells. The soil particle size distributions analysis was carried out at the

Auburn University Soil Testing Laboratory (Auburn, AL) using the hydrometer method. The soil organic carbon (SOC) was analyzed at the USDA-ARS-National Soil Dynamics Laboratory in Auburn, AL using dry combustion method for total carbon and nitrogen by Leco Truspec instrument model 2003 (Leco Corporation, St. Joseph, MN, 2004). The cone index measurement and the soil core sampling were carried out simultaneously within an approximate 24- hrs period. Within this sampling period, there were no rainfall events that minimized the risk of soil moisture differences. The measurements were obtained on June 29, 2004 and August 25, 2004 representing 'wet' and 'dry' soil moisture conditions, respectively. The sampling dates were chosen based on climatic data obtained for the Auburn University weather experimental station located near the field site (Fig. 2).

Peak cone index and depth to the peak cone index were considered as soil hardpan characterizing attributes that were predicted by analyzing the change of cone index values with depth. The analyses were carried out on the cone index data averaged over the five probe data set interpolated at every 1 cm depth increments. Visual inspection on the 200 cone index-depth profile data revealed there were two peaks. The first peak cone index that occurred in depth range of 0 – 35 cm was considered as the root restricting layer in the soil profile. A maximum value of the cone index-depth profile within this depth range (0-35 cm) was determined for the peak cone index.

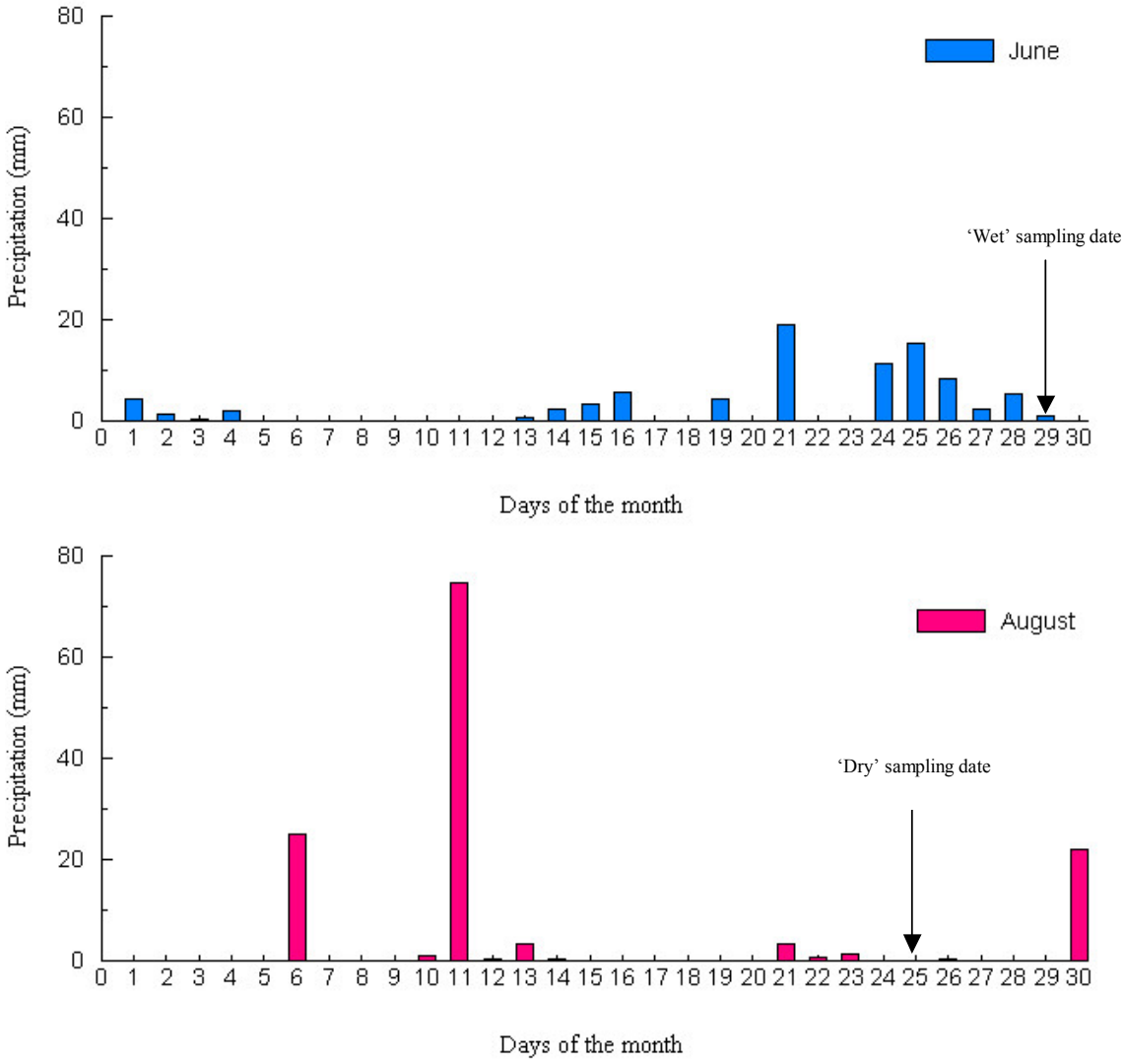

Fig. 2. Precipitation data for June, 2004 ('wet' measurement date) and August, 2004 ('dry' measurement date) for Auburn, AL.

In developing, the algorithm to define the peak cone index in the shallow depth (0-35 cm), instantaneous slope values (change in cone index per depth) were calculated and the values were tested in the following priorities, (1). If three consecutive negative slope values were obtained, the cone index and depth value at the first slope value were considered as peak cone index and its depth; (2). If the first test fails, two negative slopes were considered in deciding the peak cone index with the data values of the first negative value being used to define the hardpan; and (3) If

the second test fails, three consecutive zero slope values were considered. These zero slope values indicated that the cone index increased till it reached the root restricting peak cone index value and the cone index depth profile curve flattened with depth. The data set at the first zero slope value characterized peak cone index and depth to peak cone index.

Geo-statistical procedures PROC VARIOGRAM and PROC NLIN (SAS. Release 8.02 SAS Institute Inc., Cary, NC, 2001) were used to quantify the isotropic spatial variability and to construct theoretical semivariogram models for the soil hardpan attributes, and maximum bulk density and its depth.

A semivariogram function was determined for each variable according to equation 1 (Isaaks and Srivastava, 1989).

$$\gamma(h) = \frac{1}{2N(h)} \left\{ \sum_{i=1}^{N(h)} [Z(x_i + h) - Z(x_i)]^2 \right\} \quad (1)$$

where $\gamma(h)$ is the semivariance for interval class h, N(h) is the number of pairs separated by lag distance (separation distance between sample positions), $Z(x_i)$ is a measured variable at spatial location i, $Z(x_i + h)$ is a measured variable at spatial location i + h. The spatial structure ($\gamma(h) = C_o + C$) of a semivariogram can be described by three basic parameters: *nugget effect* (C_o), *sill* ($C_o + C$), and *range*. The *nugget effect* is the variations occurring at a scale finer than the sampling interval that could be due to sampling errors, micro-scale variability, and/or measurement errors. The *sill* (total variance) is asymptote of the semivariogram model. The *range* is a distance at which the semivariogram levels off at the sill and it indicates the distance over which the pairs of values of the variable are spatially dependent.

Spherical, exponential and linear variogram models were considered in selecting the best fitting model based on the values of weighted residual sums of squares, regression coefficient (R^2) and relative spatial structure indicator (Scale/Sill). Scale is the amount of semivariance after the nugget is reduced (Sill-Nugget). A model with the largest R^2 value, the smallest weighted residual sums of squares at the end of iteration procedure and a value of the spatial structure indicator close to 1.0 was considered the best fitting semivariogram model. A scale to sill ratio close to 1 indicates the nugget effect is negligible implying a better spatial structure (Raper et al., 2004). After selecting the best theoretical semivariogram model, ordinary kriging was used to interpolate values for un-sampled locations. Contour maps were created using Surfer (Surfer version 8.00 Golden Software Inc., 2002). All statistical comparisons were made using PROCGLM procedure (an alpha (α) level of 0.05) in SAS.

3. Results and discussion

3.1. Gravimetric soil moisture

The soil moisture distribution varied significantly by depth (Fig.3; $P < 0.0001$). The normality of residuals assumption, a requirement of analysis of variances, was fairly maintained when soil moisture and other soil variables were the depth classes of 0-35 and 35-65 cm. At the soil depth range of 0 -35 cm depth, the soil moisture sampled on June 29, 2004 (11.25 %) was significantly higher than the soil moisture (9.83 %) sampled on August 25, 2004 ($P < 0.0001$). For convenience, the soil moisture conditions were assumed ‘wet’ and ‘dry’ for the measurement dates of June 29, 2004 and August 25, 2004, respectively. At the deeper profile (35 – 65 cm), the soil moisture trend was reversed (Fig. 3). The soil moisture (17.82 %) for the second measurement date (August 25, 2004) was significantly higher than the soil moisture (15.80 %) for the first measurement date (June 29, 2004) (Table 1 and $P < 0.0001$). This may indicate a

wetting front moving downward through the soil profile. The skewness value (Table 1) and frequency distribution (not shown) showed that the soil moisture variability for the shallow depth appeared to be skewed to the left and the skewness was higher in the wet soil than in the dry soil. At the deeper soil depth, the skewness and coefficient of variation values (Table 1) were relatively small indicating the subsoil soil moisture distribution tends to be symmetrically distributed around the mean.

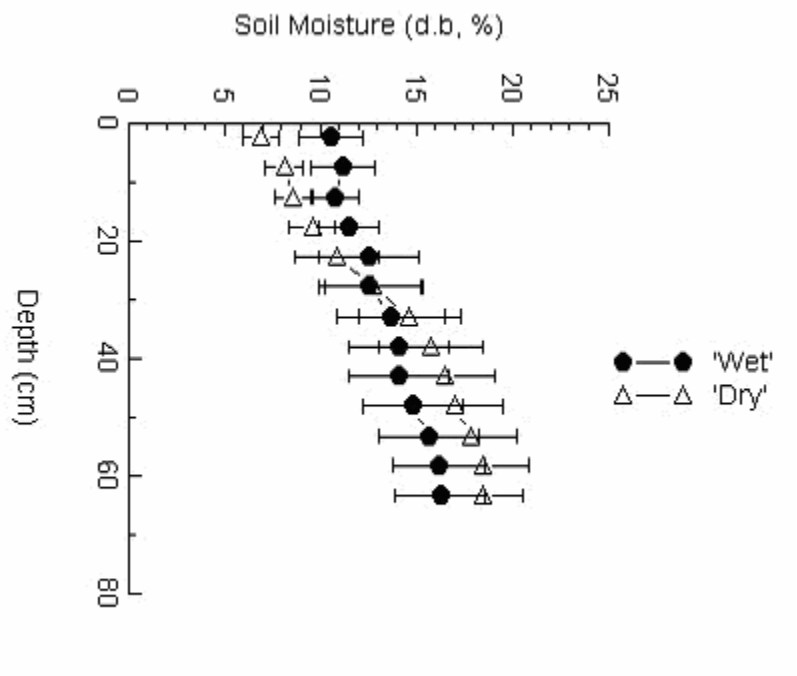

Fig. 3. Soil moisture profile for the two measurement dates of June 29, 2004 (‘Wet’) and August 25, 2004 (‘Dry’). The horizontal bars indicate standard deviations.

3.2. Soil bulk density

The average bulk density profile for the field is shown in Fig. 4. The bulk density varied by depth significantly ($P < 0.0001$). There were not statistically significant differences in the bulk density values by measurement dates ($P = 0.056$). The skewness (-0.49) and coefficient of variation (0.1) showed that the distribution of bulk density was nearly symmetrical around the mean.

Table 2

Descriptive statistics for the maximum bulk density and the depth to the maximum bulk density

	Number of values	Mean	Median	Standard deviation	Coefficient of variation	Variance	Minimum	Maximum	95% Confidence interval	Kurtosis	Skewness
Maximum bulk density (Mgm^{-3})	53	1.54	1.54	0.06	0.04	0.004	1.43	1.65	1.52-1.55	-1	0.05
Depth to the maximum bulk density (cm)	53	20.94	22.86	5.66	0.27	31.99	12.7	27.94	19.38-22.50	-1.36	-0.06

3.4. Maximum bulk density and the depth to the maximum bulk density

The variability of the maximum bulk density (Fig. 5 A) was best fit by the spherical semivariogram model ($R^2 = 0.98$ and a spatial structure indicator of 0.25). The range of the semivariogram model was 47 m. A linear semivariogram model best fit the semivariances of the predicted depth to the maximum bulk density with a sill value (14.3) nearly half of the sample variance (31.99) (Fig. 5 B). The semivariances appeared to be nearly constant over the entire separation distances indicating that the variability of the depth to the maximum bulk density was spatially independent. Contour map of the depth to the maximum bulk density showed that the predicted soil hardpan depth seems to vary across the field (Fig. 6).

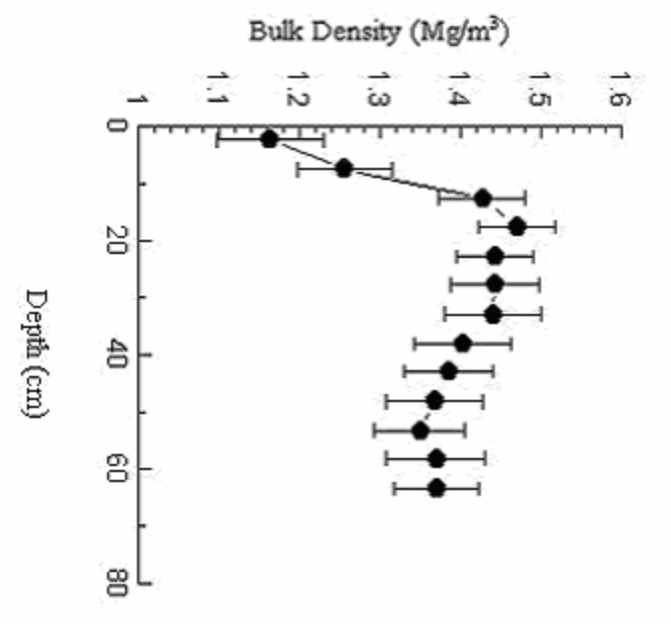

Fig. 4. Bulk density profile averaged over the two measurement dates of June, 25 2004 and August, 29 2004. The horizontal bars indicate standard deviations.

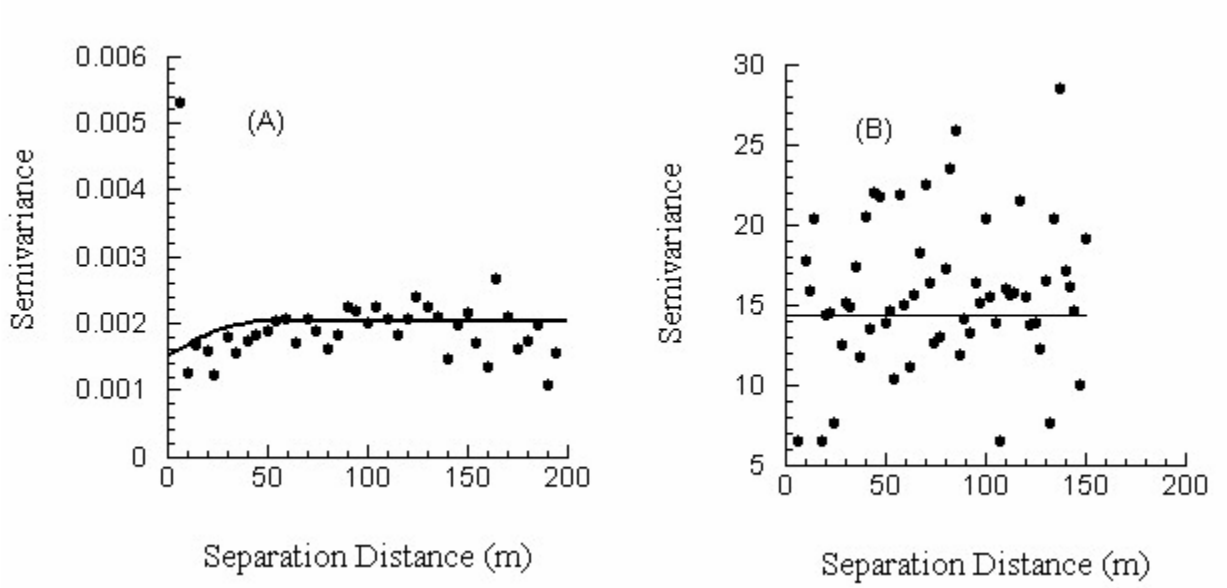

Fig.5. Semivariances (A) for the maximum bulk density with theoretical spherical semivariogram model fit and (B) depth to the maximum bulk density with theoretical linear semivariogram model fit.

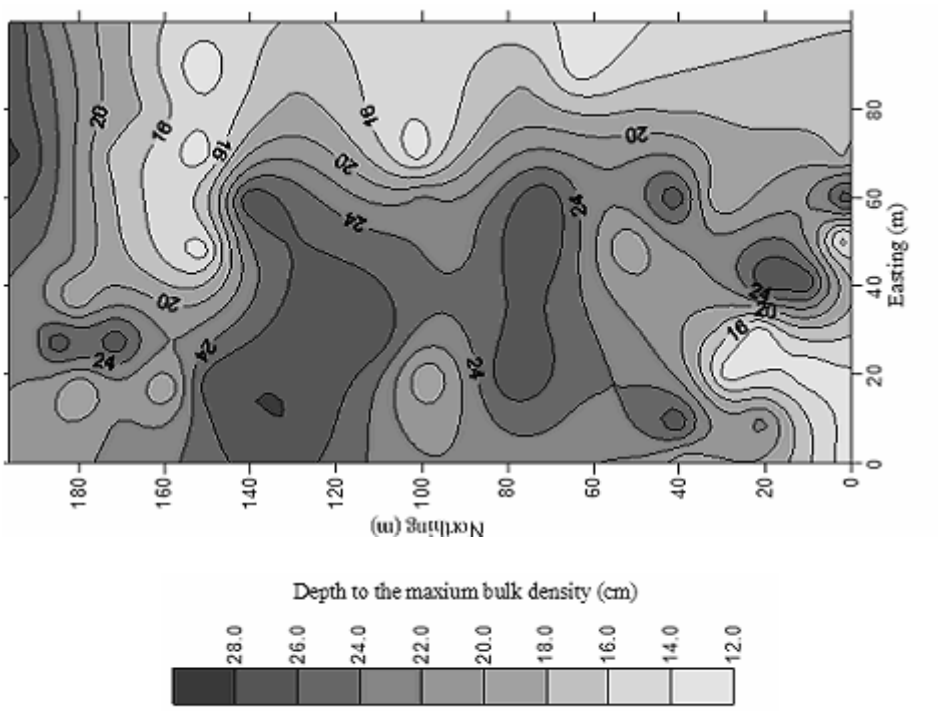

Fig. 6. Contour map of the depth to the maximum bulk density on Pacolet sandy loam soil.

3.5. Peak cone index and depth to the peak cone index

The average peak cone index was significantly higher for the dry soil condition than the value for the wet soil condition (Table 3 and $P < 0.0001$). By taking cone index measurements at the drier soil condition (August 25, 2004), the peak cone index increased by 28 %. As shown in Fig. 7 (A), the relative frequency distribution of the peak cone index for the dry soil condition appeared to shift to the right as compared to the wet soil condition. For the dry soil condition, the relative frequency distribution of the depth to the peak cone index (Fig. 7 B) indicated a slight shift to the left (small depth values). Even though the difference in the depths appeared to be small, there was strong statistical evidence that the predicted depth to the peak cone index decreased by soil drying (Table 3 and $P < 0.0001$). The predicted depth occurred within the shallow depth range (0-35cm) where the soil moisture significantly decreased by sampling date.

Table 3

Descriptive statistics of the peak cone index and the depth to the peak cone index for the two measurement dates of June 29, 2004 and August 25, 2004

		Number of values	Mean	Median	Standard deviation	Coefficient of variation	Variance	Minimum	Maximum	95% Confidence interval	Kurtosis	Skewness
June 29, 2004	Peak cone index (MPa)	198	3.29	3.2	0.88	0.27	0.78	1.23	5.86	3.23-3.36	0.11	0.42
	Depth to the peak cone index (cm)	198	21.08	21	3.36	0.16	11.29	13.5	28	20.84-21.31	-0.7	0.14
August 25, 2004	Peak cone index (MPa)	200	4.12	3.99	1.36	0.33	1.84	1.68	8.69	4.03-4.23	0.81	0.78
	Depth to the peak cone index (cm)	200	20.08	20	3.56	0.18	12.65	10	28	19.83-20.33	-0.04	-0.06

Tekeste et al. (2004) reported similar influences of soil drying on the peak cone index and the predicted depth of soil hardpan on Norfolk sandy loam soil. Comparing the soil hardpan depth prediction using the cone index and maximum bulk density method, the depths predicted at the wet and dry soil conditions from cone index data lies within the 95 % confidence interval of the depth to the maximum bulk density (Table 2).

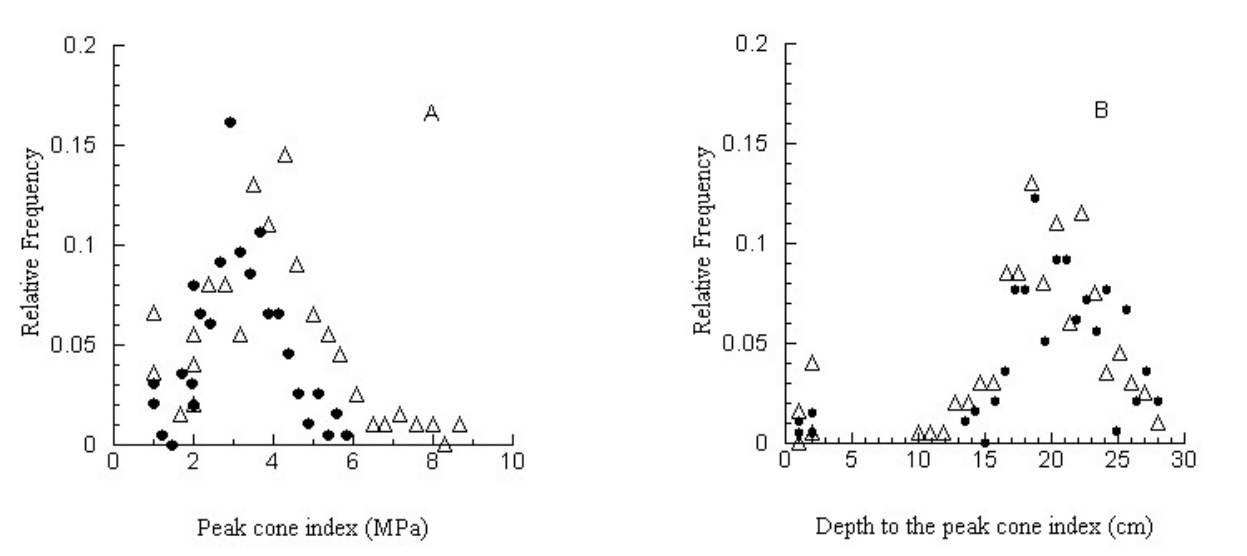

Fig. 7. Relative frequency distribution of (A) the peak cone index (MPa) and (B) the depth to the peak cone index for the two measurement dates of June 29, 2004 (‘Triangle’) and August 25, 2004 (‘Circle’).

3.6. Spatial variability analysis

Selection of sampling distance intervals is important in ensuring the quality of spatial variability analysis and interpolation of points for un-sampled locations using geostatistical techniques (Donald and Ole, 2003). A sampling interval distance less than a range, a distance over which pairs of observations exhibit spatial dependence, was considered appropriate in grid sampling. The ten-meter transect distance used in the cone index sampling was less than a range that Raper et al. (2004b) estimated for the depth of the soil hardpan on silty upland soils of Northern Mississippi.

Table 4

Descriptive semivariogram statistics for the peak cone index and the depth to the peak cone index for the two measurement dates of June 29, 2004 and August 25, 2004

		Model	Nugget u	Sill	Range	Regression coefficient	(Sill-Nugget)/Sill	WSS v
				--MPa^2--	--m--			
June	Peak cone index (Mpa)	Spherical	0.26	0.4	44	0.98	0.36	322
29, 2004	Depth to the peak cone index (cm)	Exponential	0.00	5.73	47	0.99	1.00	259
August	Peak cone index (Mpa)	Spherical	0.15	0.93	26	0.97	0.84	505
25, 2004	Depth to the peak cone index (cm)	Linear	5.80			0.98	0.15	151

u Nugget units are MPa^2 for the peak cone index and cm^2 for the depth to the peak cone index.
v WSS= Weighted Residual Sums of Squares

The spherical semivariogram was the best fitting model to the estimated semivariances of the peak cone index for both the wet and dry soil conditions (Table 4 and Fig.8). The sill for the dry soil condition was nearly twice the value for the wet soil condition. At a distance greater than the range, the square of the differences between pairs of peak cone index values would be approximately the same as the sample variance (twice the sill). Isaaks and Srivastava (1989) explained that increasing the sill has less effect on the value of kriging estimates for the sample site. The range for the dry soil condition (26 m) was smaller than for the wet soil (44 m). Smaller range value indicates that soil drying reduced the distance over which pairs of peak cone index values remain spatially dependant. At the dry soil condition, the spatial continuity of the

magnitude of soil hardpan on Pacolet sandy loam could be captured by having sampling distances less than 26 m that may improve the efficiency of future cone index sampling design. The maps for the peak cone index of the field (not shown) indicate that the values exceeded the critical root limiting cone index value of 2 MPa (Taylor and Gardner, 1963) in most parts of the field with the values being higher for the dry soil

condition.

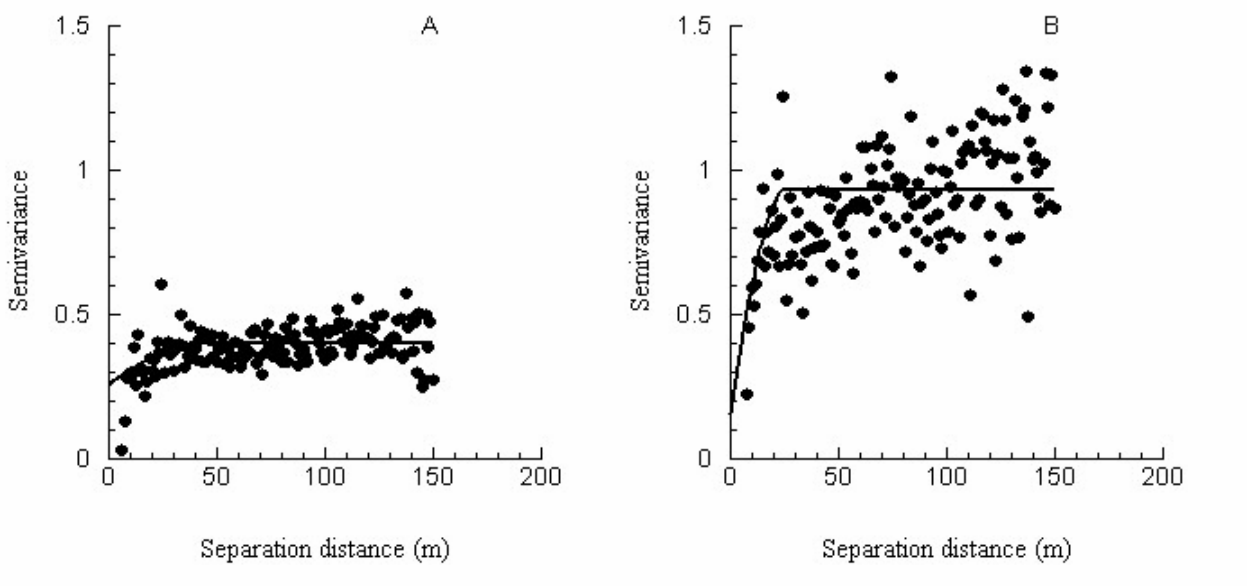

Fig. 8. Semivariances for the peak cone index and spherical theoretical model fits for the two measurement dates of June 29, 2004 (A) and August 25, 2004 (B).

Similar to the peak cone index spatial variability, soil moisture variation also affected the estimated semivariances and the semivariogram models for the depth to the peak cone index (Table 3 and Fig. 9). Exponential semivariogram model explained the spatial variability of the depth to the peak cone index with a scale to sill ratio of 1 that indicates a well defined spatial structure. For the dry soil condition, the semivariances appeared to be spatially uncorrelated that the values were nearly similar over the separation distances (Fig. 9 B). The contour maps in Fig.

10 (A and B) show that the predicted depths to the peak cone index appeared to be shallow for the dry condition in most parts of the field.

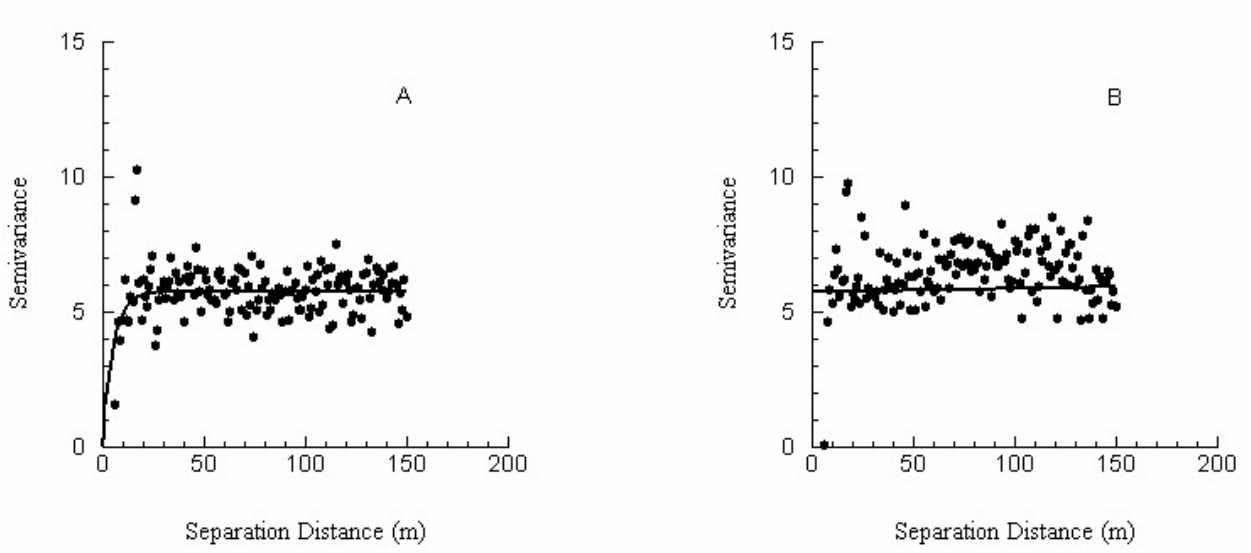

Fig. 9. Semivariances for the depth to the peak cone index and exponential theoretical model fit and linear theoretical model fit for the measurement dates of June 29, 2004 (A) and August 25, 2004 (B), respectively.

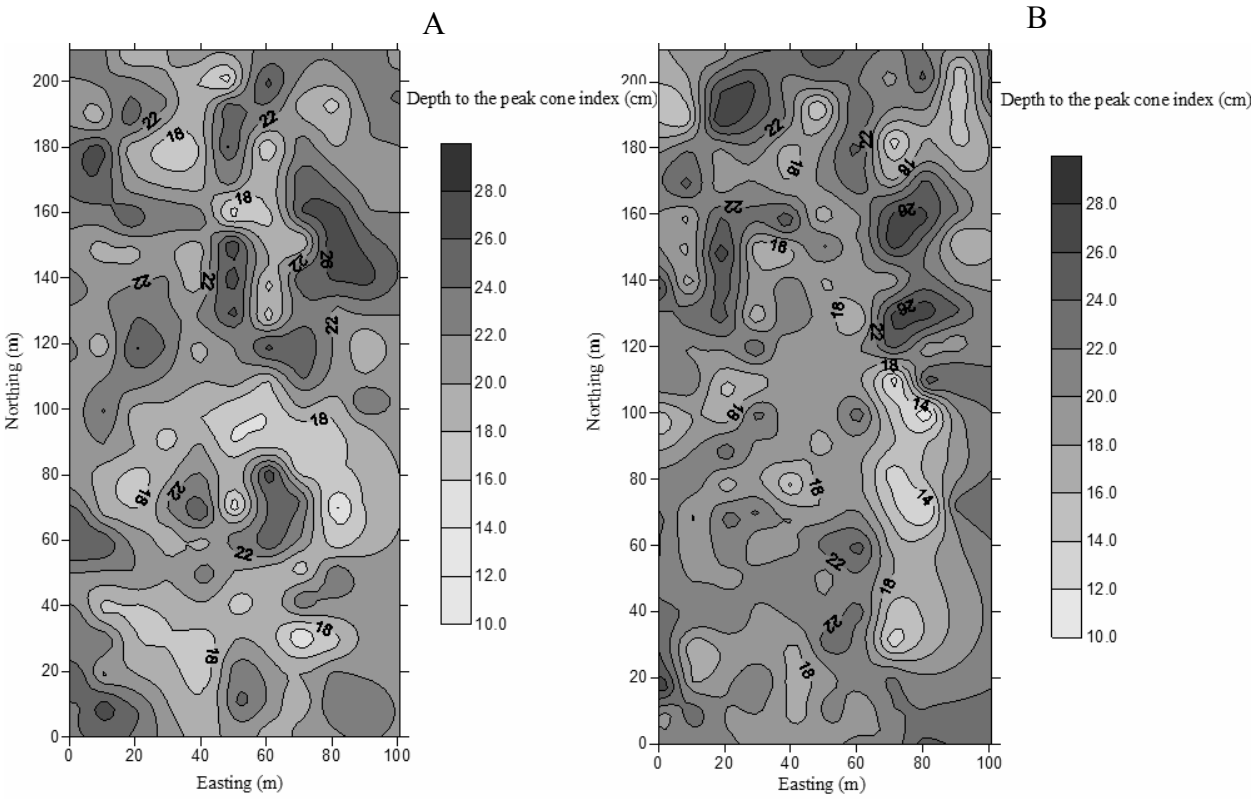

Fig. 10. Contour map of the depth to the peak cone index on Pacolet sandy loam soil for the two measurement dates of June 29, 2004 (A) and August 25, 2004 (B), respectively.

4. Conclusions

Soil drying increased the magnitude and spatial variability of the peak cone index on Pacolet sandy loam soil. The spatial pattern of the peak cone index was explained by spherical semivariogram model for wet and dry soil conditions. An exponential semivariogram model best fit the spatial variability of the depth to the peak cone index on the wet soil condition; however, in the dry soil condition the variability in the predicted depth to the peak cone index was nearly constant over the separation distances. The results suggested that soil moisture variations not only affected the values of the soil hardpan attributes (peak cone index and depth to the peak cone index) but also their estimated spatial structures which in turn may affect the prediction and soil sampling procedure.

Generally the spatial distribution pattern of the soil hardpan depths within the field seems similar as predicted by the depth to the maximum bulk density or the depth to the peak cone index values. Contour maps of peak cone index values indicate that most part of the field requires deep tillage. The depths of tillage, however, need to vary according to the predicted soil hardpan depths. This indicates that applications of depth-specific tillage on Pacolet sandy loam soils may improve the sustainability of crop management.

References

ASAE Standards, 46 Ed. 1999a. S313.3. Soil cone penetrometer. St. Joseph, Mich.: ASAE.

ASAE Standards, 46 Ed. 1999b. EP542. Procedures for using and reporting data obtained with the soil cone penetrometer. St. Joseph, Mich.: ASAE.

Busscher, W.J., Bauer, P.J., J.R. Frederick. 2005. Deep tillage management for high strength southeastern USA Coastal Plain. Soil Till.Res. (in press).

Camp, Jr. C. R. and Z. F. Lund. 1968. Effect of mechanical impendence on cotton root growth. Trans. ASAE: 189-190.

Donald R.N. and Ole, W. 2003. Spatial and temporal statistics. Sampling field soils and their vegetation. Catena Verlag GMBH, 35447 Reiskirchen, Germany.

Fulton, J. P., L. G. Wells, S. A. Shearer, and R. I. Barnhisel. 1996. Spatial variation of soil physical properties: a precursor to precision tillage. ASAE Paper No. 96-1002. St. Joseph, Mich.: ASAE.

Gill, W.R. 1968. Influence of compaction hardening of soil on penetration resistance. Trans. ASAE: 11 (6), 741-745.

Gill, W.R. and G.E. VandenBerg. 1968. Soil dynamics in tillage and traction. Agriculture Handbook No. 316. USDA-Agricultural Service, Washington. D.C.

Gorucu, S., A. Khalilian, Y.J. Han, R.B. Dodd, F.J. Wolak, and M. Keskin. 2001. Variable depth tillage based on geo-referenced soil compaction data in Coastal Plain region of South Carolina. ASAE Paper No. 011016. St. Joseph, Mich.: ASAE.

Isaaks, E.H. and R.M. Srivastava. 1989. An introduction to applied geostatistics. Oxford University Press, Inc. New York, New York.

Kenan K., E. Özgözb, and F. Akba¸s. 2003. Assessment of spatial variability in penetration resistance as related to some soil physical properties of two fluvents in Turkey. Soil Till.Res. 76, 1-11.

Mulqueen, J., J. V. Stafford, and D.W. Tanner. 1977. Evaluation of penetrometers for measuring soil strength. Journal of Terramechanics. 14, 137-151.

Naiqian, Z., M. Wang and N. Wang. 2002. Precision agriculture-a worldwide review. Computers and Electronics in Agriculture. 36, 113-132.

Perumpral, J.V. 1987. Cone penetrometer applications-A review. *Trans. ASAE* 30(4):939-944.

Raper, R. L., B. H. Washington, J.D. Jarrell. 1999. A Tractor - Mounted – Multiple probe - Soil Cone - Penetrometer. App. Eng. Agr. 15(4), 287-290.

Raper, R.L., D.W. Reeves, and C.H. Burmeste and E.B. Schwab. 2000. Tillage depth, tillage timing and cover crop effects on Cotton yield, soil strength and tillage energy requirements. App. Eng. Agr. 16(4), 379-385.

Raper, R. L., D.W. Reaves, J.N. Shaw, E. van Santen, and P.L. Mask. 2004a. Site-specific subsoiling benefits for coastal plain soils. 26 th Southern Conservation Tillage Conference, Raleigh, NC, June 8-9, 2004.

Raper, R.L., E. B. Schwab, and S.M. Dabney. 2005. Measurement and variation of site-specific hardpans for silty upland soils in the Southeastern United States. Soil Till. Res.84, 7-17.

Sanglerat, G. 1972. Interpretation of penetration diagrams- theory and practice. Developments in geotechnical engineering. Elsevier publishing company. Amsterdam, The Netherlands.

SAS/STAT. 1999-2001. Cary, N.C.: SAS Institute Inc.

Siri, G.P., D.W. Reeves, J.N. Shaw, and C.C. Mitchell. 2002. Impact of conservation tillage on soil carbon in the 'Old Rotation'. In: Proc. of 25th Annual Southern Conservation Tillage Conference for Sustainable Agriculture. June 24-26, 2002, Auburn, AL.

Soane, B. D., and C. Van Ouwerkerk. 1994. Soil compaction problems in world agriculture. In Soane, B. D., and C. Van Ouwerkerk. (Eds)., *Soil Compaction in Crop Production.* Amsterdam, The Netherlands, Elsevier.

Taylor, H. M. and Gardner, H. R. 1963. Penetration of cotton seedling taproots as influenced by bulk density, moisture content and strength of soil. Soil Sci. 96,153-545.

Tekeste, M.Z., Raper, R.L., Schwab, E.B. 2004. Effects of soil drying on soil cone penetration resistance for Norfolk Sandy Loam soils. In: Proceedings of the 7th International Conference on Precision Agriculture, July 25-28, 2004, Minneapolis, Minnesota.

CHAPTER 5

Finite Element Analysis of Cone Penetrometer for Predicting Soil Hardpan Attributes as influenced by Soil Moisture, Soil Density, and Cone Material[3]

[3] Mehari Z. Tekeste, Randy L. Raper, Ernest W. Tollner, Thomas R. Way submitted to the *Transactions of the ASABE.*

Abstract. *An accurate soil hardpan determination is important for maximum precision tillage performance. Soil cone penetrometer data are often analyzed to predict soil hardpan depths. The prediction in layered soils may be limited due to the complexity of soil reaction to cone penetration. An axisymmetric finite element (FE) model was developed to investigate soil hardpan predictions and soil deformation failures on a layered Norfolk sandy loam soil. The soil was considered as a non-linear elastic-plastic material modeled using a constitutive relationship from Drucker-Prager model with the Hardening option in ABAQUS, a commercially available FE package. ABAQUS/Explicit was used to solve the simulation of soil-cone contact pair interaction using a frictional property. The results showed that the FE model captured the soil cone penetration trend in layered soil with two deflection points indicating the start of the hardpan and the peak cone penetration resistance. The FE model predicted hardpan depth (8.62 cm) was less than the cone penetrometer predicted depth (11.03 cm). Soil moisture, bulk density and cone material significantly affected the FE and cone penetrometer predicted soil hardpan depths. The simulation also showed soil deformation zones about 3 times the diameter of the cone developed around the advancing cone.*

Keywords. *Soil hardpan, cone penetrometer, Finite Element, soil-cone interaction.*

INTRODUCTION

Soil compaction impedes root growth and reduces soil aeration and water infiltration, which consequently affects crop production systems in Southeastern US soils (Raper et al., 2004). Soil compaction can be measured using a soil-cone penetrometer, an instrument that measures insertion force of a cone into the soil (ASAE, 1999a; ASAE, 1999b). As a part of site-specific soil compaction management, the depth and magnitude of the root-restricting layer, commonly referred to as soil hardpan is predicted from the cone penetrometer data analysis. The reaction of the soil to cone penetration involves a combination of cutting, compression, shear or plastic failures, or any combination of these (Gill and VandenBerg, 1968). As the cone advances into the soil, it is generally assumed that the cone penetration force estimates the relative soil strength at a particular depth. Researchers have shown that the point cone penetration force is influenced by the soil properties in the zone of influence (Gill, 1968; Sanglerat, 1972; Mulqueen et al., 1977; Lunne et al., 1997; and Susila and Hryciw, 2003). According to Lunne et al. (1997), the zone of influence depends on layering and soil material stiffness that it can reach up to 10 to 20 times the cone diameter for stiff soil material. Mulqueen et al. (1977) and Gill (1968) had also shown that a soil wedge formed in front of the cone could erroneously increase the cone index reading.

Associated with a complex soil - cone penetrometer interaction, errors could occur in interpreting cone force – depth data that could affect the accuracy of soil hardpan detection for precision tillage. In using soil cone penetrometer to detect soil hardpan depths, a study on the dynamic response of soil to cone penetration is important to evaluate the versatility of the tool in precision tillage applications. Various approaches (Farrell and Greacen, 1965; and Rohani and Baladi, 1981; and Yu and Mitchel, 1998) have been considered to study the soil mechanical

responses during soil cone penetration including (1) bearing capacity theory; (2) cavity expansion theory; (3) steady state deformation; (4) finite element (FE) analysis; and (5) laboratory experimental methods. Most of these approaches used analytical methods whereby first a certain shape of soil failure surface was assumed and then limit equilibrium of forces over the soil-tool system was solved. Analytical approaches could have limitations to explain soil dynamic responses in cone penetration especially in layered and non-homogenous soil conditions because of the difficulty in pre-defining the soil failure shape and complexity of force equilibrium analysis.

With the availability of powerful machines of high computation speeds and FE packages that contain advanced material models, the FE method can be implemented in solving the soil cone penetration problem. FE analysis was previously used to model soil cone penetration with limited success (Markauskas et al., 2002 and Foster et al., 2005). Markauskas et al. (2002) used static elastic-plastic small strain FE analysis on sandy and clayey soils with Mohr-Columb and Tresca yield criteria, respectively. The simulation modeled a cone (60-deg and diameter, d = 35.7mm) displacement (u) of 0.2d. They also determined numerically the vertical (H=11.2d) and horizontal (D=35d) dimensions of the zone influenced during cone penetration. The small strain assumption as opposed to the large deformation property of soil material was a problem in their analysis. The authors have not attempted to compare the FE predicted forces with an experimentally measured cone penetration resistance. Soil cone penetration in a sandy loam and a clay loam soil was also modeled using the MSC/DYTRAN FE software by Foster et al. (2005). Their constitutive material parameters were estimated using the National Soil Dynamics Laboratory and Auburn University (NSDL-AU) soil compaction model. The FE force predicted for both soil types appeared to capture the general trend of measured cone force data but the

predicted force values had large fluctuations. Statistical comparisons were not carried out with the experimentally measured soil cone penetration resistance forces to evaluate the performance of the FE analysis.

Research on FE analysis is, thus, needed to explain the soil failure pattern in cone penetration and evaluate the FE method in predicting the magnitude and depth of soil hardpan as influenced by soil factors (soil moisture content and bulk density) and cone material properties in layered soils.

Our understanding of soil hardpan layer prediction could be improved for Norfolk sandy loam soil as a soil drying front moves downward in conditions similar to field soils by studying the soil response to cone penetration using the FE method.

Therefore, our objectives were, to:

- Develop FE procedure for soil cone penetration, and
- Determine the effects of soil moisture content and bulk density on FE predicted magnitude and depth of soil hardpan.

MATERIALS AND METHODS

MATERIAL PARAMETERS FOR SOIL CONSTITUTIVE MODEL

Soil was assumed as a continuum non-linear elastic-plastic material that exhibited material hardening. The soil constitutive relationship was defined using the linear form of the extended Drucker-Prager material model with a material hardening option (ABAQUS, 2004). The extended Drucker-Prager model has the capability to model frictional materials such as soil in which compressive yield strength was greater than the tensile strength and exhibited pressure-dependent yield. The Drucker-Prager model has been used to solve soil tillage (soil-tool

interaction) problems (Mouazen and Ramon, 2002 and Upadhyaya et al., 2002). The linear Drucker-Prager form requires bulk density (ρ), Young's modulus (E), Poisson's ratio (ν), angle of internal friction (ϕ), yield stress ratio in triaxial tension to triaxial compression (K) and dilation angle (ψ) for the plastic flow. Typical values of K are $0.778 \leq K \leq 1.0$ (ABAQUS, 2004). A value of K=1 was assumed during the analysis which implied that the yield surface was the von Mises circle in a deviator principal stress plane. In the associated plastic flow of the linear model, ψ=β where tan (β) was the slope in the deviator stress plane. A dilation angle (ψ) of 38^{0} was estimated from the octahedral shear stress versus octahedral normal stress of the NSDL-AU soil compaction model. A constant Poisson's ratio of 0.3 was assumed in the analysis. The NSDL-AU constitutive soil model that was developed for compactable agricultural soils subjected to different stress paths under unsaturated soil conditions was used to estimate soil mechanical parameters and the tabular data for the Drucker-Prager Hardening option. The soil mechanical parameters of NSDL-AU model are shown in table 1.

According to Bailey and Johnson (1989 and 1996), the stress-strain relationship of the NSDL-AU soil compaction model was defined using:

$$\bar{\varepsilon}_v = (A + B\sigma_{oct})(1 - e^{-C\sigma_{Oct}}) + D(\tau_{oct} / \sigma_{oct}) \quad (1)$$

Where the natural volumetric strain was defined as

$$\bar{\varepsilon}_v = \ln(V/V_o) = \ln(\rho_o / \rho) \quad (2)$$

Where:

$\bar{\varepsilon}_v$ = natural volumetric strain.

σ_{oct} =octahedral or mean normal stress [$\sigma_{oct} = (\sigma_1+\sigma_2+\sigma_3)/3$].

τ_{oct} = octahedral shear stress [$\tau_{oct} = [(\sigma_1-\sigma_2)^2 + (\sigma_2-\sigma_3)^2 + (\sigma_1-\sigma_3)^2]^{1/2}/3$].

V= volume at stress state.

V_o = initial volume.

ρ= dry bulk density at stress state.

ρ_o = Initial dry bulk density.

A, B, C and D were compactibility coefficients for a specific soil at a specific soil moisture content.

Bailey and Johnson (1989 and 1996) also assumed a linear relationship between the total natural volumetric strain and the natural plastic volumetric strain according to:

$$d\bar{\varepsilon}_v^{p} = \alpha\, d\bar{\varepsilon}_v \qquad (4)$$

Where: $\bar{\varepsilon}_v^{p}$ = natural plastic volumetric strain. α = constant.

The coefficients of the NSDL-AU soil model (eq. 1) for Norfolk sandy loam soil was developed at specific soil moisture content (6.3% d.b.). Modification of the stress-strain relationship was needed to account for different soil moisture contents. Johnson (personal communication, October 2004) suggested a relationship between the bulk density ratios of triaxial tests and Proctor Density curves. He proposed that the ratio of bulk density at soil moisture content (6.3% d.b.) to a bulk density at different soil moisture content of the same tri-axial stress test may be related to the bulk density ratios estimated from the Proctor Density curve at the corresponding soil moisture content. Mathematically the ratio of bulk density is expressed as:

$$\left[\frac{\rho_x}{\rho_i}\right]_\sigma \propto f\left\{\left[\frac{\rho_x}{\rho_i}\right]_{PD}\right\} \quad (5)$$

Where:

$\left[\frac{\rho_x}{\rho_i}\right]_\sigma$ = Dry bulk density ratios at tri-axial stress state for new soil moisture content (x) to soil moisture content (i) of 6.3% d.b.

$\left[\frac{\rho_x}{\rho_i}\right]_{PD}$ = Dry bulk density ratios from Proctor Density curve for new soil moisture content (x) to soil moisture content (i) of 6.3% d.b.

The relationship in equation (5) was evaluated using data from triaxial tests (Bailey, 2004) and from a Proctor Density curve (Grisso, 1985). A linear relationship of observed dry bulk density and predicted dry bulk density (ρ_x) for the Norfolk sandy loam soil was statistically tested using SAS (SAS. Release 8.02 SAS Institute Inc., Cary, NC, 2001). Based on the bulk density ratio relationships, the natural volumetric strain values for different soil moisture contents were estimated using;

$$\bar{\varepsilon}_{vx} = \bar{\varepsilon}_v + \ln\left(\frac{\rho_i}{\rho_x}\right)_{PD} \quad (6)$$

Where: $\bar{\varepsilon}_{vx}$ = Natural volumetric strain at new soil moisture content (x).

Tabular data of hydrostatic yield stress vs. volumetric plastic strain for the Drucker-Prager Hardening option was determined from the natural volumetric stress-strain relationship (eq. 6). The relationship defined in equation (4) was used to obtain the volumetric plastic strain values for the tabular data. Tangential Young's modulus values were estimated from the stress-strain graphs. The mean of the estimated tangential Young's modulus was used in the FE

analysis. The wet bulk density and soil moisture contents were obtained from experiments conducted in a soil column. The soil layers varied in wet bulk density and soil constitutive material parameters.

FE Problem Formulation and Procedures

FE analysis of an axisymmetric soil cone penetration problem was carried out using ABAQUS commercially available software (ABAQUS, 2004). The FE analysis was performed in three stages: pre-processing and post-processing using ABAQUS/CAE, and simulation using ABAQUS/Explicit. The ABAQUS/CAE environment comprised modules that interacted with ABAQUS/Explicit and performed the preprocessing stage including the FE geometry, specification of material properties, assembling the geometries, defining analysis steps and surface interactions, loading, boundary conditions and mesh generation. The ABAQUS/Explicit was a valuable method for quasi-static dynamic analysis and solved contact problems such as the soil cone penetration at a reduced computational time. The outputs and visualization of results were monitored in the post processing stage using the visualization module of ABAQUS/CAE.

The model was separated into two bodies, a deformable soil and a rigid cone (Fig. 1). The soil had a radius of 10.6 cm and was 22.9 cm in height. The soil body was partitioned into three layers varying in thickness similar to the soil column study: above (5.08 cm), within (2.54 cm) and below (15.2 m) soil hardpan. For each soil layer, there were separate material constitutive parameters and a table of hydrostatic yield stress vs. volumetric plastic strain. The entire soil body was meshed using a 4-node bilinear axisymmetric quadrilateral shell element with a reduced integration and hourglass control (CAX4R). The entire soil body was seeded with equal edge mesh size (0.5 x cone radius). A mesh size of the soil brick elements was smaller than the cone radius to meet the master-slave surface contact algorithm in ABAQUS/ Explicit. The

boundaries on the right and bottom edges of the axisymmetric soil model were constrained in the radial (U1) and vertical (U2) translational degrees of freedom respectively (Fig. 1). The topsoil surface where the cone penetrates was not constrained.

The cone (30^0 and base diameter, d =1.28 cm) was defined as a discrete rigid body elastic material (Young's modulus, E=193050 MPa and Poisson's ratio, ν=0.3) and modeled by a 2-node linear axisymmetric element (RAX2). A reference node was attached at the center of mass of the cone to govern the motion of the cone. Displacement (U2 = -14.0 cm) was prescribed at the reference node to simulate the cone penetration rate of 1.65 cm/s. A similar insertion rate was used when taking soil cone penetration readings in the laboratory for the FE model verification. The machine (Sintech/2G) that was used to insert the soil cone penetrometer supported a maximum rate of 1.69 cm/s. The shaft of the soil cone penetrometer was not included in the model because it is generally assumed that the force contribution from the shaft is small. The soil-cone interaction was simulated by element based surface pair contact between the rigid cone body (master surface) and the deformable soil (slave surface) with a friction property. Stainless steel (Metal), Teflon coated stainless steel (TMetal) and Teflon cone materials were modeled by specifying different values of soil-tool coefficient of friction. The cone motion was constrained from moving in the radial direction.

Equivalent plastic strain and stress variables were requested at 0.001 s interval. The resultant contact forces between the cone and the soil layers and a vertical displacement (U2) of the referenced node were also requested to simulate the cone penetration forces and displacement.

EXPERIMENT FOR VERIFICATION OF FE PREDICTION OF SOIL HARDPAN ATTRIBUTES

A soil cone penetration experiment was conducted to verify the FE prediction of soil hardpan attributes. Soil for the experiment was obtained from the Norfolk sandy loam (*Typic Paleudults*) soil bin in the NSDL in Auburn, AL. The Norfolk sandy loam particle size distribution was 72% sand, 17% silt and 11% clay (Batchelor, 1984). Two millimeter sieved soil samples were brought to a soil moisture content of 5% d. b. and kept in tight plastic bags for a week to equilibrate the soil moisture. Three layers of soil [above, within and below the soil hardpan] that varied in bulk density were created in a cylinder (20 cm diameter X 28 cm height) by applying axial loading using a rigid cylinder piston. The experiment was carried out using a split plot design with three replicates. Bulk density (within hardpan) was a main plot treatment. Soil moisture was a subplot treatment. Cone material type was a sub-sub plot treatment. The soil column samples were first wetted to near saturation and put in a greenhouse located at the NSDL until the soil moisture suction measured using tensiometers at the hardpan depth reached 10 kPa (soil moisture level I) and 60 kPa (soil moisture level II). Once the soil samples reached the target soil moisture levels, cone penetration readings were taken using soil cone penetrometer with a randomly selected cone material of Metal, TMetal and Teflon.

A separate experiment was conducted with three replicates to determine the soil-tool [Metal, TMetal and Teflon] coefficients of friction according to the Coulomb friction criterion. Soil samples (2 mm sieved) equilibrated to 5% and 10% (d.b.) soil moisture contents were filled in a wooden box. For each soil moisture content, the soil was compressed to two bulk densities (1.22 and 1.67 Mg m^{-3}). A bar (0.6 cm thickness, 15 cm length and 15 cm width) made of Teflon, Stainless Steel and Teflon-coated steel was laid on top of the soil. For the Teflon coated stainless steel, dry powder Teflon (® Fluorotelometer powder) was sprayed on a stainless steel piece and

dried before taking a measurement. The pull force required to slide the bar in the soil-tool interface with a normal weight of 2, 11 and 22 kg on top of the bar was measured using a load cell. The coefficients of soil-material friction were determined by estimating the slope of a linearly fitted line to the normal force vs. average sliding force data.

DATA ANALYSIS

Treatment effects of soil moisture, bulk density and cone material on FE prediction of the magnitude and depth of a soil hardpan were analyzed using appropriate statistical procedures in SAS (SAS. Release 8.02 SAS Institute Inc., Cary, NC, 2001). Similarly, FE predictions of the soil hardpan were compared with the soil cone penetrometer data analysis method. An F-test statistic with an alpha (α) level of 0.05 was used for all treatment and method comparisons.

RESULTS AND DISCUSSION

The bulk density within the hardpan was used to classify the three compaction treatments, namely compaction I, compaction II and compaction III. The bulk density in the compaction II and compaction III treatments were significantly greater than the above and below hardpan positions ($P < 0.0001$). To investigate the effects of soil parameters on FE prediction, statistical analyses were performed for only the compaction II (1.64 Mg m $^{-3}$, within soil hardpan) and compaction III (1.71 Mg m $^{-3}$, within soil hardpan) because no statistical variations in bulk density values were observed among the soil layers for compaction I.

A linear relationship was observed between the predicted bulk density from equation (5) and the observed bulk density from tri-axial stress test with high correlation coefficient ($r^2 = 0.96$) and 99 % confidence intervals of [–0.14, 0.02] and [0.97, 1.07] for the intercept and slope, respectively. For the FE analysis, the bulk density values (Table 2) that were obtained in the soil

column study were used for the bulk density (ρ_x) in equation (6) to determine the natural volumetric strains. The stress-strain relationships for the three layers of the three compaction treatments were shown in figure 2. The differences in bulk density values were manifested in the stress-strain relationships. The natural volumetric strains for the within hardpan layer were smaller than the above and below hardpan (Fig. 2 (B and C)). Tangential Young's modulus values were estimated from each of the curves in figure 3. The mean value of the tangential Young's modulus for each soil layer was estimated for use in the FE analysis.

SOIL HARDPAN ATTRIBUTES PREDICTION USING CONE PENETROMETER AND FINITE ELEMENT

The FE simulation had a similar trend to the penetration resistance forces of the cone penetrometer readings (Figs. 3 and 4). The FE predicted contact forces had oscillatory responses typically occurring in ABAQUS/ Explicit simulation. A moving average filtering technique was performed on the FE data to remove noise. After data smoothing, the FE trend showed two deflection points, one near the start of the soil hardpan and another one near the peak cone penetration force. For most treatment conditions, contact forces obtained with the FE analysis overestimated and underestimated the soil cone penetration resistance forces for soil moisture level II (4.17% d.b.) and level I (8.78% d.b.), respectively (Figs. 3 and 4). FE force data values observed in this study appear to be similar to the force data reported by Foster et al. (2005) for Norfolk sandy loam soil. The large differences in the FE force values and cone penetrometer data could possibly be due to the fact that the FE model may not account for all soil failure modes (shear, tensile and cutting) that occurred during cone penetration because the soil constitutive model used in the analysis incorporated only the hydrostatic compaction behavior. A constant Poisson's ratio assumption may also be another possible reason for the differences.

Results for the depth to the peak cone penetration forces predicted by the FE method and cone penetrometer were statistically compared. The FE predicted soil hardpan depths (8.62 cm) smaller than the cone penetrometer method (11.03 cm) ($P < 0.0001$).

The influences of soil parameters on the prediction of soil hardpan depths were analyzed separately for FE and cone penetrometer methods. In both methods, the peak or the deflection point in the force readings occurred below the soil hardpan thickness measured in the laboratory experiment (Table 5, depth to the top hardpan + hardpan thickness). The soil moisture content and cone material strongly affected the cone penetrometer prediction of soil hardpan depths. There were no interaction effects of soil moisture content and cone material on the predicted depths. The mean soil hardpan depth in the wet soil condition (8.78% d.b.) was 11.01 cm and in the dry (4.17% d.b.) the depth was 8.32 cm. Varying the coefficient of soil-tool frictions (Table 4) also affected the soil hardpan depth prediction with the depth from the cone made from Metal (7.19 cm) being shallower than TMetal (9.96 cm) and Teflon (11.86 cm) ($P < 0.0001$). When a Teflon cone was used, the predicted depth increased by 65 % as compared to the ASAE standard stainless steel (Metal) cone.

Similarly the FE predicted soil hardpan depths were affected by the soil moisture contents, soil bulk density, cone material and their interactions ($P < 0.0001$). The FE predicted depth for the dry soil moisture conditions (9.14 cm) was greater than for the wet soil moisture conditions (7.54 cm). This was contrary to the cone penetrometer prediction of the soil hardpan depth that soil drying decreased the predicted depth. The reason for this was not determined. The FE predicted soil hardpan depths varied statistically by the soil-tool friction property (Teflon 8.68 cm, Metal 8.27 cm, TMetal 8.07 cm).

Stress and soil deformation patterns

The FE results showing the soil responses to the cone penetration are shown in figure 5 (A and B). The element on the surface rose up as the cone advanced into the soil. The stress concentration near the rigid cone body was highest near the cone and decreased as the radial distance from the cone increased. The stress and deformation distribution showed the effect of friction that as the coefficient of friction for metal cone was used, the stress and plastic strain ranges were higher as compared to the range for soil-teflon and soil-Tmetal (figure not shown). The plastic zone extended nearly three times the diameter of the cone suggesting that the cone penetration resistance force was a measure of soil reaction within the zone of influence.

CONCLUSIONS

From the finite element analysis of cone penetration on Norfolk sandy loam soil in predicting soil hardpan, the following conclusions were drawn.

1). The finite element procedure was successfully developed in ABAQUS to simulate soil cone penetration in a layered Norfolk sandy loam soil that varied values in soil moisture content and bulk density.

2). In both the FE and cone penetrometer methods, when metal was used ($\mu_{soil\text{-}metal} = 0.50$) the predicted depth was shallower than when Teflon ($\mu_{soil\text{-}Teflon} = 0.31$) cone material was used.

3). In dry soil moisture condition (4.17% d.b.), the soil hardpan was predicted at shallower depth using a cone penetrometer than at wet soil moisture condition (8.78% d. b.).

4). Use of a finite element analysis that accounts for the confining and shearing stresses of the NSDL-AU soil model and assuming variable Poisson's ratio may further improve the prediction of cone penetration force values.

ACKNOWLEDGEMENTS

The authors would like to acknowledge the contribution of Dr. Clarence Johnson of Auburn University and Dr. Alvin Bailey of the USDA-ARS-NSDL at Auburn, AL for their suggestion on NSDL-AU soil compaction model modifications and provision of tri-axial stress data.

Table 1. Soil parameters and coefficients of the NSDL-AU soil compaction model for Norfolk sandy loam soil.

	Soil moisture (% d.b.)	Initial bulk density (Mg m^{-3})	Poisson's ratio υ	Soil-soil material angle of friction [a]	A [b]	B (kPa^{-1})	C (kPa^{-1})	D	α [c]
Value	6.3	1.35	0.3	58°	-0.241	-0.0002	0.0126	-0.1122	0.926

[a] Material angle of friction for Norfolk sandy loam soil from Chiroux et al.(2005).

[b] A, B, C and D are model coefficients for the NSDL-AU soil compaction model from Bailey and Johnson (1989).

[c] α is the slope of a straight regression line fit to data in a graph of the plastic natural volumetric strain as a function of total natural volumetric strain, from Foster et al. (2005).

Table 2. Dry bulk density from the laboratory experiment at three positions (above, within and below the hardpan) for three compaction levels of Norfolk sandy loam soil.

	Compaction I			Compaction II			Compaction III		
	Mean	SD	95 % Confidence Interval	Mean	SD	95 % Confidence Interval	Mean	SD	95 % Confidence Interval
					Mg m				
Above Hardpan	1.32	0.08	1.28-1.36	1.27	0.09	1.22-1.31	1.27	0.08	1.23-1.31
Within Hardpan	1.32	0.09	1.28-1.36	1.64	0.11	1.59-1.68	1.71	0.09	1.66-1.75
Below Hardpan	1.25	0.04	1.23-1.27	1.48	0.06	1.46-1.51	1.54	0.06	1.51-1.57

Table 3. Soil moisture at three positions (above, within and below the hardpan) at the two soil moisture levels and three compaction levels of Norfolk sandy loam soil.

	Soil Moisture Level I						Soil Moisture Level II					
	Compaction I		Compaction II		Compaction III		Compaction I		Compaction II		Compaction III	
	Mean	SD	Mean	SD	Mean	SD	Mean	SD	Mean	SD	Mean	SD
	(% d.b)											
Above Hardpan	6.20	1.94	6.08	1.95	7.72	1.38	2.47	0.30	3.02	0.32	2.40	0.15
Within Hardpan	8.08	1.53	8.08	2.22	9.25	1.40	4.41	0.55	4.97	0.21	3.83	0.23
Below Hardpan	10.26	3.08	9.53	3.25	10.31	1.99	5.05	0.79	5.43	0.26	4.21	0.26

Table 4. Coefficient of friction for soil - cone materials (Metal, TMetal and Teflon) at two soil moisture contents and bulk densities of Norfolk sandy loam soil.

Soil Moisture	Bulk Density	Soil -Tool Friction Property					
(% d.b.)	(Mg m $^{-3}$)	μ_{Metal}	SD	μ_{TMetal}	SD	μ_{Teflon}	SD
5	1.22	0.37	0.03	0.27	0.03	0.33	0.01
	1.67	0.51	0.05	0.36	0.01	0.31	0.02
10	1.22	0.49	0.01	0.29	0.03	0.31	0.01
	1.67	0.62	0.01	0.35	0.04	0.3	0.01

Table 5. Actual depth to the top of the hardpan, hardpan thickness and below hardpan measured in soil layers in soil column.

	Compaction I			Compaction II			Compaction III		
	Mean	SD	95 % Confidence Interval	Mean	SD	95 % Confidence Interval	Mean	SD	95 % Confidence Interval
	cm								
Depth to Top Hardpan	2.53	0.15	2.46-2.60	5.15	0.48	4.92-5.36	5.28	0.4	5.08-5.48
Hardpan Thickness	5.07	0.34	4.92-5.22	4.09	0.28	3.97-4.22	3.92	0.22	3.81-4.03
Below Hardpan	18.67	0.59	18.39-18.94	15.87	1.12	15.36-16.38	15.19	0.56	14.91-15.47

Table 6. Cone penetrometer and FE predicted soil hardpan depth.

		Cone penetrometer predicted peak depth (cm)						FE predicted peak depth (cm)		
		Metal		Tmetal		Teflon		Metal	Tmetal	Teflon
		Mean	SD	Mean	SD	Mean	SD	Mean	Mean	Mean
		cm								
Soil Moisture Level I	Compaction I	6.32	2.42	12.64	1.76	13.74	0.72	11.3	11.8	11.3
(8.78 % d. b.)	Compaction II	9.06	1.37	10.31	1.39	13.42	0.72	6.82	7.09	7.76
	Compaction III	7.06	2.62	11.99	2.71	14.26	0.1	7.36	7.63	8.57
Soil Moisture Level II	Compaction I	11.63	1.91	9.72	0.89	8.88	0.15	6.28	7.09	7.36
(4.17 % d. b.)	Compaction II	6.36	0.04	8.54	0.23	10.01	0.63	9.66	9.12	9.12
	Compaction III	6.28	1.41	8.99	0.35	9.75	0.67	9.25	8.44	9.25

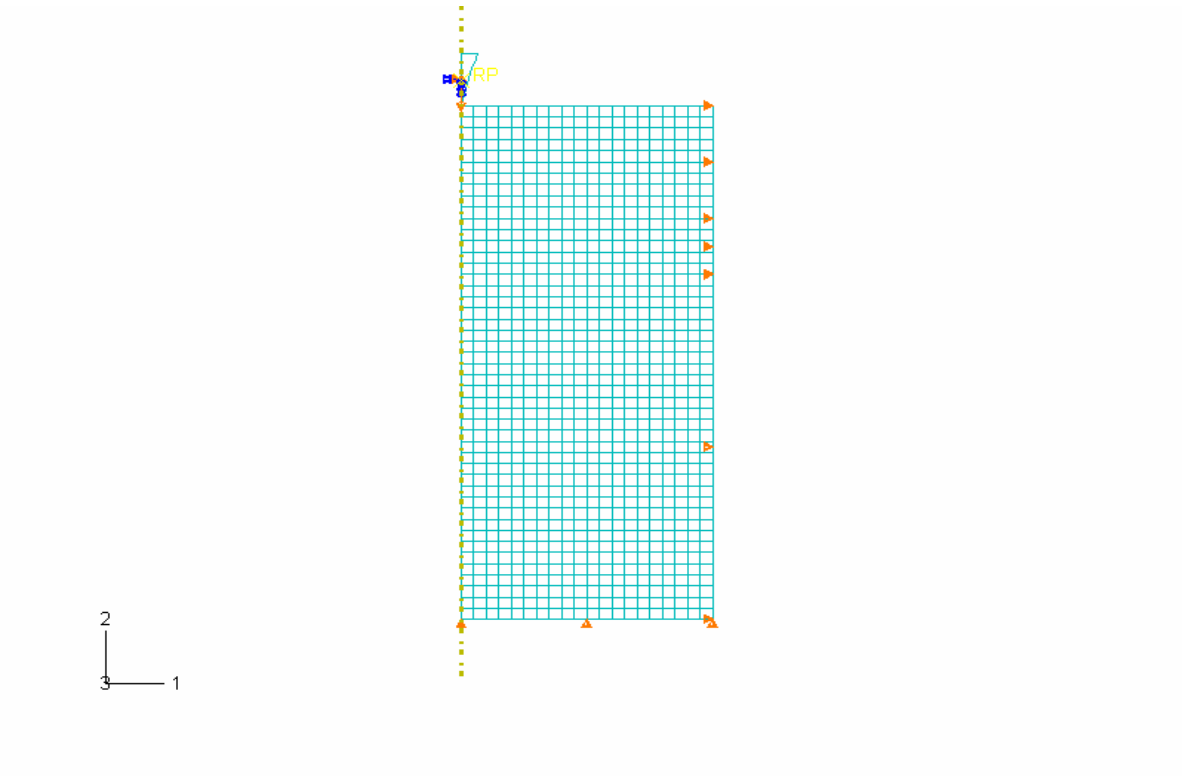

Figure1. Two-dimensional FE mesh of the soil and the cone. The arrows indicate boundary conditions that constraint the translational degrees of freedom of the left and bottom edges of the soil and governing the vertical motion of the cone.

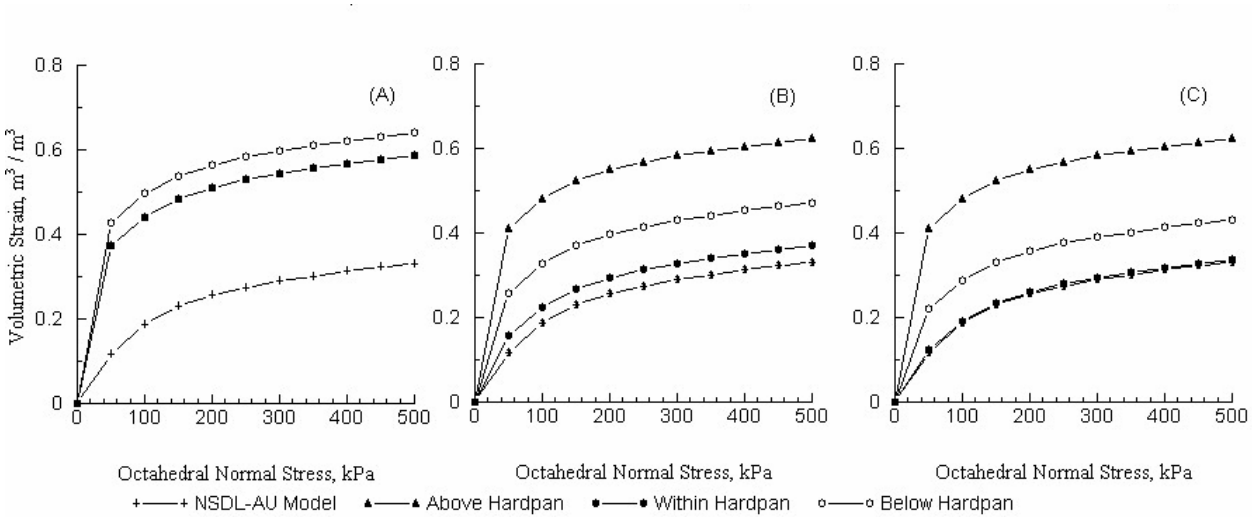

Figure 2. Natural volumetric strains vs. octahedral stress for compaction I (A), compaction II (B) and compaction III (C) and the three soil layer positions (Above, within and below hardpan).

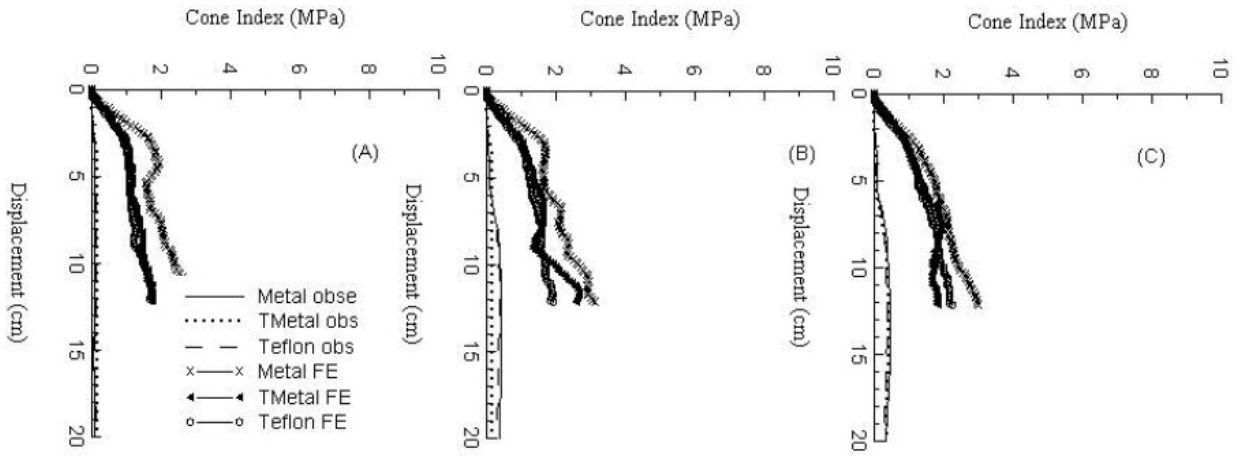

Figure 3. FE predicted versus (line and symbol) observed penetration resistance forces (line) for soil moisture level I (Wet) and for compaction I (A), compaction II (B) and compaction III (C) and cone material types.

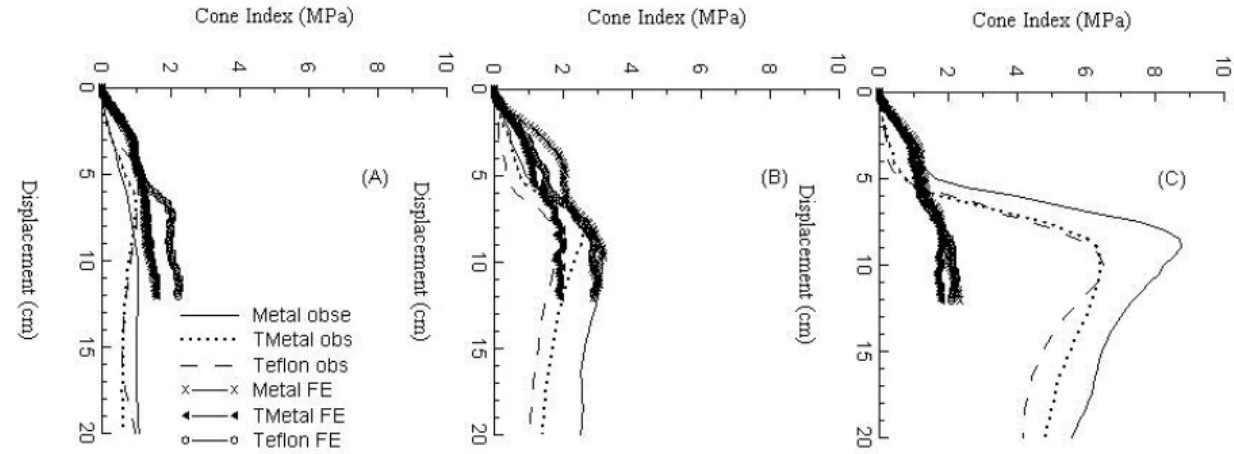

Figure 4. FE predicted (lines with symbols) vs. observed penetration resistance (lines) for soil moisture level II (Dry) and for compaction I (A), compaction II (B) and compaction III (C), and cone material types.

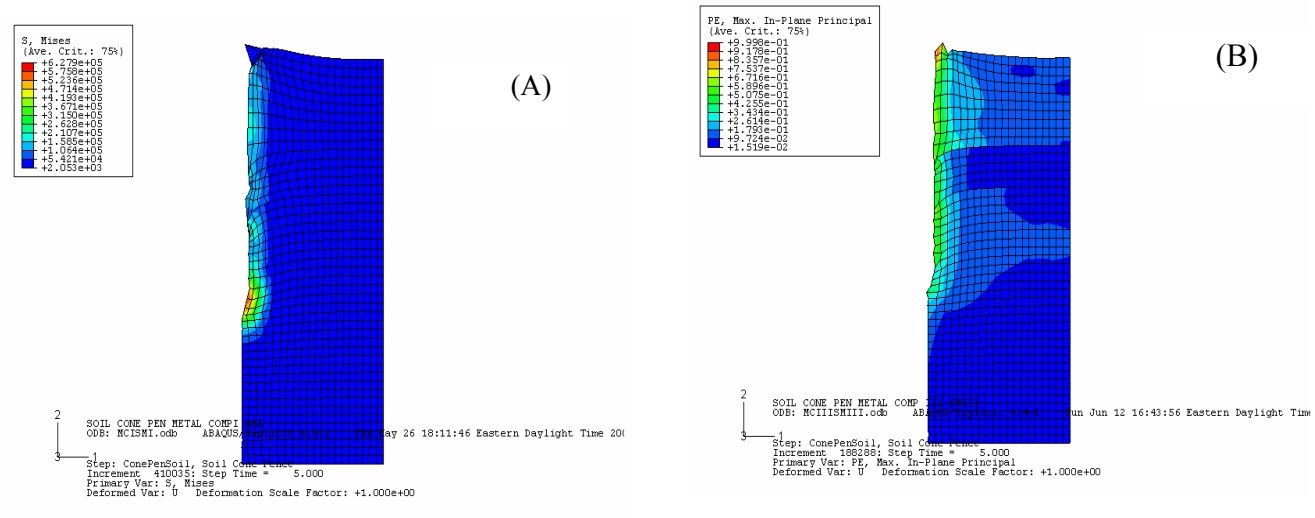

Figure 5. FE analysis results showing von Misses soil stress (A) and volumetric plastic soil strain (B) for Norfolk sandy loam soil during cone penetration.

REFERENCES

ABAQUS, Version 6.4. 2004. ABAQUS, Inc. U.S.A.

ASAE Standard, 46Ed. 1999a. S313.3. Soil cone penetrometer. St. Joseph, Mich.: ASAE.

ASAE Standard, 46Ed. 1999b. EP542. Soil cone penetrometer. St. Joseph, Mich.: ASAE.

Bailey, A.C. 2004. Unpublished data. Auburn, Ala.: USDA-ARS National Soil Dynamics Laboratory.

Bailey, A.C. and C. E. Johnson. 1989. A soil compaction model for cylindrical stress states. Transactions of the ASAE 32(3): 822 -825.

Bailey, A.C. and C. E. Johnson. 1996. Soil critical state behavior and the NSDL-AU model. ASAE Paper No. 96-1064. St. Joseph, Mich.: ASAE.

Batchelor, J. A. 1984. Properties of bin soils. National Tillage Machinery Laboratory, USDA-ARS, Auburn, AL.

Farrell, D.A. and E.L. Greacen. 1965. Resistance to penetration on fine probes in compressible soil. Division of Soils,CSIRO, Adelaide, Australia.

Chiroux, R.C., W.A. Foster Jr., C.E. Johnson, S.A. Shoop and R.L. Raper. 2005. Three-dimensional finite element analysis of soil interaction with rigid wheel. *Applied Mathematics and Computation*. 162:707-722.

Foster,Jr. W.A., C.E. Johnson, R.C. Chiroux and T.R. Way. 2005. Finite Element Simulation of Cone Penetration. Applied Mathematics and Computation 162: 735-749.

Grisso, R.D., Jr. 1985. Compaction of agricultural soil by continuous deviatoric stress. Unpublished Ph.D. Dissertation. Auburn University, AL.

Gill, W.R. and G.E. VandenBerg. 1968. Soil Dynamics in Tillage and Traction. Agriculture Handbook No. 316. USDA-Agricultural Research Service, Washington. D.C.

Johnson, C.E. and A.C. Bailey. 2002. Soil Compaction. In Advances in Soil Dynamics Vol. 2: 155-178. St. Joseph,Mich:ASAE.

Markauskas, D. , R. Kacianauskas, M. Suksta. 2002. Modeling the cone penetration test by the finite element method. Foundation of Civil and Environmental Engineering. No. 2. Poznan University of Technology,Poznan, Poland.

Mouazen, A.M. and H. Ramon. 2002. A numerical –statistical hybrid modeling scheme for evaluation of draught requirements of a subsoiler cutting a sandy loam soil, as affected by moisture content, bulk density and depth. Soil and Tillage Research 63:155-165.

Mulqueen, J., J. V. Stafford, and D.W. Tanner. 1977. Evaluation of penetrometers for measuring soil strength. *Journal of Terramechanics*. 14: 137-151.

Lunne, T., P.K. Robertson, and J.J.M. Powell. 1997. Cone penetration testing in geotechnical practices. Blackie academic and professional, London, UK.

Perumpral, J.V. 1987. Cone penetrometer applications-A review. Transactions of the ASAE 30(4):939-944.

Raper,R.L. and D.C. Erbach. Effect of variable linear elastic paratemeters on finite element prediction of soil compaction. Transactions of the ASAE 33(3):731-736.

Raper, R. L., D.W. Reaves, J.N. Shaw, E. van Santen, and P.L. Mask. 2004. Site-specific subsoiling benefits for coastal plain soils. 26 th Southern Conservation Tillage Conference, Raleigh, NC, June 8-9, 2004.

Rohani, B. and G. Y. Baladi. 1981. Correlation of mobility cone index with fundamental engineering properties of soil. International Society for Terrain-Vehicle Systems. Vol 3:959-990. Alberta,Canada.

Upadhyaya,S.K.,U.A. Rosa and D. Wulfsohn. 2002. Application of the finite element method in agricultural soil mechanics. In Advances in Soil Dynamics Vol. 2: 117-1153. St. Joseph,Mich:ASAE.

Sanglerat, G. 1972. Interpretation of penetration diagrams- theory and practice. Developments in geotechnical engineering. Elsevier publishing company. Amsterdam, The Netherlands.

Susila, E. and R. D. Hryciw. 2003. Large displacement FEM modeling of the cone penetration test (CPT) in normally consolidated soil. *Int. J. Numer. Anal. Meth.* Vol. 27:585-602.

Yu, H.S. and J.K. Mitchel.1998. Analysis of cone resistance: Review of Methods. Journal of Geotechnical and Geoenvironmental Engineering. Vol. 124:140-149. ASCE.

CHAPTER 6

Acoustic Compaction Layer Detection[4]

[4] Mehari Z. Tekeste (co-author), Tony E Grift, and Randy. L. Raper. Published in 2005 at the *Transactions of the ASAE*. 48(5):1-8

ABSTRACT. *The ASAE standardized tool to detect the depth and strength of compaction layers in the field is the cone penetrometer. Since this method is point-to-point, researchers have experimented with on-the-fly alternatives that can be used as, or in combination with, a standard tillage tool. On-the-fly compaction layer sensing also enables adaptive tillage, where the soil is only tilled as deep as necessary, which can lead to significant energy savings and erosion reduction. Wedged tips, strain gauges mounted on a deflecting tine, air bubbles pushed into the soil, as well as ground-penetrating radar have been tested for this purpose. In this research, passive acoustics was used to detect the compaction layer by recording the sound of a cone being drawn through the soil. The premise was that a more compacted layer should cause higher sound levels, which might reveal the depth and strength of the compaction layer. Two experiments were conducted in the soil bins of the USDA-ARS National Soil Dynamics Laboratory in Auburn, Alabama. First, constant-depth tests (15 and 30 cm) at three compaction levels (0.72, 2.8, and 3.6 MPa) revealed the relationship of sound amplitude with depth and compaction. Second, to test the detection capability, the cone was gradually inserted in the soil, passing through an artificial compaction layer. A windowed, short-time Fourier transform (STFT) analysis showed that the compaction layer is detectable since the sound amplitude was positively related to depth and compaction levels, but only in the highest frequency range of the spectrum. This led to the conjecture that the soil-cone interface acts as a low-pass filtering mechanism, where the cutoff frequency becomes higher in the compaction layer due to a more intimate contact between sensor and soil.*

Keywords. *Plow pan, Precision tillage.*

INTRODUCTION

Soil compaction, caused by either natural causes or human interference, is a major yield-limiting factor. This is because soil compaction: (1) reduces soil pore size, (2) changes pore size distribution, (3) increases soil strength, (4) reduces air and water permeability, (5) increases heat capacity and bulk density, and most importantly, (6) increases root penetration resistance (Al-Adawi and Reeder, 1996). Distinctively high-strength soil layers are commonly termed "hardpans" or "plow soles." Hardpans impede plant roots from uptake of nutrients and soil water reserves in the deeper soil strata. They also decrease water infiltration, which can accelerate loss of nutrients due to erosion and runoff. Under wet conditions, roots above the hardpan layer may suffocate due to water logging. The overall deterioration of soil quality due to compaction can result in a decrease of crop productivity and may increase the cost of fertilization.

Hardpan properties are not uniform across the field, but vary in depth and strength due to soil and crop factors, as well as farming and tillage practices (Clark, 1999; Fulton et al., 1996; Raper et al., 2001). Farmers often practice conventional subsoiling to mechanically disrupt the hardpan layer. This is done by adjusting the depth of the subsoiling implement at a uniform level, based on observational judgment and/or cone index measurements. Due to the depth variability of the hardpan, this means either that the compaction layer is not disrupted at all or that energy is wasted by tilling deeper than necessary. A "site-specific tillage scheme," where the tillage depth was adapted to the hardpan location, was investigated by Raper et al., (2003) and was found to yield energy savings of 25% compared to conventional tillage while the yield of corn (*Zea mays L.*) remained unaffected. To realize sensor-based, variable-depth subsoiling, instrumentation is needed that accurately measures the location of the hardpan and conveys this information to an

actuation mechanism. Map-based variable-depth subsoiling can then be implemented by adding positioning functionality such as a GPS.

Soil cone penetrometers, as standardized according to ASAE Standard S313.3 (*ASAE Standards*, 1999a), measure the soil penetration resistance as a function of depth to assess soil strength. The result is reported as the cone index (CI) according to ASAE Standard EP 542 (*ASAE Standards*, 1999b). The cone index is defined as the force required to insert the penetrometer probe into the soil divided by the cone base area. Raper et al., (1999) developed a tractor-mounted, multiple-probe soil cone penetrometer (MPSCP) with the capability of obtaining a set of five cone index measurements in a single insertion to improve the data acquisition speed. A major drawback of the cone penetrometer method is that it is strongly affected by other soil factors, such as water content, bulk density, and soil type (Ayers and Perumpral, 1982; Perumpral, 1987; Raper et al., 1999; Utset and Cid, 2001). Since the cone index measurement is based on vertical insertion of the probe, a stop-and-go sampling procedure is currently employed. This makes the procedure time consuming and difficult to implement in a continuous sensor-based variable-depth tillage practice. An alternative, as developed by Hall and Raper (2005), is termed the On-the-go Soil Strength Sensor (OSSS). This method used a wedge-shaped tip that was drawn horizontally through the soil, and the measured force on the tip resulted in the mechanical penetration resistance as a function of depth. The study reported that the wedge index (defined as the force divided by the wedge base area, similar to cone index) was less sensitive to water content variations than the standard cone penetrometer, and the data appeared to be correlated to bulk density and cone index. Chung and Sudduth (2003) have further explored the idea of using multiple horizontal penetrometers to estimate soil mechanical resistance at five depths. Adamchuk et al. (2001) used an array of strain gauges attached to the

backside of a vertical smooth blade to measure soil mechanical resistance at three depth intervals.

In this study, an alternative on-the-fly approach to hardpan location measurement was developed, based on measuring the sound level produced by a cone-shaped tip being drawn through the soil. Acoustics has been applied before to measure texture among four soil types (Liu et al., 1993). Oelze et al. (2002) measured the sound propagation velocity in soils and determined soil surface roughness using acoustic backscatter (Oelze et al., 2003).

In contrast to the on-the-fly methods discussed, the acoustic sensor (microphone) can be very small, which allows embedding into production tillage tines. In addition, since this study uses sound in the audible range (20 Hz to 20 kHz), inexpensive microphones can be used as a sensor. The premise behind the acoustic plow pan detection method was that the produced sound level is related to: (1) soil density, since more particles sliding across the cone surface will likely produce more sound, and (2) soil strength, since more energy is required to break up harder aggregates, also resulting in higher sound levels. Although water content was expected to have an effect on the acoustic measurement, it was kept constant and is recommended as a future research extension.

The objective of this study was to investigate whether a passive acoustic method is capable of detecting the location and strength of a hardpan under constant soil water levels.

MATERIALS AND METHODS

ACOUSTIC MEASUREMENT SYSTEM

The measurement system consisted of a tine with a cone containing a standard 8 mm condenser microphone (model 189958, Jameco Electronics, Belmont, Cal.) with a frequency range from 20 Hz to 20 kHz. The tine, cone, and microphone mounting are shown in figure 1.

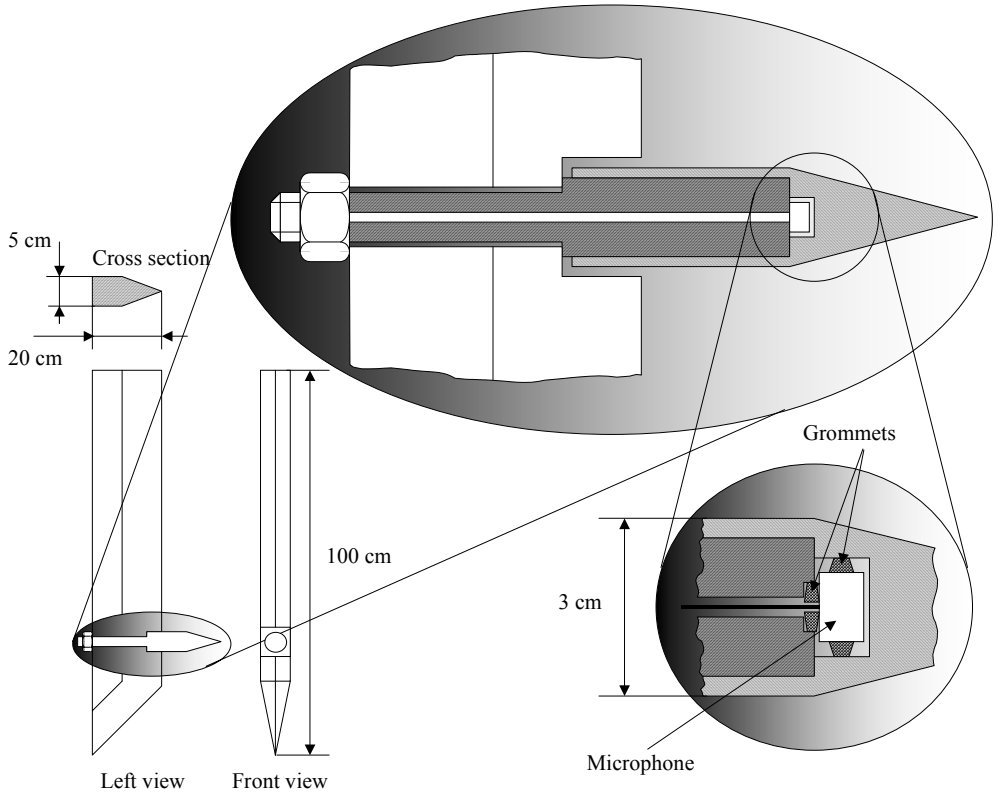

Figure 1. Tine (left) with mounted cone (top) and microphone in grommets (bottom right).

The tine has a sharp front edge, and the cone was mounted on a shaft that was bolted onto the tine. The shaft is hollow, which allows the electrical connections of the microphone to be passed through and fed upward through a protective conduit welded on the back of the tine. The microphone was mounted in rubber grommets to minimize contact sound transmitted through the tine. The data acquisition was performed using a portable computer with a built-in sound card controlled by MatLab's (2000) data acquisition toolbox. The sampling rate was set to 22,050 samples/second.

EXPERIMENTS

Before experiments in the soil, a dry run in air was made to obtain an indication of the noise that was detected by the microphone due to the tractor that drove the measurement cart. This was thought to be a good starting point for filtering the noise that would propagate into the soil.

During all experiments, the forward speed of the tine was kept constant at 0.44 m/s. To study the effects of depth and density on the acoustic signals, constant-depth experiments were carried out at 15 and 30 cm with a compaction layer located at 25.4 cm depth (fig. 2).

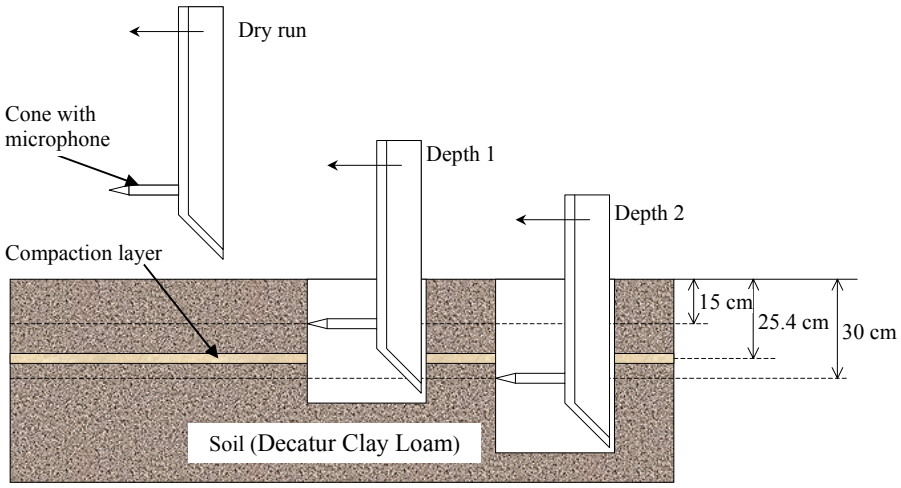

Figure 2. Constant-depth experimental arrangement, showing the two cone depths (15 and 30 cm) and the location of the compaction layer.

Before the start of the constant-depth experiments, a hole was dug and the sensor was lowered to the desired depth. The duration of the constant-depth experiments was 20 s, covering a distance of approx. 8.8 m.

To test whether the acoustic method is capable of detecting the location of a compaction layer, variable-depth experiments were conducted by starting the cone at the surface, followed by a gradual penetration into the soil, through the compaction layer, until a depth of 30 cm was reached (fig. 3).

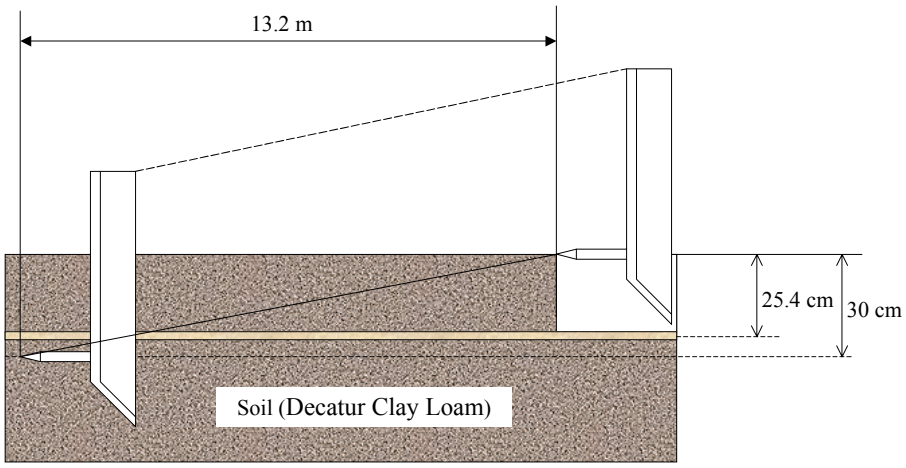

Figure 3. Variable-depth experimental arrangement, showing the sensor's gradual soil penetration.

The compaction layer was installed at a depth of 25.4 cm, and consequently the highest peaks in sound amplitude were expected towards the end of the run. The duration of the variable-depth experiments was 30 s, covering a distance of approx. 13.2 m.

SOIL PREPARATION

Experiments were conducted in a Decatur clay loam (rhodic Paleudults) soil bin located at the USDA-ARS National Soil Dynamics Laboratory in Auburn, Alabama. The soil bins are 7 m wide, 58 m long, and 1.5 m deep. The soil consisted of 26.9% sand, 43.4% silt, and 29.7% clay (Batchelor, 1984). The soil was wetted and mixed with a rotary tiller so that the entire soil bin attained a uniform soil water level. Three soil density levels were created by varying the number of times a compression wheel was used. "Single pass" density amounted to a forward and backward movement of a rigid wheel on the soil. For the "double pass" density, the "single pass" procedure was repeated. For the plots with "single pass" and "double pass" conditions, a hardpan was installed at a target depth of 25.4 cm. For the "no pass" density, no hardpan was installed. Finally, the soil surface was leveled using a blade. The soil bin was divided into two blocks, each consisting of three 12 × 4 m plots. Each plot was further divided into two equal subplots. Half of

the subplots were used for variable-depth experiments, and the remaining half for the 15 and 30 cm constant-depth experiments (fig. 4).

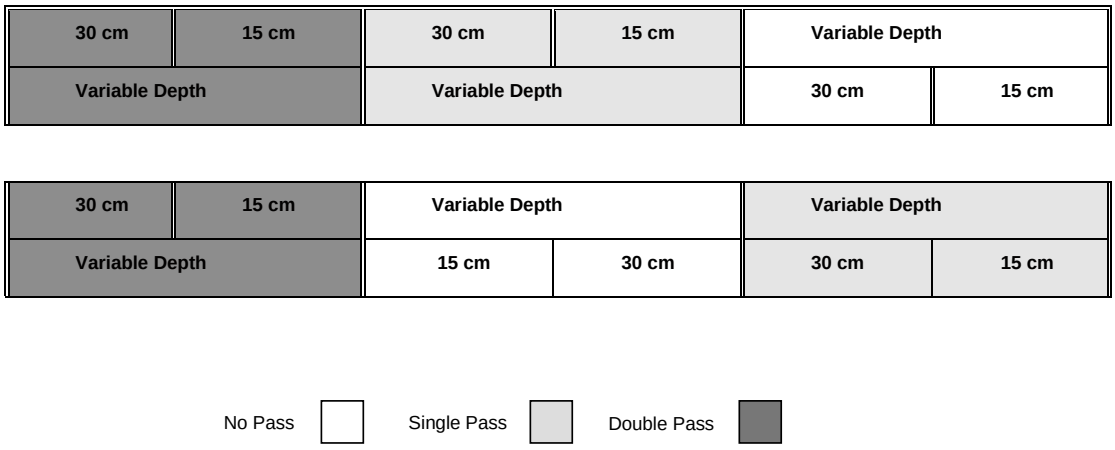

Figure 4. Experimental plot design for the constant-depth (15 and 30 cm) and variable-depth experiments and density treatments (no pass, single pass, and double pass).

RESULTS AND DISCUSSION

Before experimentation, the dry bulk density, soil water content (in and above the hardpan), as well as the peak cone index value and corresponding location were measured (table 1). The table entries are averages of five sampling repetitions.

Table 1. Dry bulk density, soil water content, peak cone index and depth to peak cone index.

	Dry Bulk Density (g/cm^3)		Soil Water Content (% w/w)		Peak Cone Index (CI)	
Density	Above Hardpan	Within Hardpan	Above Hardpan	Within Hardpan	CI (MPa)	Depth (cm)
No pass	1.16	1.18	9.5	12.6	0.72	25.5
Single pass	1.19	1.47	10.1	13.1	2.8	26.3
Double pass	1.14	1.65	10.5	12.8	3.6	25.5

From table 1 it is clear that dry bulk density did not vary appreciably for the "no pass" condition, since no hardpan was installed (the measurement was taken at 25.4 cm, where the hardpan was installed for the "single pass" and "double pass" conditions). In the "single pass" and "double pass" conditions, however, a major increase in dry bulk density was observed due to

compaction. The soil water content level was measured using a gravimetric method with oven drying at 105°C for 72 h. The water content levels in the hardpan were consistently higher than above it, which was attributed to a drying effect from the surface soil downward. Since the soil water differences overall are small, this implies that the soil strength variability is mainly dictated by the bulk density. The cone index values were obtained using a cone penetrometer (Rimik, Agridry Rimik Pty, Ltd., Toowomba, Australia). As expected, the peak values were found close to the hardpan location of 25.4 cm.

CONSTANT-DEPTH EXPERIMENTS

Figure 5 shows the fast Fourier transform (FFT) of a typical signal produced when the tine was drawn through the soil at 15 cm depth and no compaction layer was installed ("no pass"). The *x*-axis (frequency) is scaled from 0 to 1, where 1 represents the Nyquist frequency (11,025 Hz). The sound amplitude is expressed in artificial units since the true microphone output sensitivity was unknown, combined with the unknown attenuation factors of the soil-metal-air interface of the cone itself.

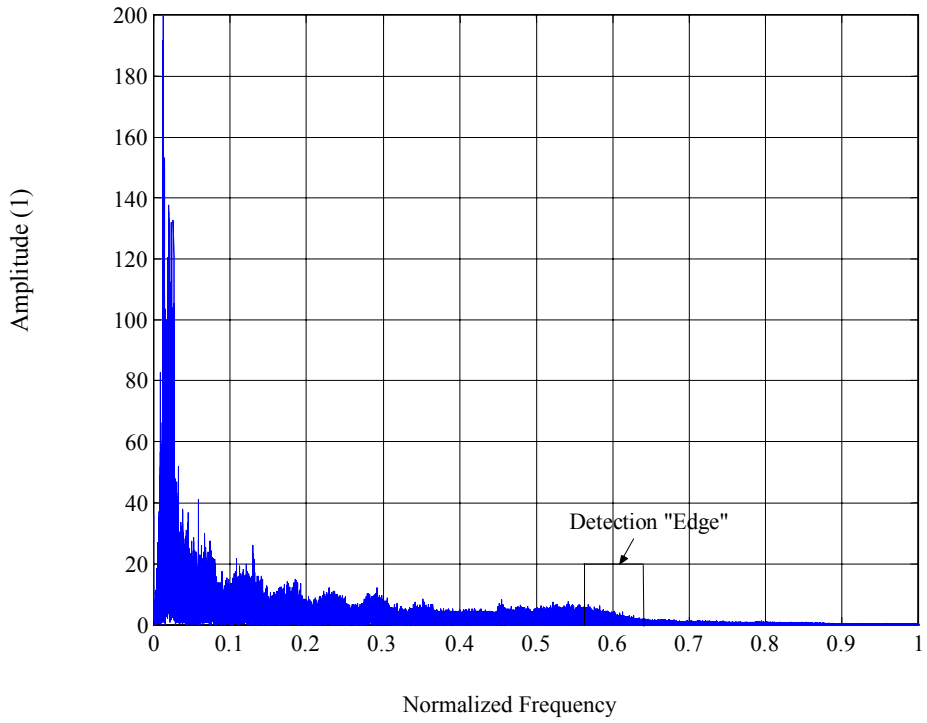

Figure 5. Acoustic signal amplitude vs. normalized frequency for constant depth (15 cm) and "no pass" density, with the detection edge at approximately 0.6 (6600 Hz).

The frequency spectrum shows a dominant peak in the lower range and several higher-order harmonics. The main peaks below 0.3 (3300 Hz) were also visible in the dry run data; these were caused by the tractor that drove the measurement cart.

After conducting constant-depth experiments at 15 and 30 cm, and studying the raw data similar to figure 5, it was discovered that differences among treatments always occurred in the highest range of the spectrum (in the range 0.57 to 0.63, or 6,300 to 7,000 Hz). This range was termed the "detection edge" and led to the conjecture that higher-frequency signals are always present, but they transfer into the microphone only when there is a more intimate contact between the cone and the medium, such as in a compaction layer. This inherent low-pass filtering mechanism causes higher-frequency signals for higher densities and higher soil strength. The detection edge range was used for filtering in the variable-depth experiments.

Six constant-depth experiments were carried out to study relationships among two depths and three treatments ("no pass," "single pass," and "double pass" densities), as shown in figure 6. The spectra were high-pass filtered using a cut off of 0.3 (3300 Hz) to suppress the sound introduced by the drive tractor, and visual comparisons were made among two depths and three treatments.

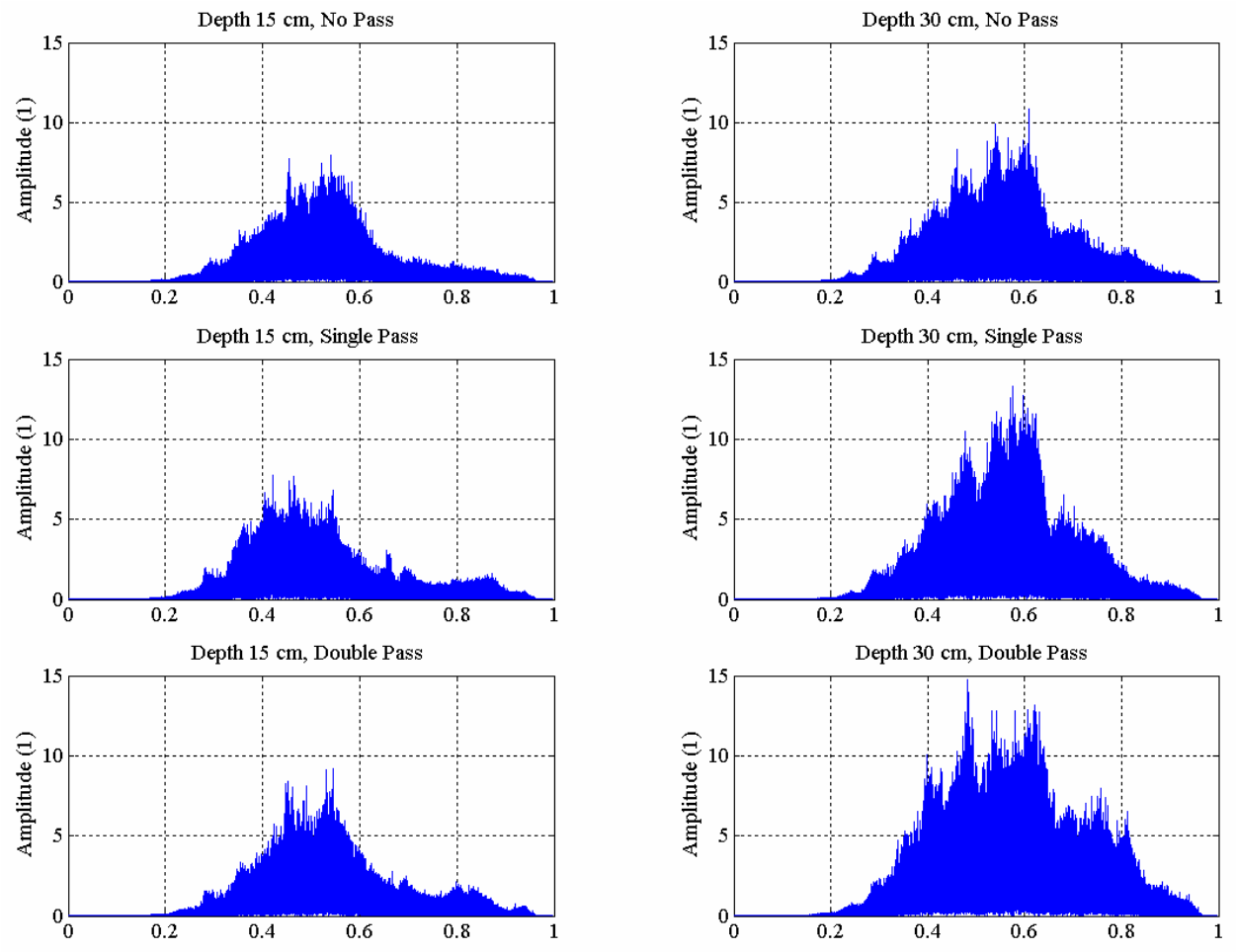

Figure 6. Comparison of depth effect (left plots = 15 cm, right plots = 30 cm) and density effect (top row = no pass, center row = single pass, and bottom row = double pass) on acoustic signal Fourier transform.

The left column of figure 6 plots represent experiments at 15 cm depth (above the hardpan) and since the dry bulk densities were similar among treatments (1.16, 1.19, and 1.14 g/cm^3, from table 1), the signal FFTs were expected to be similar, which is confirmed in the graphs.

The right column plots represent experiments at 30 cm, just below the hardpan location (in the "single pass" and "double pass" cases). From table 1, the dry bulk density increased from 1.18 g/cm^3 (no pass) to 1.47 g/cm^3 (single pass) to 1.65 g/cm^3 (double pass). The acoustic plots also show a visible increase in amplitude, especially around 0.6 (6600 Hz), which implies that the amplitude is a function of soil density.

A depth effect on the amplitude can be seen in the top row plots. Here, the depths are 15 cm and 30 cm, but no hardpan was installed. Even without this external soil compression, an overall increase in amplitude is visible.

VARIABLE-DEPTH EXPERIMENTS

For the variable-depth experiments, the acoustic data were band-pass filtered with the frequency window values obtained from the constant-depth experiments (0.57 to 0.63, or 6,300 to 7,000 Hz). The cone index (CI) data as a function of depth were combined with the cone depth as a function of time, yielding CI as a function of time. The filtered acoustic data as a function of time were compared to the CI data as a function of time, as shown in figures 7 through 9. This procedure was repeated for the three density treatments (no pass, single pass, and double pass).

Figure 7 shows the CI and acoustic data for the "no pass" condition (no hard pan). The solid line represents the CI in this plot as a function of time. It is clear that the CI slightly increased due to the depth increase over time (at 30 s a depth of 30 cm was reached, see figure 3). The filtered sound amplitude showed a similar increase over time and depth. The distinct extremes in the sound data from approximately 12 to 14 s and at approximately 24 s are unexplained and may be caused by soil discontinuities, such as larger clumps or rocks.

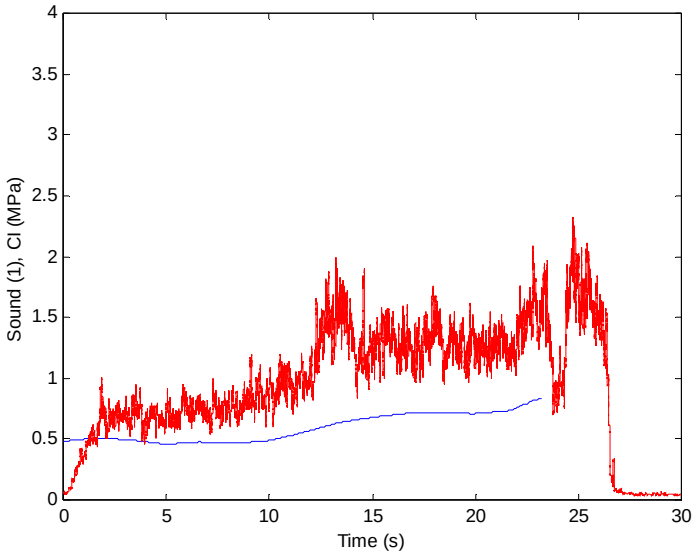

Figure 7. Cone index (solid line) and filtered acoustic data vs. time for variable-depth experiment under "no pass" density condition. The CI remaining low indicates no hardpan, and the acoustic signal shows a similar pattern as CI.

Figure 8 shows the CI and acoustic data for the "single pass" experiment (hardpan at 25.4 cm). Although the hard pan was intended and visualized as a narrow plane located at 25.4 cm, the CI data show that it is much wider than expected. However, this does not compromise the comparison of acoustic measurements with CI data. From figure 8, it is clear that the filtered acoustic data has the same overall shape as the CI data, although the relationship appears to be non-linear. In addition, there seems to be a time (depth) lag, which might be caused by the physical size of the cone (30 mm diameter). The larger the cone size, the more the plow pan becomes smoothed in the data, since the sound generation is integrated over the whole area of the cone. In future experiments, the cone size should be as small as possible.

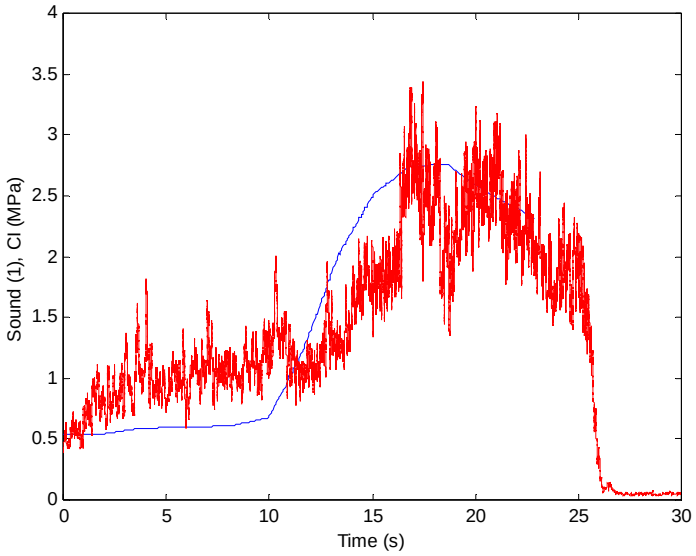

Figure 8. Cone index (solid line) and filtered acoustic data vs. time for variable-depth experiment under "single pass" density condition. The CI reaches a peak at the hardpan location, and the acoustic signal shows a similar pattern.

Figure 9 shows the CI and acoustic data for the "double pass" experiment (hardpan at 25.4 cm). The hardpan starts and peaks at approximately the same location as in the "single pass" case (fig. 8), but it is more intense. The sound data are slightly higher in the hardpan range, and the contour is similar to the true hard pan CI. Again, a time (depth) lag is present, and there are some unexplained peaks (such as at 17 s). These were attributed to true local variations in density caused by clumps or embedded objects.

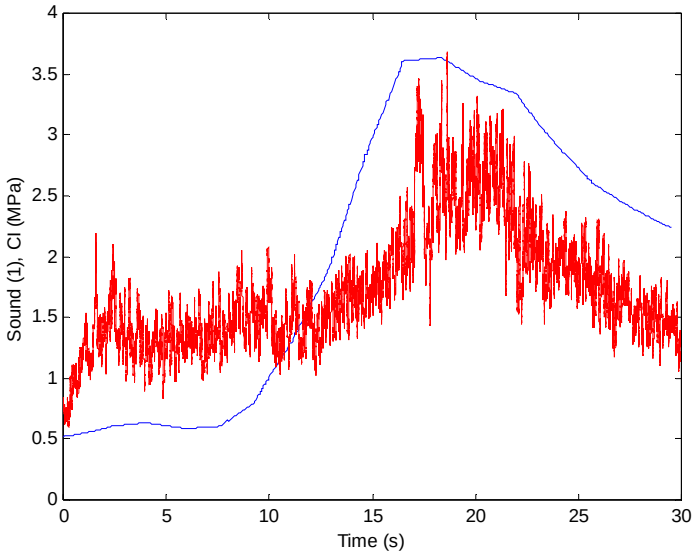

Figure 9. Cone index (solid line) and filtered acoustic data vs. time for variable-depth experiment under "double pass" density condition. The CI has a wider range and higher peak values, indicating a denser hardpan, and the acoustic signal shows a similar pattern.

CONCLUSIONS

An acoustic compaction layer detection system was developed using a microphone-fitted cone mounted on a tine. To observe the acoustic effects of depth and soil density, constant-depth experiments at 15 and 30 cm depth were conducted under three densities, "no pass" (no hardpan), "single pass" (single compression hardpan), and "double pass" (double compression hardpan).

Results showed that both soil depth and density had a detectable effect on the sound levels produced. In addition, the highest acoustic sensitivity to density was in the upper range of the frequency spectrum. This led to the conjecture that the soil-sensor interface introduces a low-pass filtering mechanism where the cutoff frequency depends on the level of the contact between medium and sensor. In other words, the higher-frequency signals are always present, but they do not transfer into the microphone due to the low-pass filtering effect of the soil-cone interface. The inherent low-pass filtering mechanism is an advantage. It allows detection of the location of

the higher-density soil layers (hardpans) by only observing the highest frequency range of the signals (termed "detection edge"), as demonstrated in this research.

To test the system's potential for detecting hardpans, variable-depth experiments were carried out in which the cone gradually penetrated the soil from the surface downward until it passed the hardpan. The data were filtered using the detection edge range to isolate density effects. High levels of agreement were found between cone index measurements and associated sound levels, which clearly demonstrated the methods' potential to detect hardpans. Some unexplained peaks were encountered in the data that may be attributed to embedded dense objects.

In future research, experiments are needed among soil types and varying soil water levels. In addition, since the frequency content of the data varies over time, a wavelet analysis may be appropriate. Further fundamental research is needed to explain why the soil-cone interface forms a low-pass filtering mechanism for propagation of sound into the sensor.

REFERENCES

Adamchuk, V. I., M. T. Morgan, and H. Sumali. 2001. Application of a strain gauge array to estimate soil mechanical impedance on-the-go. *Trans. ASAE* 44(6): 1377-1383.

Al-Adawi, S. S., and R. C. Reeder. 1996. Compaction and sub-soiling effects on corn and soybean yields and soil physical properties. *Trans. ASAE* 39(5): 1641-1649.

ASAE Standards. 1999a. S313.3: Soil cone penetrometer. St. Joseph, Mich.: ASAE.

ASAE Standards. 1999b. EP542: Procedures for using and reporting data obtained with the soil cone penetrometer. St. Joseph, Mich.: ASAE.

Ayers, P. D., and J. V. Perumpral. 1982. Moisture and density effect on cone index. *Trans. ASAE* 25(5): 1169-1172.

Batchelor, J. A. 1984. Properties of bin soils. Auburn, Ala.: USDA-ARS National Tillage Machinery Laboratory.

Chung, S., and K.A. Sudduth. 2003. Characterization of soil strength data for an on-the-go sensor. American Soc. of Agricultural Engineering Meetings Papers. Mid-Central Conf. Paper MC03-203.

Clark, R. L. 1999. Evaluation of the potential to develop soil strength maps using a cone penetrometer. ASAE Paper No. 993109. St. Joseph, Mich.: ASAE.

Fulton, J. P., L. G. Wells, S. A. Shearer, and R. I. Barnhisel. 1996. Spatial variation of soil physical properties: A precursor to precision tillage. ASAE Paper No. 961002. St. Joseph, Mich.: ASAE.

Hall, H.E., and R. L. Raper. 2005. Development and concept evaluation of an on-the-go soil strength measurement system. *Trans. ASAE* 48(2): 469-477.

Liu, W., L. D. Gaultney, and M. T. Morgan. 1993. Soil texture detection using acoustic methods. ASAE Paper No. 931015. St. Joseph, Mich.: ASAE.

MatLab. 2000. MatLab, ver. 6.0. Natick, Mass.: The Math Works, Inc.

Oelze, M. L., W. D. O'Brien, and R. J. Darmody. 2002. Measurement of attenuation and speed of sound in soils. *SSSA J.* 66(3): 788-796.

Oelze, M. L., J. M. Sabatier, and R. Raspet. 2003. Roughness measurements of soil surfaces by acoustic backscatter. *SSSA. J.* 67(1): 241-250.

Perumpral, J. V. 1987. Cone penetrometer applications - A review. *Trans. ASAE* 30(4): 939-944.

Raper, R. L., B. H. Washington, and J. D. Jarrell. 1999. A tractor-mounted, multiple-probe soil cone penetrometer. *Applied Eng. in Agric.* 15(4): 287-290.

Raper, R. L., E. B. Schwab, and S. M. Dabney. 2001. Measurement and variation of site-specific hardpans. ASAE Paper No. 011008. St. Joseph, Mich.: ASAE.

Raper, R. L., D. W. Reeves, J. Shaw, E. van Santen, P. Mask, and T. E. Grift. 2003. Reducing draft requirements and maintaining crop yields with site-specific tillage. In: Proceedings of the 16th International Soil Tillage Research Organization Proceedings (ISTRO) Conference. July 13-18, 2003, Brisbane, Australia. p. 961-965.

Utset, A., and G. Cid. 2001. Soil penetrometer resistance spatial variability in a ferrasol at several soil moisture conditions. *Soil Till. Res.* 61(3): 193-202.

CHAPTER 7

Conclusion and Future Studies

In this dissertation work, the goals were achieved based on results obtained in the laboratory experiments, field experiments, and computer simulation studies of soil cone penetration.

CAUSE-EFFECT RELATIONSHIPS

a). Depth-specific soil moisture variations were observed at short soil depth increments when a Norfolk sandy loam soil bin was subjected to drying. The soil moisture distributions were affected by the degree of compaction and amount of drying. In the double pass compaction (1.76 Mg m^{-3}), the changes in soil moisture were very small in the deeper soil profile (below 5.5 cm).

b). The effects of soil drying on predicted hardpan parameters in the Norfolk sandy loam soil bin were dependent not only on the magnitude of soil drying index (intensity of soil dryness) but also on the bulk density of the hardpan. The higher the antecedent bulk density (1.76 Mg m^{-3}) of the hardpan in the double pass compaction treatment, the lesser was the soil moisture variation and its effect on the peak cone index and the depth to the peak cone index. For the single pass compaction (1.66 Mg m^{-3}), peak cone index increased and its depth appeared to decrease with soil drying. The effect of soil drying on the predicted depth to the top of the hardpan layer was significant only for the double pass compaction treatment.

c). Further research is needed to develop soil measurement systems that have a capability of sensing soil variables such as soil moisture, soil texture, and soil strength in real time. Some of

the problems with soil strength measurement by cone penetrometer could be solved using a measurement system that contains vane (torsion) and cone (penetration) in a single unit. The measurement can obtain soil strength property of shear and compression behaviors that could improve the accuracy of soil strength measurement and minimize the effects of soil moisture on cone penetration resistance.

d). Soil hardpan can be identified by locating the top of the hardpan (cone index profile started to abruptly change) or the peak cone index. Roots may experience mechanical impedance at the depth of the top of the hardpan layer. When the cone index at the top of the hardpan layer exceeds the critical cone index value (2MPa), roots may not grow deeper to penetrate the hardpan layer. Studies may be needed to investigate the effects of application of tillage depths adjusted according to the depth of the peak cone index and the depth of the top of the hardpan layer on tillage fuel consumption.

SPATIAL VARIABILITY ANALYSIS

Soil drying increased the magnitude and spatial variability of the peak cone index on Pacolet sandy loam soil. The spatial pattern of the peak cone index was explained by spherical semivariogram model for wet and dry soil conditions with range values of 44 and 26 m, respectively. An exponential semivariogram (range=47m) model best fit the spatial variability of the depth to the peak cone index on the wet soil condition; however, in the dry soil condition the variability in the predicted depth to the peak cone index was nearly constant over the separation distances. The results suggested that soil moisture variations not only affected the values of the soil hardpan attributes (peak cone index and depth to the peak cone index) but also their estimated spatial structures which in turn may affect the prediction and soil sampling procedure.

Generally the spatial distribution patterns of the soil hardpan depths within the field were similar as predicted by the depth to the maximum bulk density or the depth to the peak cone index values. Contour maps of peak cone index values indicated that most of the field required deep tillage. The depths of tillage, however, need to vary according to the predicted soil hardpan depths. This indicated that applications of depth-specific tillage on Pacolet sandy loam soils may improve the sustainability of crop management.

The advantages of spatial variability analysis and variable depth soil compaction mapping have to be evaluated on soil quality, crop yield, environmental quality of nutrient losses and erosion. Many studies indicated that the effects of soil compaction on crop yield have been affected by uncontrolled environmental variables such as drought, natural disasters (e.g. Hurricane). This could be a problem to isolate the effects of new tillage tool designs or precision tillage inputs on crop yield in conventional or conservation cropping systems. A future study could be proposed by developing a field based economical greenhouse with controlled environment on rainfall, humidity and temperature; and advanced soil instrumentation. The design of the experimental plots in the greenhouse should allow operation of heavy machinery. Precision agriculture and conservation systems research on tillage tool designs and advanced soil measurement systems could be performed under controlled environments and field soil conditions. Conventional testing method in soil bins has potential limitations that the soils are disturbed and have lost natural soil structure.

FINITE ELEMENT MODELING

a). The finite element model based on a large strain formulation and surface contact (frictional property) pairs of soil-cone materials was successfully developed in ABAQUS/Explicit

algorithm solutions to simulate soil cone penetration in a layered coarse textured soils (Norfolk sandy loam) that varied values in soil moisture contents and bulk density.

b). Similar to cone penetrometer, the finite element model predicted the top of soil hardpan and the position of the peak cone penetration resistance. In both the FE and cone penetrometer methods, when metal was used ($\mu_{soil\text{-}metal} = 0.50$) the predicted depth was shallower than when Teflon ($\mu_{soil\text{-}Teflon} = 0.31$) cone material was used.

c). In dry soil moisture condition (4.17% d. b.), the soil hardpan was predicted at shallower depth using a cone penetrometer than at wet soil moisture condition (8.78% d. b.).

d). In future studies, finite element analysis may be needed with a soil constitutive model that accounts a combination of soil failure modes that occur during cone penetration testing. In addition, variable material parameters such as Poisson's ratio may further improve the prediction of cone penetration force values. Dilation is an important mechanical behavior of soil that seems to not be in the triaxial experimental test for the NSDL-AU soil constitutive model. During dilation until failure, soil yield stress in sand increased which appeared to be as significant as the intensity of density of the hardpan layer under dry soil moisture content. In their study on cemented sands, Abdulla and Kiousis (1997) found that volumetric compression of a dilatant sand increased as a function of cementation and confinement which appeared to be similar with the subsoil properties of hardpan, in particular the tillage pans which are highly cemented.

e). ABAQUS environment has a capability of finite element modeling of 3D complex soil-tool interaction that include different tool shapes, tool motion of a natural frequency (sinusoidal motion) similar to the real-time mechanical impedance sensors which could be addressed by applying a boundary condition to the reference node of the rigid body (tillage tool) with displacement amplitude step curve. The advantage of finite element analysis is to investigate

soil deformation and stress distributions of soil-tool interaction problems in real-time sensors that could be otherwise difficult to study in laboratory or soil bin studies.

ACOUSTIC BASED COMPACTION SENSOR

An acoustic compaction layer detection system was developed using a microphone-fitted cone mounted on a tine. High levels of agreement were found between cone index measurements and associated sound levels, which clearly demonstrated the acoustic real-time soil compaction methods' potential in detecting soil hardpans. The higher-frequency signals "detection edge" of the sound level produced at the soil-sensor interface was sensitive to the soil depth and bulk density levels. In future research, experiments are needed among soil types and varying soil water levels. In addition, since the frequency content of the data varies over time, a wavelet analysis may be appropriate.

Analysis of the magnitude and locations of hardpans in southeastern US soils was successfully carried out using a cone penetrometer and an on-the-go acoustic based soil compaction sensor. Soil hardpans exhibited spatial variability suggesting application of precision tillage may improve the sustainability of agricultural production systems in the region. The finite element simulation of cone penetration enhanced the advancement of soil compaction analysis in predicting hardpan locations in layered and heterogeneous soils. In further research, improvements on the finite element formulation was proposed to improve the prediction of soil strength contained in the hardpans.

Appendices

A. NON-LINEAR FINITE ELEMENT MODELING OF SOIL CONE PENETRATION IN LAYERED NORFOLK SANDY LOAM SOILS- CONSIDERING PRECOMPRESSION STRESS STATE

INTRODUCTION

Finite element method is important numerical technique to solve complex engineering problems. Soil-tool interaction modeling using finite element model had enabled in design of tillage tools, prediction of soil deformations under loading from tractor vehicle and tillage implements. The availability of powerful machines and advanced soil models has increased the usefulness of the numerical technique in engineering applications. Finite element simulation is comprised of discretization of the simulated body, nodal displacement analysis, propagation of applied loads, and stress-strain analysis. First, the geometry of the simulated body or assembly of bodies is discretized into finite elements. The elements, the building blocks of the body, are connected by shared nodes which collectively are called the finite element mesh. The finite element code numerically solves the displacement of nodes and propagation of loads to all the nodes of the body. Once, the nodal displacements are known, the stress and strains in each element are determined using kinematics and constitutive equations. For the stress-strain analysis, constitutive material models that are applicable to the engineering problem are needed. The nodal displacements can be determined using either the implicit or explicit method (ABAQUS, 2004). For quasi-dynamic problems such as the soil cone penetration, ABAQUS/Explicit is

preferred over the implicit method. The ABAQUS/Explicit solution determines the nodal displacement using advanced numerical technique called center difference integration rule (Eq. 1) from one increment to the next. The steps in ABAQUS/Explicit solutions involve nodal calculations of the dynamic equilibrium (Eq. 1.1) and explicit integration through time using the center difference integration rule (Eq. 1.2, 1.3) ; and elemental calculations using kinematics for the strain increments (dε) and the constitutive equations ($\sigma_{(t+\Delta t)} = f\left(\sigma_{(t)}, d\varepsilon\right)$) for stress computations. Then the nodal internal forces ($I_{(t+\Delta t)}$) are assembled and all the steps are repeated for the next time increment (t +Δt).

$$\ddot{u} = M^{-1}\left(P_{(t)} - I_{(t)}\right) \quad 1$$

$$\dot{u}_{(t+\Delta t/2)} = \dot{u}_{(t+\Delta t/2)} + \frac{\left(\Delta t_{t+\Delta t} + \Delta t_t\right)}{2}\ddot{u}_t \quad 2$$

$$u_{t+\Delta t} = u_t + \Delta t_{(t+\Delta t)}\dot{u}_{(t+\Delta t/2)} \quad 3$$

CONSTITUTIVE SOIL MODELS

The stress and strain relationships for a material under loading can be established using constitutive equations. Engineering standard tests such as triaxial testing can be used to uniquely define the stress and strain relationships in the constitutive equation. The constitutive relationships depend on many factors including homogeneity, isotropy, material continuity and reaction to various loading conditions (Chen and Mizuno, 1990). Loading in agricultural practices can vary depending on duration, rate and magnitude of loading, and loading paths (Koolen and Kuiper, 1983 and Wulfsohn and Adams, 2002). In production agriculture and forestry, the main force systems can be categorized into load bearing and soil loosening (Gill and Vanden Berg, 1968 and Koolen and Kuiper, 1983). Gill and Vanden Berg (1968) prepared a

handbook, ‘the ark of soil dynamics ‘, on soil dynamics in tillage and traction that explained the engineering mechanics of soil-tillage tools and soil-traction systems. Agricultural soils are heterogeneous, as they vary in soil moisture content, bulk density, soil structure, mineral compositions and layering. Gill (1968) and Koolen and Kuiper (1983) described soil deformation modes that could occur in soil-tool-machinery interactions as: soil compaction (change in volume); soil distortion at constant volume (plastic flow); distortion combined with compaction; expansion (dilation) that could occur with shear failure and tensile failure; and cutting. The soil deformation types vary depending on the soil moisture contents, bulk density and loading. Wet and deformable soils (e.g. high clay content soils) may exhibit deformation at constant volume. Relatively dry soils under high lateral to axial stress ratio, distortion combined with compaction predominates the soil deformation. In dense soils (e.g. high sand content soils) and soils with relatively low lateral to axial stress ratios, failure planes with dilation could occur.

Constitutive modeling of soil behavior under general loading and field soil conditions could be complicated. In modeling soil constitutive relationships, idealization of the soil material behavior and assumptions of continuum mechanics are essential. For stress and strain analysis, soil is assumed to be a continuum material even though it is a multiphase material with inter-and intra-soil pores. Continuum mechanics based stress and strain analysis has solved numerous engineering problems using the finite element method (Upadhyaya, 2002). Idealization of soil material for the development of a constitutive relationship should reflect the important characteristics of the experimental data or soil failures related to the simulated engineering problem.

Soil deformation contains elastic (recoverable) and plastic (irrecoverable) strains upon loading and unloading paths. Elastic strains account for small fractions of the total soil

deformation (Koolen and Kuiper, 1983 and Shen and Kushwaha, 1998). The reversible behavior of elastic strains upon removal of loading could be of linear or non-linear forms (Chen and Mizuno, 1990). The simplest form of linear-elastic constitutive relationship for an isotropic soil material that incorporates the volumetric and distortional (shape change) effects is shown in equation 1.4 (Wulfsohn, 2002).

$$\begin{Bmatrix} \varepsilon_v^e \\ \varepsilon_s^e \end{Bmatrix} = \begin{bmatrix} 1/K & 0 \\ 0 & 1/G \end{bmatrix} \begin{Bmatrix} p \\ q \end{Bmatrix} \qquad 4$$

Where: $K = \frac{E}{3(1-2\nu)}$ is bulk modulus; $G = \frac{E}{2(1+\nu)}$ is shear modulus; P = $\sigma_{oct} = \frac{1}{3}(\sigma_1 + \sigma_2 + \sigma_3)$ is octahedral normal stress and q = $(\sigma_1 - \sigma_3)$ is deviatoric stress.

Non-linear elastic models could be of bi-linear, multi-linear and hyperbolic forms and the material parameters (bulk modulus (K) and shear modulus (G)) are not constant but depend on stress and/or strain invariants (Chen and Mizuno, 1990 and Shen and Kushwaha, 1998).

Soil behaviors under loading are generally considered having non-linear elastic-plastic properties with geometric non-linearity (large strain deformation) (Upadhyaya, 2002). A review on deformation or flow theory of plasticity that can be used to model the plastic behaviors of the stress and strain relationships is given in Chen and Mizuno (1990). Formulation of plastic theories requires the definition of yield criteria that mathematically defines the stress conditions under which plastic deformation occurs. Yielding in soils define the onset of plasticity or the point at which elastic behavior ceases. Gill and VandenBerg (1968) and Koolen (1994) noted yielding in soil could be of compression; shear failure (change in shape and volume); or plastic flow (shearing with out change in volume). A yield criterion, *f*, is a function of stress and could be defined as:

$$f(\sigma_{ij}, k) = 0 \qquad 5$$

The yield criterion assumes that the plastic strain occurs when the stress state (σ_{ij}) reach a critical value, *k,* which could be a constant value for a perfectly plastic material or a variable for work hardening or softening materials (Chen and Mizuno,1990 and Wulfsohn, 2002). Soil behavior under wheels often exhibits work hardening as the soil becomes stronger by compaction (Koolen, 1994). The yield surface may change in size and shape as soil behavior attains work hardening (Koolen and Kuiper, 1983 and Wulfsohn, 2002).

Numerous yield criteria have been proposed for constitutive soil models that are generally defined when a maximum stress state (e.g. shear stress) or maximum strain energy reaches a critical value (Chen and Mizuno, 1990 and Shen and Kushwaha, 1998). The Mohr-Coulomb failure criterion, Drucker-Prager's yield criterion, and Cam-Clay yield criteria (Table 1.1) have important applications in soil mechanics (Atkinso and Bransby, 1978; Chen and Mizuno, 1990 and Wood, 1990). Chen and Mizuno (1990) provided the developments of each criterion, advantages and disadvantages of them. The bases for yield criteria definitions for soils were the Tresca's and von Mises yield criteria, which were originally developed for metals.

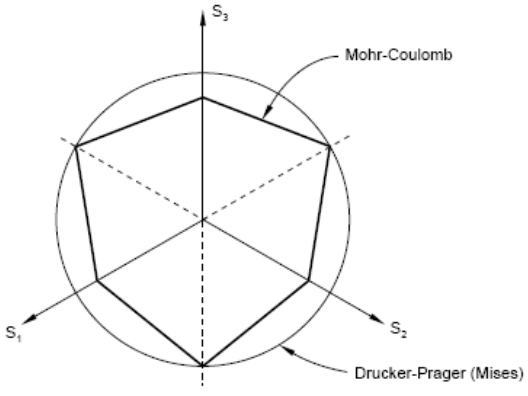

Figure 1. Yield surfaces in deviatoric plane; (After Shoop, 2001 and ABAQUS, 2004).

The model parameters of the constitutive models are defined in the pressure-deviatoric plane (p-q plane) and/or the pressure-volume plane (v-p or v-ln p plane). The Drucker-Prager, and Mohr-Coulomb yield surfaces in deviatoric plane as shown in figure 2.3 (Shoop, 2001 and ABAQUS, 2004). The volume parameter could be defined using bulk density, void ratios, bulk weight volume (1/bulk density) or natural volumetric strain (Koolen and Kuiper, 1983; Bailey and Johnson, 1989 and Wood, 1990).

Table 1.1 Yield criteria for soil constitutive models.

Yield criterion	Yield equation	Description
Mohr-Coulomb	$f(\sigma_{ij}) = \sigma_1 - \sigma_3 - [\sin\phi(\sigma_1 - \sigma_3) + 2c\cos\phi]; k_o = 0$	Simple frictional model; based on Mohr-Coulomb law ($\tau = c + \sigma \tan\phi$); hexagonal pyramid surface on hydrostatic axis; and corner of the surface complicates in finite element analysis
Drucker-Prager	$f(\sigma_{ij}) = \alpha I_1 + \sqrt{J_2} = k$	Constants α and k may be related to Coulomb's material constants c and phi; this is *extended von Mises criterion*
Cam-Clay	$f(\sigma_{ij}) = \frac{q}{p\,ln(p_c / p)}; k = M$	Based on critical state soil and can be separated into three components: critical state line (CSL) q=Mp; normal consolidation line (NCL) q=0, $V = N - \lambda\, ln\, p$ and unloading-reloading line (URL) $V = V_k - \kappa\, ln\, p$

Several soil behavioral models have been developed to predict the effects of force systems from surface loads, tires and soil engaging tools on the bases of yield criteria in Table 1.1 and pseudo-analytic theories such as Bousinnesq and Froehlich (Söhne, 1958; Raper and Erbach, 1990; Gupta and Raper, 1994; Markauskas et al., 2002; Chrioux et al., 2005 and Foster et al., 2005). The Drucker-Prager criterion based constitutive modeling was used in finite

element analysis for solving various soil-tool interactions problems (Fielke, 1999; Mouazen and Ramon, 2002 and Upadhyaya et al., 2002). Bailey et al. (1986) developed a non-linear elastic model to predict natural volumetric strains of unsaturated agricultural soils under hydrostatic stress. Bailey and Johnson (1989) modified the hydrostatic stress compaction model by Bailey et al. (1986) to include soil behaviors under compressive normal and shearing stresses. The model which is also called National Soil Dynamics Laboratory-Auburn University (NSDL-AU) soil compaction model was developed from triaxial tests on four different soil types, each at a specific soil moisture contents. The details on the NSDL-AU model parameters and their descriptions are available in the later chapter on finite element modeling. The three dimensional yield diagrams of NSDL-AU are related to the Critical State Soil Mechanics theory and its parameters are compared with the modified Cam-clay model (Bailey and Johnson, 1996). Raper and Erbach (1990) developed a finite element program that used the hydrostatic stress and natural volumetric strain NSDL-AU model to predict soil stresses under flat plate and spherical disc loads. Their finite element predicted soil stresses were fairly similar to the stresses measured by soil Stress State Transducers (SST) that were placed within the soil profile. Raper et al. (1994) reported improvements in the finite element predictions of soil stresses when they used the modified NSDL-AU soil constitutive model which accounted both the normal and shearing stresses. Numerous models of soil compaction due to traffic have been evaluated by Defossez and Richard (2002). Further details on soil deformation-load related soil physical properties, measurement methods and soil-plant dynamics are available in ASABE monographs "compaction of agricultural soils" (Barnes et al., 1971) and "Advances in Soil Dynamics-volume 1" (Upadhyaya et al., 1994).

The NSDL-AU soil compaction model was used to estimate the extended Drucker-Prager soil constitutive model parameters in chapter 5 of the dissertation. Tabular data of hydrostatic yield stress vs. volumetric plastic strain for the Drucker-Prager Hardening option was determined from the NSDL-AU natural volumetric stress-strain relationship (Tekeste et al., 2005, chapter 5 of the dissertation). The finite element (FE) successfully simulated the soil cone contact problem with adaptive meshing. The FE predicted forces, however, were not close to the observed cone penetration forces obtained using cone penetrometer. The soil material property in the NSDL-AU model may not accounted for the soil mechanical behavior in cone penetration. For improving the finite element simulation of cone penetration in layered soils, inclusion of the volumetric strain due to shearing stress and modification of the 'virgin' stress strain relationship of the NSDL-AU to account for the pre-compression stress concept were proposed in Appendix A. The NSDL-AU model coefficients (A, B, C and D) were determined using no-linear curve fitting on the tri-axial testing data on Norfolk sandy loam soil. The loading path employed in the NSDL-AU parameters estimation was that loading was applied when the σ_{oct} (Octahedral normal stress) was constant (500 kPa) while the shear stresses were applied (Bailey and Johnson, 1996). The volumetric strain due to the shearing component of the NSDL-AU model ($D\frac{\tau_{oct}}{\sigma_{oct}}$) was small about 2 % of the total volumetric strain. The finite element analysis using the total volumetric strain from the tri-axial test data (Bailey, 2004) did not improve the magnitude of the finite element contact forces.

The strain and stress of the NSDL-AU was modified to account the pre-compression stress state of the layered soil and the relationship between tri-axial stress state and proctor density curve for soil moisture content variations. In the stress-strain of the NSDL-AU model, the volumetric strain at pre-compression (the greatest stress the soil ever experienced) equivalent

to the initial bulk density of the soil hardpan layer was first determined. Assuming the plastic strain contains nearly 90 % of the total deformation from equation 4 in chapter 5 ($d\bar{\varepsilon}_v^p = \alpha d\bar{\varepsilon}_v$), new yield stress and equivalent plastic strain tables were prepared for the hardening part of the extended Drucker-Prager model (ABAQUS, 2004). Variable elastic parameters of Young's Modulus and Poisson's ratio as a function of octahedral stress were used according to Raper et al. (1994). The stress-strain relationships (Fig. A 1.2) indicated the variation in the magnitude of volumetric strains when the curve was modified to account the pre-compression stress state. For the hardpan layer (Fig. A 1.2), the plastic strain values were decreased by nearly 15 times from the original NSDL-AU strain values indicating a soil initially compressed to 1.71 kg m^{-3} bulk density had small deformation for the stress range considered in the analysis.

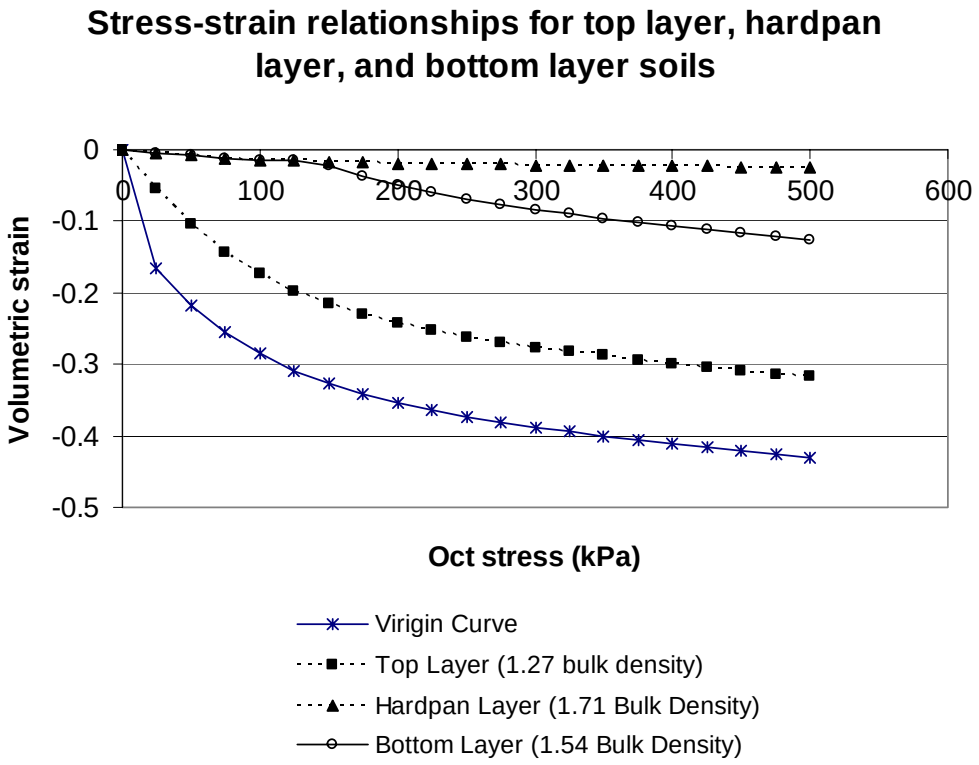

Figure A 1.2. Stress-strain relationships of the NSDL-AU virgin curve and the three layers (Top, Hardpan and Bottom) of the Norfolk sandy loam soil.

The finite element predicted contact forces have improved when the soil material model for the Norfolk sandy loam soil was modified. Figure A 1.3 shows the finite element predicted and cone penetrometer soil cone penetration resistance forces. The finite element results with the pre-compression stress appeared to be similar to the observed data better than the previous finite element analysis presented in chapter 5 of the dissertation.

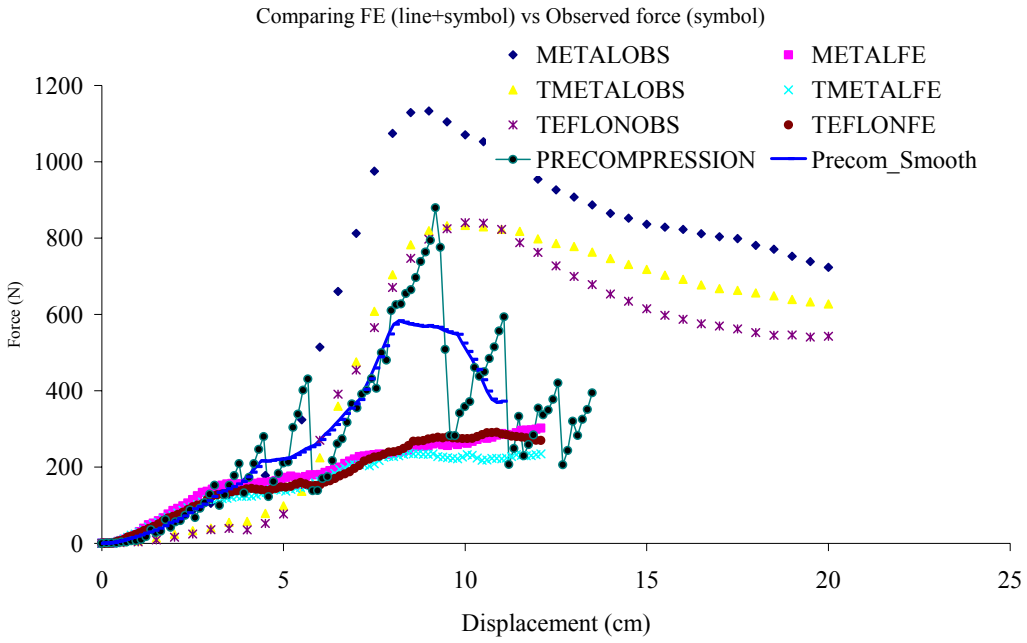

Figure A 1.3. FE predicted (lines with symbols) vs. observed penetration resistance (lines) for dry soil moisture (3.48 % d.b.) and 1.71 kg m^{-3} bulk density (within hardpan). The modified FE results (Pre-compression) are shown both for ABAQUS/Explicit (Oscillated forces) and smoothed curve.

REFERENCES

ABAQUS, Version 6.4. 2004. Abaqus theory manual. ABAQUS, Inc. USA.

Atkinson, J.H. and Bransby, P.L. 1978. The mechanics of soils: An introduction to critical soil mechanics. McGraw Hill, London.

Barnes, K.K., W.M. Carleton, H.M. Taylor, R.I., Throchmorton and G.E. Vanden Berg. 1971. Compaction of Agricultural Soils. ASAE monograph no. 1, St. Joseph, MI. 126-153.

Bailey, A.C., C.E. Johnson, and R.L. Schafer. 1986. A model for agricultural soil compaction. *J. Agric. Eng. Res.* 33:257-262.

Bailey, A.C. and C.E. Johnson. 1996. Soil critical state behavior in the NSDL-AU model. ASAE Paper 96-1064. St. Joseph, Mich.: ASAE.

Bailey, A.C. and C.E. Johnson. 1996. A soil compaction model for cylindrical stress states. *Trans. ASAE* 32(3): 822-825.

Beer F.P., E.R. Johnson and J.T. DeWolf. 2005. Mechanics of materials. 3rd ed. McGraw Hill, London.

Chen, W.F. and E. Mizuno. 1990. Non-linear Analysis in soil mechanics: Theory and Implementation. Developments in geotechnical engineering vol. 53. Elsevier Science Publishing Company Inc. 655 Avenu of the Americas, New York, NY 10010, U.S.A.

Chiroux, R.C., W.A. Foster Jr., C.E. Johnson, S.A. Shoop and R.L. Raper. 2005. Three-dimensional finite element analysis of soil interaction with rigid wheel. *Applied Mathematics and Computation*. 162:707-722.

Coduto, D.P. 1999. Geotechnical engineering principles and practices. Prentice-Hall, Inc. Upper Saddle River, New Jersey.

Defossez, P. and G. Richard. 2002. Models of soil compaction due to traffic and their evaluation. *Soil Till. Res.* 67: 41-64.

Fielke, J.M. 1999. Finite element modeling of the interactions of cutting edge of tillage implements with soil. *J. Agric. Engg. Res.* 74: 91-101.

Foster,Jr. W.A., C.E. Johnson, R.C. Chiroux and T.R. Way. 2005. Finite Element Simulation of Cone Penetration. *Applied Mathematics and Computation.* 162: 735-749.

Gill, W.R. 1968. Influence of compaction hardening of soil on penetration resistance. *Trans. ASAE* 11(6): 741-745.

Gill, W.R. and G.E. VandenBerg. 1968. Soil dynamics in tillage and traction. Agriculture Handbook No. 316. USDA-Agricultural Research Service, Washington. D.C.

Huang, W., D. Sheng, S.W. Sloan and H.S. Yu. 2004. Finite element analysis of cone penetration in cohesionless soil. *Computers and Geotechnics.* 31(7):517-528.

Koolen, A.J. and H. Kuipers. 1983. Agricultural soil mechanics. Advanced series in agricultural sciences 13. Springer-Verlan Berlin Heidelberg, Germany.

Lunne, T., P.K. Robertson, and J.J.M. Powell. 1997. Cone penetration testing in geotechnical practices. Blackie academic and professional, London, UK.

Markauskas, D. , R. Kacianauskas, M. Suksta. 2002. Modeling the cone penetration test by the finite element method. *Foundation of Civil and Environmental Engineering*. No. 2. Poznan University of Technology,Poznan, Poland.

Mouazen, A. M. and M. Neményi. 1999. Finite element analysis of subsoiler cutting in non-homogeneous sandy loam soil. *Soil Till. Res.* 51(1-2): 1-15.

Raper, R.L., C.E. Johnson and A.C. Bailey. 1994. Coupling normal and shearing stresses to use in finite-element analysis of soil compaction. *Trans. ASAE* 37(5):1417-1422.

Raper, R.L. and D.C. Erbach, 1990b. Prediction of soil stresses using the finite element method. *Trans. ASAE,* 33: 725–30.

Rohani, B. and G. Y. Baladi. 1981. Correlation of mobility cone index with fundamental engineering properties of soil. International Society for Terrain-Vehicle Systems. Vol 3:959-990. Alberta, Canada.

Sanglerat, G. 1972. Interpretation of penetration diagrams- theory and practice. Developments in geotechnical engineering. Elsevier publishing company. Amsterdam, The Netherlands.

Shen, J. and R.L. Kushwaha, 1998. Soil–Machine Interaction, A Finite Element Perspective. New York: Marcel Dekker, Inc.

Söhne, W. 1958. Fundamentals of pressure distribution and soil compaction under tractor tyres. Agric. Eng. 39,276-281.

Shoop, S.A. 2001. Finite element modeling of tire-terrain interaction. Technical report ERDC/CRREL TR-01-16.

Tekeste, M. Z., R.L. Raper, E. W. Tollner and T.R. Way. 2002. Finite element anlaysis of cone penetrometer for predicting soil hardpan attributes as influenced by soil moisture, soil density and cone material. Chpt 5 of this dissertation, Submitted to the *Trans. ASAE.*

Upadhyaya, S. K., W. J. Chancellor, J. V. Perumpral, R. L. Schafer, W. R. Gill, and Glen E. VandenBerg (editors). 1994. Advances in Soil Dynamics. Vol. 1. American Society of Agricultural Engineers. 313p.

U.S. Army Corps of Engineers. 1948. Trafficability of soils—Development of testing instruments. Technical memo 3-240, 3d suppl. Vicksburg, MS:U.S. Army Corps of Engineers Waterways Experiment Station.

Voorhees W.B. 1991. Compaction effects on yield-are they significant? *Trans. ASAE* 34(4): 1667-1672.

Wood, M.D. 1990. Soil behavior and critical state soil mechanics. Cambridge University Press: Cambridge.

Wulfsohn, D., and B. A. Adams. 2002. Elastoplastic soil mechanics. In *Advances in Soil Dynamics Volume 2*, 1- 116. St. Joseph, Mich.: ASAE.

Yu, H.S., J.K. Mitchell, 1998. Analysis of cone resistance: review of methods. *J Geotechnical and Geoenvironmental Engg.* 141 (2): 140-149.

B. IMAGES AND PICTURES

Figure B 2.1. Soil compression in the USDA-ARS NSDL facility in Auburn, AL precision farming lab.

Figure B 2.2 Soil columns drying in greenhouse at the NSDL facility in Auburn, AL.

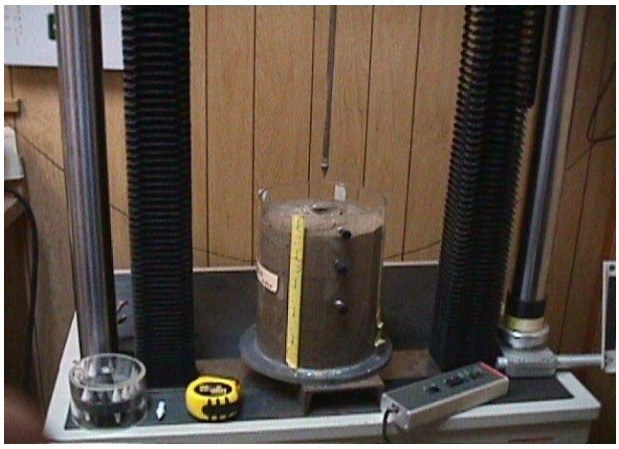

Figure A 2.3 Soil cone penetration reading using Sintech/2G at the USDA-ARS- NSDL facility in Auburn, AL precision farming lab.

Figure A 2.4 Soil cone materials (Teflon, Telflon metal and Metal) coefficient of friction measurement at the USDA-ARS- NSDL facility in Auburn, AL precision farming lab.

Figure A 2.5 Data acquisition for soil cone materials (Teflon, Telflon metal and Metal) coefficient of friction measurement at the USDA-ARS- NSDL facility in Auburn, AL precision farming lab.

Figure B 2.6 Soil cone penetration reading using multiple-probe soil cone penetrometer on the Norfolk sandy loam soil bin at the USDA-ARS- NSDL facility in Auburn, AL.

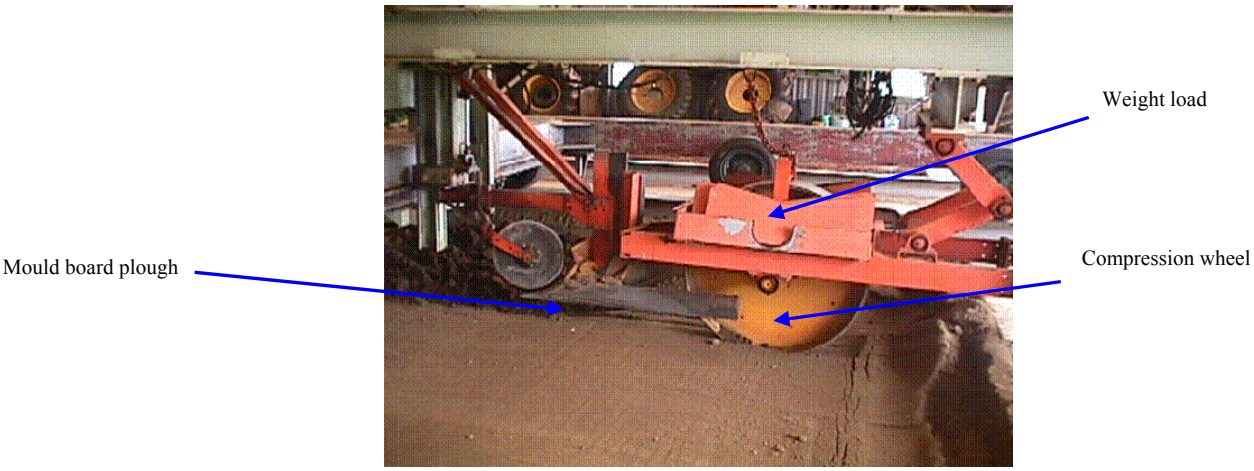

Figure B 2.7 Soil bin preparation on the Norfolk sandy loam soil bin at the USDA-ARS- NSDL facility in Auburn, AL.

Figure B 2.8 Soil core sampling for soil moisture determination using air-jack hammer on the Norfolk sandy loam soil bin at the USDA-ARS- NSDL facility in Auburn, AL.

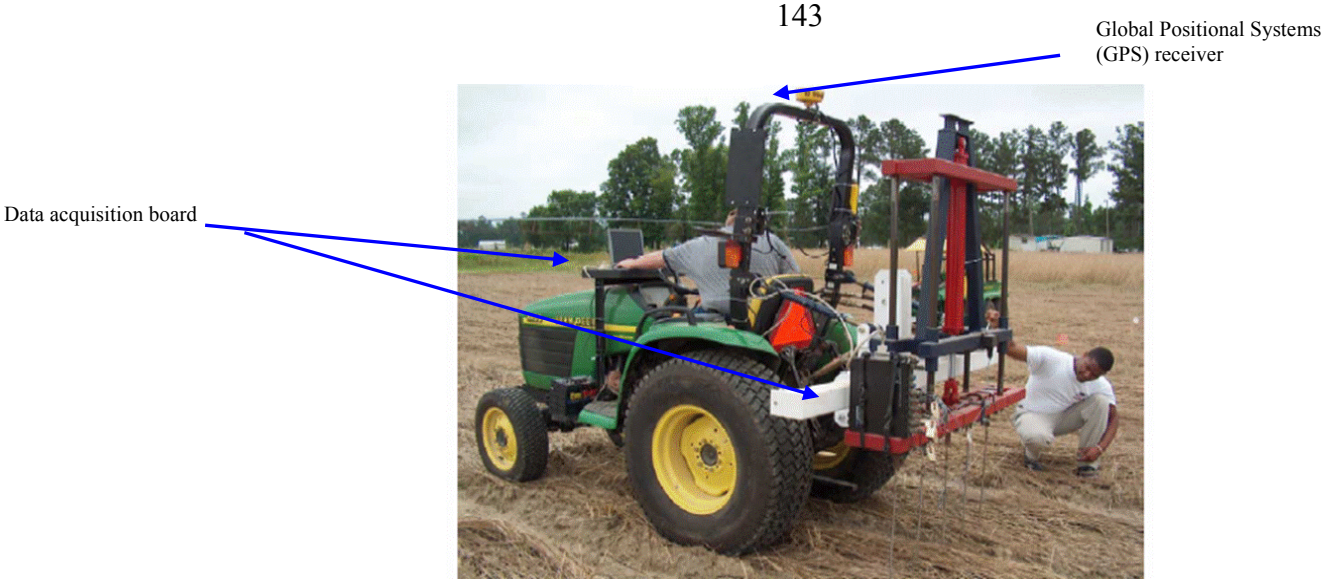

Figure B 2.9 Soil cone penetration sampling using multiple-probe-cone penetrometer on Pacolet sandy loam soil near the Old Rotation Experimental Plots of the Auburn University and USDA-ARS- NSDL in Auburn, AL.

Figure B 2.10 A dual-frequency RTK, AgGPS ® 214, GPS receiver (cm level accuracy) with ground station for digital elevation data acquisition on Pacolet sandy loam soil near the Old Rotation Experimental Plots of the Auburn University and USDA-ARS- NSDL in Auburn, AL.

Figure B 2.11 Soil core sampler for bulk density and soil moisture determination on the Pacolet sandy loam soil near the Old Rotation Experimental Plots of the Auburn University and USDA-AR

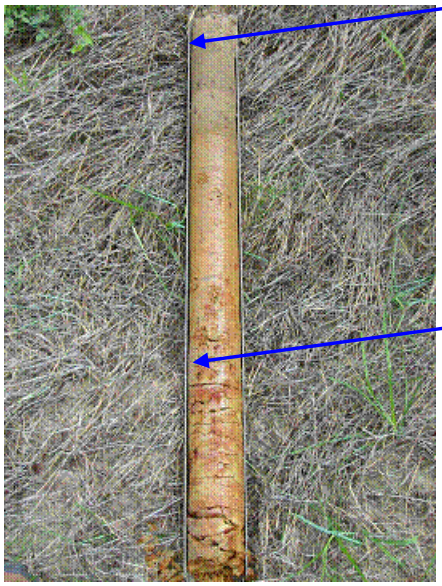

Figure B 2.12 Soil core sample (26 inches depth) of the Pacolet sandy loam soil near the Old Rotation Experimental Plots of the Auburn University and USDA-ARS- NSDL in Auburn, AL.

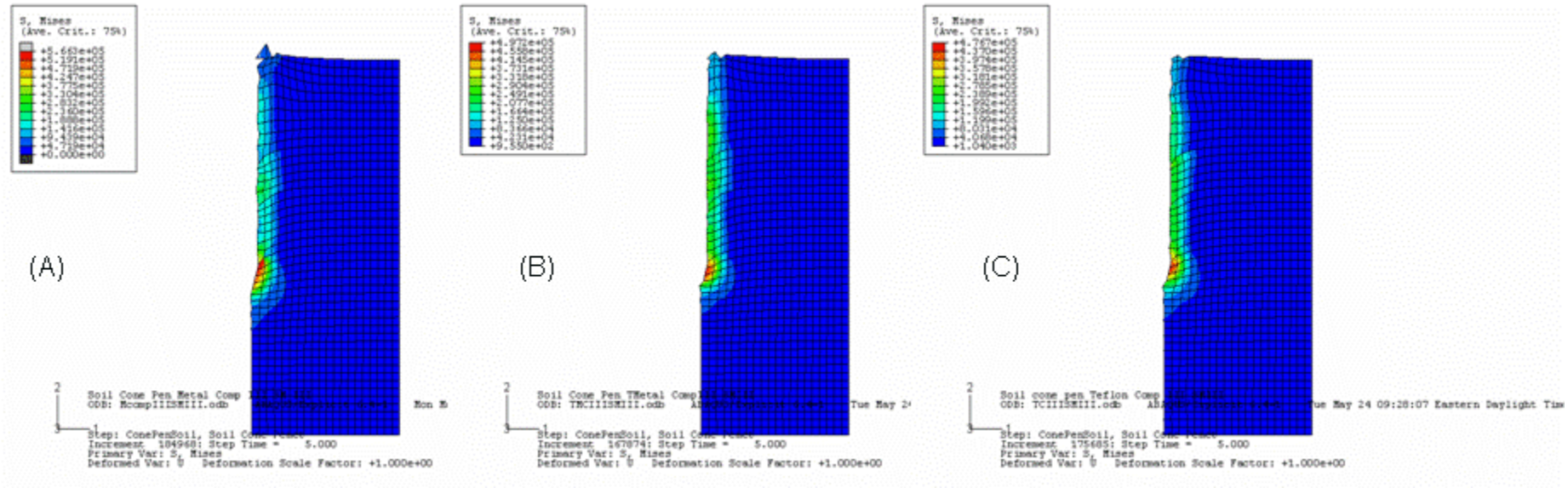

Figure B 2.13 FE analysis results showing Von Misses stresses from soil cone penetration simulation on Norfolk sandy loam soil with bulk density (Within hardpan) of 1.76 Mg m $^{-3}$ and soil moisture level II (3.48 % d.b.) for cone materials of Metal (A), TMetal (B), and Teflon (C).

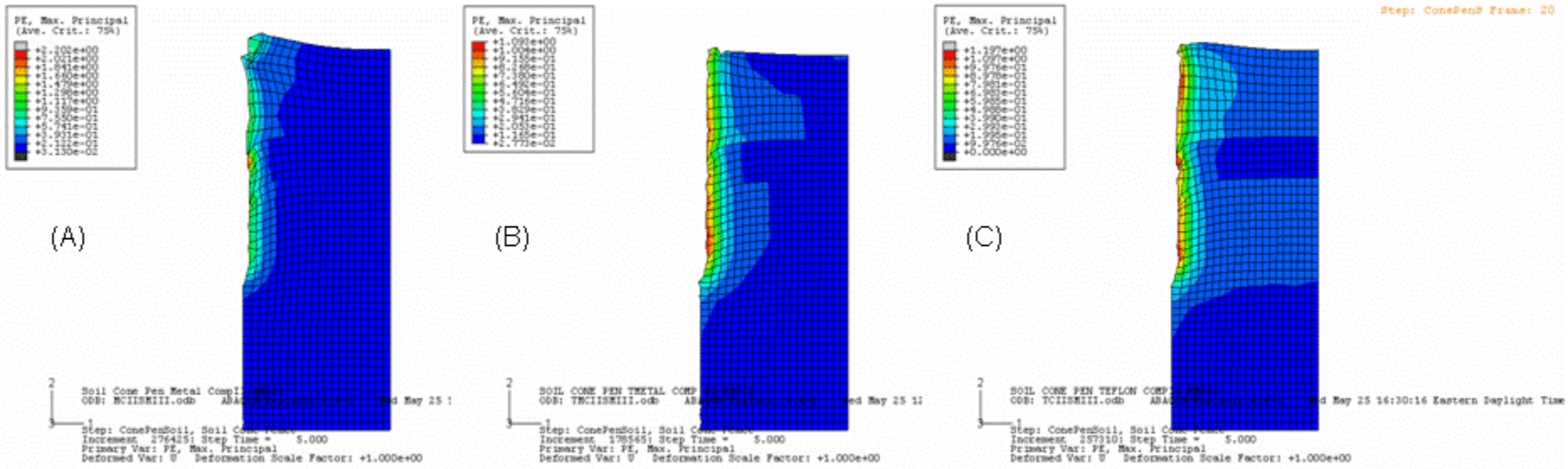

Figure B 2.14 FE analysis results showing plastic strains from soil cone penetration simulation on Norfolk sandy loam soil with bulk density (Within hardpan) of 1.76 Mg m $^{-3}$ and soil moisture level II (3.48 % d.b.) for cone materials of Metal (A), TMetal (B), and Teflon (C).

C. ABAQUS/EXPLICIT INPUT FILE

```
*Heading
 NSDLAU vol strain modified to account precompression stress
** UNITS: Kg,N,m,Sec
** Job name: precompre18_06vardensityMetal Model name: Model-1
*Preprint, echo=NO, model=NO, history=NO, contact=NO
**
** PARTS
**
*Part, name=Cone
*End Part
**
*Part, name=Soil
*End Part
**
**
** ASSEMBLY
**
*Assembly, name=Assembly
**
*Instance, name=Soil-2, part=Soil
         0., 0.358153180000023,           0.
*Node
      1,  0.101599999,   29.9247456

    480, 0.0943428576,    29.992815
*Element, type=CAX4R
  1,   1,   9, 117,  74
434, 480,  97,   7,  98
*Nset, nset=_PickedSet16, internal, generate
   1,  480,    1
*Elset, elset=_PickedSet16, internal, generate
   1,  434,    1
*Nset, nset=_PickedSet25, internal, generate
   1,  480,    1
*Elset, elset=_PickedSet25, internal, generate
   1,  434,    1
*Nset, nset=Set-1, generate
   1,  480,    1
*Elset, elset=Set-1, generate
   1,  434,    1
*Nset, nset=_PickedSet27, internal, generate
   1,  480,    1
*Elset, elset=_PickedSet27, internal, generate
   1,  434,    1
*Nset, nset=_PickedSet28, internal, generate
   1,  480,    1
```

```
*Elset, elset=_PickedSet28, internal, generate
  1,  434,    1
*Nset, nset=_PickedSet37, internal
  5,   6,   7,   8,  77,  78,  79,  80,  81,  82,  83,  84,  85,  86,  87,  88
473, 474, 475, 476, 477, 478, 479, 480
*Elset, elset=_PickedSet37, internal, generate
337,  434,    1
*Nset, nset=_PickedSet38, internal
  1,   2,   5,   6,   9,  10,  11,  12,  13,  14,  15,  16,  17,  18,  19,  20
391, 392, 393, 394, 395, 396, 397, 398, 399, 400, 401, 402
*Elset, elset=_PickedSet38, internal, generate
295,  336,    1
*Nset, nset=_PickedSet39, internal
  1,   2,   3,   4,   9,  10,  11,  12,  13,  14,  15,  16,  17,  18,  19,  20
367, 368, 369, 370, 371, 372, 373, 374, 375, 376
*Elset, elset=_PickedSet39, internal, generate
  1,  294,    1
*Nset, nset=_PickedSet40, internal
  5,   6,   7,   8,  77,  78,  79,  80,  81,  82,  83,  84,  85,  86,  87,  88
473, 474, 475, 476, 477, 478, 479, 480
*Elset, elset=_PickedSet40, internal, generate
337,  434,    1
*Nset, nset=_PickedSet41, internal
  1,   2,   5,   6,   9,  10,  11,  12,  13,  14,  15,  16,  17,  18,  19,  20
391, 392, 393, 394, 395, 396, 397, 398, 399, 400, 401, 402
*Elset, elset=_PickedSet41, internal, generate
295,  336,    1
*Nset, nset=_PickedSet42, internal
  1,   2,   3,   4,   9,  10,  11,  12,  13,  14,  15,  16,  17,  18,  19,  20
367, 368, 369, 370, 371, 372, 373, 374, 375, 376
*Elset, elset=_PickedSet42, internal, generate
  1,  294,    1
*Nset, nset=_PickedSet43, internal
  5,   6,   7,   8,  77,  78,  79,  80,  81,  82,  83,  84,  85,  86,  87,  88
473, 474, 475, 476, 477, 478, 479, 480
*Elset, elset=_PickedSet43, internal, generate
337,  434,    1
*Nset, nset=_PickedSet44, internal
  1,   2,   5,   6,   9,  10,  11,  12,  13,  14,  15,  16,  17,  18,  19,  20
391, 392, 393, 394, 395, 396, 397, 398, 399, 400, 401, 402
*Elset, elset=_PickedSet44, internal, generate
295,  336,    1
*Nset, nset=_PickedSet45, internal
  1,   2,   3,   4,   9,  10,  11,  12,  13,  14,  15,  16,  17,  18,  19,  20
367, 368, 369, 370, 371, 372, 373, 374, 375, 376
*Elset, elset=_PickedSet45, internal, generate
  1,  294,    1
*Nset, nset=_PickedSet46, internal
  5,   6,   7,   8,  77,  78,  79,  80,  81,  82,  83,  84,  85,  86,  87,  88
473, 474, 475, 476, 477, 478, 479, 480
```

```
*Elset, elset=_PickedSet46, internal, generate
 337,  434,    1
*Nset, nset=_PickedSet47, internal
   1,   2,   5,   6,   9,  10,  11,  12,  13,  14,  15,  16,  17,  18,  19,  20
 391, 392, 393, 394, 395, 396, 397, 398, 399, 400, 401, 402
*Elset, elset=_PickedSet47, internal, generate
 295,  336,    1
*Nset, nset=_PickedSet48, internal
   1,   2,   3,   4,   9,  10,  11,  12,  13,  14,  15,  16,  17,  18,  19,  20
 367, 368, 369, 370, 371, 372, 373, 374, 375, 376
*Elset, elset=_PickedSet48, internal, generate
   1,  294,    1
*Nset, nset=_PickedSet49, internal
   5,   6,   7,   8,  77,  78,  79,  80,  81,  82,  83,  84,  85,  86,  87,  88
 473, 474, 475, 476, 477, 478, 479, 480
*Elset, elset=_PickedSet49, internal, generate
 337,  434,    1
*Nset, nset=_PickedSet50, internal
   1,   2,   5,   6,   9,  10,  11,  12,  13,  14,  15,  16,  17,  18,  19,  20
 391, 392, 393, 394, 395, 396, 397, 398, 399, 400, 401, 402
*Elset, elset=_PickedSet50, internal, generate
 295,  336,    1
*Nset, nset=_PickedSet51, internal
   1,   2,   3,   4,   9,  10,  11,  12,  13,  14,  15,  16,  17,  18,  19,  20
 367, 368, 369, 370, 371, 372, 373, 374, 375, 376
*Elset, elset=_PickedSet51, internal, generate
   1,  294,    1
*Nset, nset=_PickedSet52, internal
   5,   6,   7,   8,  77,  78,  79,  80,  81,  82,  83,  84,  85,  86,  87,  88
 473, 474, 475, 476, 477, 478, 479, 480
*Elset, elset=_PickedSet52, internal, generate
 337,  434,    1
*Nset, nset=_PickedSet53, internal
   1,   2,   5,   6,   9,  10,  11,  12,  13,  14,  15,  16,  17,  18,  19,  20
 391, 392, 393, 394, 395, 396, 397, 398, 399, 400, 401, 402
*Elset, elset=_PickedSet53, internal, generate
 295,  336,    1
*Nset, nset=_PickedSet54, internal
   1,   2,   3,   4,   9,  10,  11,  12,  13,  14,  15,  16,  17,  18,  19,  20
 367, 368, 369, 370, 371, 372, 373, 374, 375, 376
*Elset, elset=_PickedSet54, internal, generate
   1,  294,    1
*Nset, nset=_PickedSet55, internal
   5,   6,   7,   8,  77,  78,  79,  80,  81,  82,  83,  84,  85,  86,  87,  88

 473, 474, 475, 476, 477, 478, 479, 480
*Elset, elset=_PickedSet55, internal, generate
 337,  434,    1
*Nset, nset=_PickedSet56, internal
   1,   2,   5,   6,   9,  10,  11,  12,  13,  14,  15,  16,  17,  18,  19,  20
```

```
 391, 392, 393, 394, 395, 396, 397, 398, 399, 400, 401, 402
*Elset, elset=_PickedSet56, internal, generate
 295,  336,    1
*Nset, nset=_PickedSet57, internal
   1,   2,   3,   4,   9,  10,  11,  12,  13,  14,  15,  16,  17,  18,  19,  20
 367, 368, 369, 370, 371, 372, 373, 374, 375, 376
*Elset, elset=_PickedSet57, internal, generate
   1,  294,    1
*Nset, nset=_PickedSet58, internal
   5,   6,   7,   8,  77,  78,  79,  80,  81,  82,  83,  84,  85,  86,  87,  88

 473, 474, 475, 476, 477, 478, 479, 480
*Elset, elset=_PickedSet58, internal, generate
 337,  434,    1
*Nset, nset=_PickedSet59, internal
   1,   2,   5,   6,   9,  10,  11,  12,  13,  14,  15,  16,  17,  18,  19,  20
 391, 392, 393, 394, 395, 396, 397, 398, 399, 400, 401, 402
*Elset, elset=_PickedSet59, internal, generate
 295,  336,    1
*Nset, nset=_PickedSet60, internal
   1,   2,   3,   4,   9,  10,  11,  12,  13,  14,  15,  16,  17,  18,  19,  20

 367, 368, 369, 370, 371, 372, 373, 374, 375, 376
*Elset, elset=_PickedSet60, internal, generate
   1,  294,    1
*Nset, nset=_PickedSet61, internal
   5,   6,   7,   8,  77,  78,  79,  80,  81,  82,  83,  84,  85,  86,  87,  88

 473, 474, 475, 476, 477, 478, 479, 480
*Elset, elset=_PickedSet61, internal, generate
 337,  434,    1
*Nset, nset=_PickedSet62, internal
   1,   2,   5,   6,   9,  10,  11,  12,  13,  14,  15,  16,  17,  18,  19,  20
 391, 392, 393, 394, 395, 396, 397, 398, 399, 400, 401, 402
*Elset, elset=_PickedSet62, internal, generate
 295,  336,    1
*Nset, nset=_PickedSet63, internal
   1,   2,   3,   4,   9,  10,  11,  12,  13,  14,  15,  16,  17,  18,  19,  20
 367, 368, 369, 370, 371, 372, 373, 374, 375, 376
*Elset, elset=_PickedSet63, internal, generate
   1,  294,    1
*Nset, nset=_PickedSet64, internal
   5,   6,   7,   8,  77,  78,  79,  80,  81,  82,  83,  84,  85,  86,  87,  88
 473, 474, 475, 476, 477, 478, 479, 480
*Elset, elset=_PickedSet64, internal, generate
337,  434,    1
*Nset, nset=_PickedSet65, internal
   1,   2,   5,   6,   9,  10,  11,  12,  13,  14,  15,  16,  17,  18,  19,  20
 391, 392, 393, 394, 395, 396, 397, 398, 399, 400, 401, 402
*Elset, elset=_PickedSet65, internal, generate
```

```
 295,  336,    1
*Nset, nset=_PickedSet66, internal
   1,   2,   3,   4,   9,  10,  11,  12,  13,  14,  15,  16,  17,  18,  19,  20
 367, 368, 369, 370, 371, 372, 373, 374, 375, 376
*Elset, elset=_PickedSet66, internal, generate
   1,  294,    1
*Nset, nset=_PickedSet67, internal
   5,   6,   7,   8,  77,  78,  79,  80,  81,  82,  83,  84,  85,  86,  87,  88
 473, 474, 475, 476, 477, 478, 479, 480
*Elset, elset=_PickedSet67, internal, generate
 337,  434,    1
*Nset, nset=_PickedSet68, internal
   1,   2,   5,   6,   9,  10,  11,  12,  13,  14,  15,  16,  17,  18,  19,  20
 391, 392, 393, 394, 395, 396, 397, 398, 399, 400, 401, 402
*Elset, elset=_PickedSet68, internal, generate
 295,  336,    1
*Nset, nset=_PickedSet69, internal
   1,   2,   3,   4,   9,  10,  11,  12,  13,  14,  15,  16,  17,  18,  19,  20
 367, 368, 369, 370, 371, 372, 373, 374, 375, 376
*Elset, elset=_PickedSet69, internal, generate
   1,  294,    1
*Nset, nset=_PickedSet70, internal
   5,   6,   7,   8,  77,  78,  79,  80,  81,  82,  83,  84,  85,  86,  87,  88
 473, 474, 475, 476, 477, 478, 479, 480
*Elset, elset=_PickedSet70, internal, generate
 337,  434,    1
*Nset, nset=_PickedSet71, internal
   1,   2,   5,   6,   9,  10,  11,  12,  13,  14,  15,  16,  17,  18,  19,  20
 391, 392, 393, 394, 395, 396, 397, 398, 399, 400, 401, 402
*Elset, elset=_PickedSet71, internal, generate
 295,  336,    1
*Nset, nset=_PickedSet72, internal
   1,   2,   3,   4,   9,  10,  11,  12,  13,  14,  15,  16,  17,  18,  19,  20
 367, 368, 369, 370, 371, 372, 373, 374, 375, 376
*Elset, elset=_PickedSet72, internal, generate
   1,  294,    1
** Region: (SoilBottomLayer:Picked), (Controls:EC-1)
*Elset, elset=_PickedSet72, internal, generate
   1,  294,    1
** Section: SoilBottomLayer
*Solid Section, elset=_PickedSet72, controls=EC-1, material=BottomLayer
1.,
** Region: (SoilHardpanLayer:Picked), (Controls:EC-1)
*Elset, elset=_PickedSet71, internal, generate
295,  336,    1
** Section: SoilHardpanLayer
*Solid Section, elset=_PickedSet71, controls=EC-1, material=Hardpan
1.,
** Region: (SoilTopLayer:Picked), (Controls:EC-1)
*Elset, elset=_PickedSet70, internal, generate
```

```
 337,  434,    1
** Section: SoilTopLayer
*Solid Section, elset=_PickedSet70, controls=EC-1, material=TopLayer
1.,
*End Instance
**
*Instance, name=Cone-1, part=Cone
         0., 7.45899750000003,           0.
*Node
      1,           0.,   22.9224453
     23, 0.00215333328,   22.9224453
*Element, type=RAX2
 1,  1,  4
23, 23,  1
*Node
     24,           0.,   22.9108009,           0.
*Nset, nset=Cone-1-RefPt_, internal
24,
*Nset, nset=_PickedSet7, internal
 24,
*Nset, nset=_PickedSet8, internal
 24,
*Nset, nset=_PickedSet9, internal
 24,
*Elset, elset=Cone-1, generate
  1,  23,   1
*Element, type=MASS, elset=_PickedSet9_ConeTip_
24, 24
*Mass, elset=_PickedSet9_ConeTip_
0.0025,
*End Instance
**
*Nset, nset=SoilLayers, instance=Soil-2, generate
   1,  480,    1
*Elset, elset=SoilLayers, instance=Soil-2, generate
   1,  434,    1
*Nset, nset=_PickedSet243, internal, instance=Soil-2
  3,  4, 42, 43, 44, 45, 46, 47, 48, 49, 50, 51, 52, 53, 54
*Elset, elset=_PickedSet243, internal, instance=Soil-2, generate
 281,  294,    1
*Nset, nset=_PickedSet245, internal, instance=Soil-2
  1,  4,  5,  7, 55, 56, 57, 58, 59, 60, 61, 62, 63, 64, 65, 66
 67, 68, 69, 70, 71, 72, 73, 74, 75, 76, 92, 93, 94, 95, 96, 97
*Elset, elset=_PickedSet245, internal, instance=Soil-2
   1,  15,  29,  43,  57,  71,  85,  99, 113, 127, 141, 155, 169, 183, 197, 211
 225, 239, 253, 267, 281, 308, 322, 336, 350, 364, 378, 392, 406, 420, 434
*Nset, nset=ConeTip, instance=Cone-1
 24,
*Elset, elset=__PickedSurf259_SNEG, internal, instance=Cone-1, generate
 11,  20,   1
```

```
*Surface, type=ELEMENT, name=_PickedSurf259, internal
__PickedSurf259_SNEG, SNEG
*Surface, type=NODE, name=SoilLayers_CNS_, internal
SoilLayers, 1.
*Rigid Body, ref node=Cone-1.Cone-1-RefPt_, elset=Cone-1.Cone-1
*End Assembly
**
** ELEMENT CONTROLS
**
*Section Controls, name=EC-1, hourglass=ENHANCED
1., 1., 1.
*Amplitude, name=DisPen, time=TOTAL TIME
0., 0., 1., 0.015, 2., 0.03, 3., 0.045
4., 0.06, 5., 0.075
**
** MATERIALS
**

*Material, name=BottomLayer
*Density, dependencies=1
1540.0,,0.0001.
1547.6,,25000.
1553.4,,50000.
1557.8,,75000.
1561.3,,100000.
1564.0,,125000.
1575.6,,150000.
1599.2,,175000.
1618.9,,200000.
1635.5,,225000.
1649.9,,250000.
1662.5,,275000.
1673.9,,300000.
1684.3,,325000.
1694.0,,350000.
1703.2,,375000.
1712.1,,400000.
1720.6,,425000.
1729.0,,450000.
1737.2,,475000.
1745.4,,500000.
*Drucker Prager
58., 1.,38.
*Drucker Prager Hardening, type=SHEAR
 0.0001,         0.
 25000., 0.00454501
 50000.,  0.0080049
 75000.,  0.0106566
100000.,  0.0127065
125000.,  0.0143087
```

```
150000.,   0.021154
175000.,  0.0349548
200000.,  0.0462667
225000.,   0.055729
250000.,  0.0638172
275000.,  0.0708848
300000.,  0.0771946
325000.,  0.0829421
350000.,  0.0882722
375000.,  0.0932928
400000.,  0.0980837
425000.,   0.102704
450000.,   0.107199
475000.,     0.1116
500000.,   0.115931
*Elastic, dependencies=1
   2e+06,   0.18, ,100000.
 3.5e+06,   0.28, ,200000.
 5.5e+06,   0.32, ,300000.
 6.5e+06,  0.325, ,400000.
   7e+06,  0.325, ,500000.
*Material, name=Cone
*Density
 7908.4,
*Elastic
 1.9305e+10, 0.3
*Material, name=Hardpan
*Density, dependencies=1
1710.0,      ,1.00E-05.
1718.4,      ,25000.
1724.8,      ,50000.
1729.8,      ,75000.
1733.6,      ,100000.
1736.6,      ,125000.
1739.0,      ,150000.
1740.9,      ,175000.
1742.5,      ,200000.
1743.8,      ,225000.
1744.9,      ,250000.
1745.9,      ,275000.
1746.8,      ,300000.
1747.6,      ,325000.
1748.4,      ,350000.
1749.1,      ,375000.
1749.7,      ,400000.
1750.4,      ,425000.
1751.0,      ,450000.
1751.6,      ,475000.
1752.2,      ,500000.
**
```

```
*Drucker Prager
58., 1.,38.
*Drucker Prager Hardening, type=SHEAR
  1e-06,        0.
 50000., 0.0080049
100000., 0.0127065
150000., 0.0155777
200000.,  0.017436
250000., 0.0187348
300000., 0.0197247
350000., 0.0205444
400000., 0.0212705
450000.,  0.021945
500000., 0.0225912
*Elastic, dependencies=1
   2e+06,   0.18, ,200000.
 3.5e+06,   0.28, ,400000.
 5.5e+06,   0.32, ,600000.
 6.5e+06,  0.325, ,800000.
   7e+06,  0.325, ,  1e+06
*Material, name=TopLayer
*Density, dependencies=1
1270.0,      ,1.00E-05.
1341.3,      ,25000.
1410.7,      ,50000.
1466.4,      ,75000.
1510.9,      ,100000.
1546.7,      ,125000.
1575.6,      ,150000.
1599.2,      ,175000.
1618.9,      ,200000.
1635.5,      ,225000.
1649.9,      ,250000.
1662.5,      ,275000.
1673.9,      ,300000.
1684.3,      ,325000.
1694.0,      ,350000.
1703.2,      ,375000.
1712.1,      ,400000.
1720.6,      ,425000.
1729.0,      ,450000.
1737.2,      ,475000.
1745.4,      ,500000.
*Drucker Prager
58., 1.,38.
*Drucker Prager Hardening, type=SHEAR
 0.0001,        0.
 25000., 0.0505645
 50000., 0.0973197
 75000.,  0.133153
```

```
100000.,  0.160855
125000.,  0.182506
150000.,  0.199655
175000.,  0.213456
200000.,  0.224768
225000.,   0.23423
250000.,  0.242318
275000.,  0.249386
300000.,  0.255696
325000.,  0.261443
350000.,  0.266773
375000.,  0.271794
400000.,  0.276585
425000.,  0.281205
450000.,    0.2857
475000.,  0.290101
500000.,  0.294432
*Elastic, dependencies=1
   2e+06,   0.18, ,100000.
 3.5e+06,   0.28, ,200000.
 5.5e+06,   0.32, ,300000.
 6.5e+06,  0.325, ,400000.
   7e+06,  0.325, ,500000.
**
** INTERACTION PROPERTIES
**
*Surface Interaction, name=IntProp-1
*Friction
 0.34,
** ----------------------------------------------------------------
**
** STEP: ConePenSoil
**
*Step, name=ConePenSoil
Soil Cone Penet
*Dynamic, Explicit
, 5.
*Bulk Viscosity
0.06, 1.2
**
** BOUNDARY CONDITIONS
**
** Name: BC-5 Type: Symmetry/Antisymmetry/Encastre
*Boundary
ConeTip, ZSYMM
** Name: Bottom Type: Displacement/Rotation
*Boundary
_PickedSet243, 2, 2
** Name: RP Type: Displacement/Rotation
*Boundary, amplitude=DisPen
```

```
ConeTip, 1, 1
ConeTip, 2, 2, -1.8
ConeTip, 6, 6
** Name: TopRight Type: Displacement/Rotation
*Boundary
_PickedSet245, 1, 1
*Adaptive Mesh Controls, name=Ada-1, smoothing objective=GRADED
1., 0., 0.
*Adaptive Mesh, elset=SoilLayers, frequency=9999, op=NEW
**
** INTERACTIONS
**
** Interaction: Cone_SoilLayerInt
*Contact Pair, interaction=IntProp-1, mechanical constraint=KINEMATIC, cpset=Cone_SoilLayerInt
_PickedSurf259, SoilLayers_CNS_
**
** OUTPUT REQUESTS
**
*Restart, write, number interval=1, time marks=NO
**
** FIELD OUTPUT: ConeTip
**
*Output, field
*Node Output
RF, U
**
** FIELD OUTPUT: F-Output-1
**
*Node Output, nset=SoilLayers
U,
*Element Output, elset=SoilLayers, directions=YES
PE, S, PEEQ
**
** HISTORY OUTPUT: ConeSoil
**
*Output, history, time interval=0.05
*Contact Output, cpset=Cone_SoilLayerInt
CFT, XT
**
** HISTORY OUTPUT: ReactionForce
**
*Node Output, nset=ConeTip
RF2, U2
*End Step
```